THESIS REPORT

Ph.D.

The Design of Tendon-Driven Manipulators with Isotropic Transmission Characteristics

by Y-J. Ou
Advisor: L-W. Tsai

Ph.D. 94-3

Sponsored by
the National Science Foundation
Engineering Research Center Program,
the University of Maryland,
Harvard University,
and Industry

Abstract

Title of Dissertation: The Design of Tendon-Driven Manipulators with Isotropic Transmission Characteristics

Yeong-Jeong Ou, Doctor of Philosophy, 1994

Dissertation directed by: Professor Lung-Wen Tsai
Department of Mechanical Engineering
and
Institute for Systems Research

This dissertation deals with the synthesis of the mechanical power transmission structure in tendon-driven manipulators. The force transmission characteristics from the end-effector space to the actuator space has been investigated. It is shown that tendon forces required to generate an output force at the end-effector are functions of the transmission structure matrix and the manipulator Jacobian matrix. The sufficient and necessary conditions for a transmission structure to be admissible are summarized and an efficient algorithm to check admissible structures is derived.

Based on the analysis of static force transmission, a general theory is developed for the synthesis of tendon-driven manipulators with isotropic transmission characteristics. It is shown that an n-dof (degree of freedom) manipulator can

possess these characteristics if it is made up of $n+1$ or $2n$ tendons and if its link lengths and pulley sizes are designed according to two equations of constraint. Design equations for synthesizing a manipulator to possess isotropic transmission characteristics are derived.

To demonstrate the theory, two examples are used: (1) a two-dof planar manipulator and (2) a three-dof spatial manipulator. The tendon forces in each manipulator with different transmission structures are compared. It is shown that manipulators with an isotropic transmission structure have more uniform force distribution among their tendons.

To further understand the isotropic transmission characteristics, the properties of a manipulator with an isotropic transmission structure are then discussed from many different perspectives. The discussion includes the tension control algorithm, maximum tensions, kinematic performance, antagonistic forces among tendons, and survivability of a transmission structure with $2n$ tendons.

Finally, a new design methodology is developed to determine tendon routings and pulley sizes of a special three-dof tendon-driven manipulator. This design methodology ensures that each tendon will subject equal maximum tension when an external force is applied to the end-effector in all possible directions. The design is further enhanced when the criteria of isotropic transmission are imposed. A design example is presented to demonstrate the features and to compare with the Salisbury finger.

The Design of Tendon-Driven Manipulators with Isotropic Transmission Characteristics

by

Yeong-Jeong Ou

Dissertation submitted to the Faculty of the Graduate School
of The University of Maryland in partial fulfillment
of the requirements for the degree of
Doctor of Philosophy
1994

Advisory Committee:

Professor Lung-Wen Tsai, Chairman/Advisor
Professor Patrick F. Cunniff
Professor Edward B. Magrab
Associate Professor W. P. Dayawansa
Assistant Professor Ioannis Minis

Dedication

To

My Parents

and

My Beloved Wife

Acknowledgements

I would like to express my sincere gratitude to my dissertation advisor, Prof. Lung-Wen Tsai. This work has been the result of numerous discussions with him. Without his encouragement, guidance, constructive criticism and support, this study would not be possible.

I am grateful to Dr. Cunnif, Dr. Magrab, Dr. Dayawanasa and Dr. Minis for their serving my advisory committee, reading this thesis, and providing informative comments. Special thanks are due to Dr. Kenneth Salisbury at MIT AI Laboratory for providing dimensions of the Salisbury hand.

This work was supported in part by the U.S. Department of Energy under Grant DEF05-88ER13977, and in part by the NSF Engineering Research Centers Program NSFD CDR 8803012. Such support does not constitute an endorsement by the supporting agencies of the views expressed in the thesis.

Table of Contents

List of Tables

List of Figures

Nomenclature

$\mathbf{A}$	a matrix which relates tendon displacements and joint angles
$\mathbf{A}^T$	structure matrix which is the transpose of $\mathbf{A}$
$\mathbf{A}_m^T$	structure matrix with m columns (m transmission lines)
$\mathbf{A}^{+T}$	pseudo-inverse of $\mathbf{A}^T$
C_i	$Cos(\theta_i)$
C_{ij}	$Cos(\theta_i + \theta_j)$
c_m	$1/(\mu\alpha_m)$
$\underline{f}$	output force vector at the end-effector
$\underline{f}^*$	force vector applied at the end-effector (= - $\underline{f}$)
$\mathbf{H}$	null space matrix of $\mathbf{A}^T$ whose columns span the null space of $\mathbf{A}^T$
$\tilde{\mathbf{H}}_m$	null space matrix of $\tilde{\mathbf{P}}_m^T$ whose columns span the null space of $\tilde{\mathbf{P}}_m^T$
$\underline{h}$	one-dimensional null vector of $\mathbf{A}_{n+1}^T$
h_j	j-th component of $\underline{h}$
$\mathbf{I}_n$	identity matrix of dimension n
$\mathbf{J}$	Jacobian matrix for a non-redundant manipulator
$\tilde{\mathbf{J}}$	Jacobian matrix evaluated at an isotropic point
$\mathbf{J}^T$	transpose of $\mathbf{J}$
$\mathbf{J}^{-T}$	inverse of $\mathbf{J}^T$
$\mathbf{L}$	Cholesky factorization of matrix $\mathbf{W}$ ($\mathbf{W} = \mathbf{L}^T\mathbf{L}$)
ℓ	link length
$\mathbf{P}_m$	matrix whose column vectors represent coordinates of all m apexes of a regular polytope
$\tilde{\mathbf{P}}_m$	pseudo-triangular matrix whose column vectors represent coordinates of all m apexes of a regular polytope

$\mathbf{Q}$	orthonormal matrix
$\mathbf{Q}_1$	rectangular matrix with orthonormal columns
$\mathbf{R}$, $\mathbf{R}_1$	upper triangular matrix with positive diagonal entries
$\underline{S}$	tendon displacement vector
S_i	$Sin(\theta_i)$
S_{ij}	$Sin(\theta_i + \theta_j)$
$\mathbf{U}$	rotation matrix
$\mathbf{W}$	positive definite weighting matrix
$\underline{\dot{x}}$	generalized velocity vector of the end-effector
α_{n+1}^2	$(n+1)/n$
α_{2n}^2	2
β, μ	arbitrary non-zero constants
$\underline{\lambda}$	arbitrary vector for the homogenous solution of $\underline{\xi}$
$\underline{\theta}$	joint angle vector
$\underline{\tau}$	joint torque vector
$\underline{\xi}$	tendon force vector
$\underline{\xi}_h$	homogenous solution of tendon force vector $\underline{\xi}$
$\underline{\xi}_p$	particular solution of tendon force vector $\underline{\xi}$
ϕ, ψ	direction of an external force $\underline{f}^*$
$(\ )_j$	j-th row of the matrix in the parentheses

Chapter 1

Introduction

1.1 Background

Today's industrial robots mostly have a motor mounted on one link to drive its adjacent link via a gear reduction unit. This means that the motor in the proximal joint must be powerful enough to lift all the outer motors. An individually joint driven manipulator thus tends to be bulky and heavy. As flexible automation increases in industry, so is the need for more precise, lightweight, and compact manipulators. By introducing power transmission mechanisms, motors can be placed in a location away from the joints. Therefore, light weight and compact manipulators can be produced. With the introduction of a power transmission mechanism to a system, the possibility of bringing in friction, noise, vibration, and wear increases. Therefore, the importance of the proper selection and design of a transmission mechanism for a system can never be over-emphasized.

Among the several means of power transmission, tendon (belt) has advantages of being quiet and clean, not needing lubrication, being able to absorb shock, easy installation and lower maintenance costs. Two major features of using tendons as the power transmission elements in manipulators are : (1) Actuators can be installed on or somewhere close to the base to reduce the size and inertia of a manipulating system. (2) A properly pretensioned tendon has no backlash, and therefore improves the precision of a manipulator. These merits have made tendons better suited than other transmission systems in many power-transmission applications; especially, in a dexterous hand design where the requirements of small volume and light weight are important.

Another reason to choose tendon power transmission in robots, especially for dexterous hands, is that it is analogous to tendons in human hands. The human tendon-sheath system has nearly the lowest friction known to man. To date, however, the design of tendon-driven manipulators still suffers from the lack of comprehensive knowledge necessary to take advantage of tendon technology (Jacobsen, et al., 1984; Jacobsen, et al., 1986). The understanding of tendon technology is essential to improving robot's capability.

1.2 Overview of Tendon-Driven Manipulators

Several descriptions of tendon-driven manipulators can be found in the literature. Okada (1977) used endless type tendons (belts) in the transmission system of a three fingered hand. Though only n actuators are needed to actuate an n-dof manipulator, pretension is required to prevent the belts from slacking. For high

speed operations, pretension causes excessive friction and, therefore, degrades the efficiency of the system. Rovetta (1977) and Sugano and Kato (1987) developed similar transmission devices using springs for pretensioning the tendons. The three-fingered UB hand II (Melchiorri and Vassura, 1992) and the five-fingered Anthrobot-2 (Ali, et al., 1993) also adopted the n-joint-n-actuator actuation scheme.

To avoid high pretension, Jacobsen, et al. (1984) used two tendons (two actuators), antagonistically pulled against each other, to drive each joint of the Utah/MIT dexterous hand. Figure 1.1 shows its finger structure and tendon routings. The device inevitably increases the number of tendons, actuators, and the complexity of the controller. On the other hand, Morecki, et al. (1980) employed seven tendons to actuate a six-dof manipulator. They showed that $n + 1$ is the minimum number of tendons required to achieve full control of an n-dof manipulator. Salisbury designed a three-fingered Salisbury hand (1990) (formerly called the Stanford/JPL hand) in which each finger has three degrees of freedom, and is actuated by four tendons (see Fig. 1.2). Both the Morecki and Salisbury's designs require no pretension and, therefore, result in lower tendon forces. The number of actuators needed outnumber that used in belt driven devices by only one.

1.3 Motivation and Preview

Most of the previous studies on tendon-driven manipulators have focused on the mechanics of manipulation and control of specific designs (Salisbury and Roth,

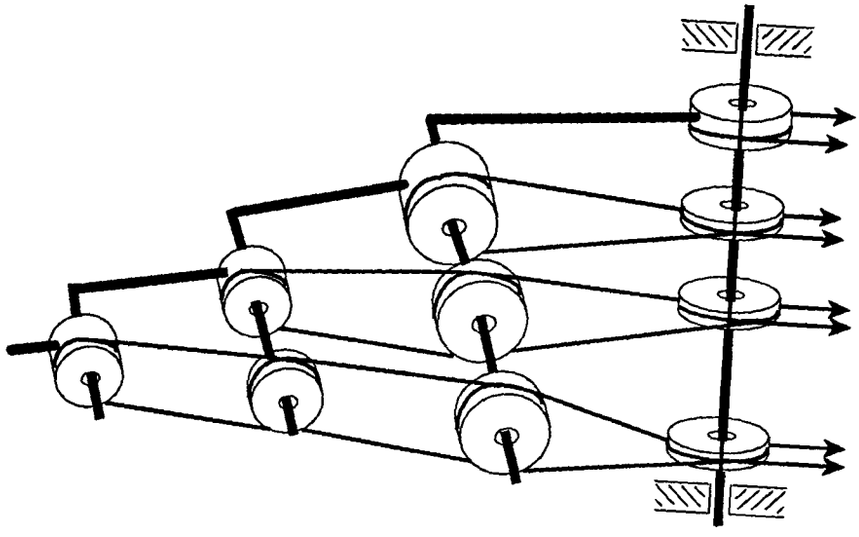

Figure 1.1: The link structure and tendon routings of the Utah/MIT finger

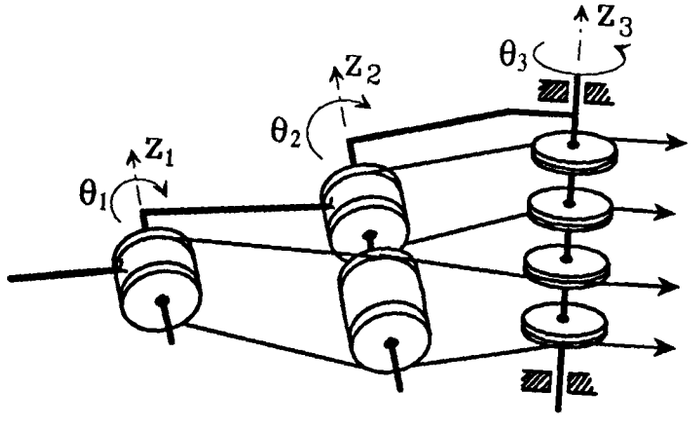

Figure 1.2: The link structure and tendon routings of the Salisbury finger

1983; Jacobsen, et al., 1989). The construction of actuation systems seems to rely on the designer's intuition. Those ad hoc approaches often fail to achieve an optimal implementation of tendons for power transmission.

In order to better design tendon-driven manipulators, Lee and Tsai (1991a) developed a methodology for the synthesis of kinematic structures with pseudo-triangular structure matrices. However, they only focused on those types of structures in which pulleys mounted on one common joint axis are all of the same size.

This study aims at improving this limitation by allowing the pulleys to assume different sizes, and developing a theory for synthesizing tendon-driven manipulators with isotropic transmission characteristics.

In Chapter 2 we look at the fundamental kinematic and static force equations. The force transmission characteristics, from the end-effector space to the actuator space, is investigated. It is shown that tendon forces required to generate an output force at the end-effector are functions of the transmission structure matrix, and the manipulator Jacobian matrix. The sufficient and necessary conditions for a transmission structure to be admissible are summarized and an efficient algorithm to check for admissible structures is derived.

In Chapter 3 we explore the concept of isotropic transmission structures and present a methodology for the kinematic synthesis of tendon-driven manipulators with isotropic transmission characteristics. Design equations for synthesizing a manipulator that possesses isotropic transmission characteristics are derived. Based on the analysis of static force transmission from the actuator space to

the end-effector space, a general theory is developed for the synthesis of tendon-driven manipulators with isotropic transmission characteristics. It is shown that an n-dof (degree of freedom) manipulator can possess these characteristics if it is made-up of $n+1$ or $2n$ tendons and if its link lengths and pulley sizes are designed according to two equations of constraint.

In Chapter 4 we use the criteria developed in Chapter 3 to derive the isotropic transmission structure with $n+1$ and $2n$ tendons. Two design examples: one two-dof planar manipulator and one three-dof spatial manipulator are presented to demonstrate the characteristics. Some fundamental design constraints of isotropic transmission structures with $n+1$ and $2n$ tendons are discussed. It is shown that manipulators which possess isotropic transmission characteristics do have more uniform force distribution among their tendons.

In Chapter 5 we discuss the attributes of isotropic transmission structures and compare the similarity and difference between isotropic transmission structures with $n+1$ tendons and $2n$ tendons from many different perspectives, including the tension control algorithm, maximum tensions, kinematic performance, antagonistic forces among tendons, and survivability of transmission structures with $2n$ tendons.

In Chapter 6 we develop a design methodology to determine the tendon routings and pulley sizes of a particular three-dof tendon-driven manipulator. This design methodology ensures that all tendons subject to equal maximum tensions in its entire workspace when an external force is applied at the end-effector in all possible orientations. The design is further enhanced when the criteria of

isotropic transmission are imposed. An example is presented to demonstrate the features and to compare with the finger of the Salisbury hand.

Finally, in Chapter 7 we review the study and summarize the findings, and give suggestions for further research.

Chapter 2

Preliminaries

2.1 Introduction

In the process of designing or synthesizing a mechanism, one inevitable process is the system analysis. The analysis of a representative model provides adequate understanding of the functions and the responses of a physical system in operation. Nonetheless, even the simplest physical component in a mechanism sometimes can be very complex to analyze. It is necessary for a designer to first establish a simple and yet workable model so that the fundamental characteristics of a system can be examined.

In this chapter, the general assumptions for a tendon-driven manipulator in this work are listed. Then, by studying kinematic equations of these models, the relationships among system states are determined. Such state variables include tendon displacements, joint angular displacements, and end-effector position (or

orientation). Meanwhile, by assuming that an external force is applied at the end-effector, static equations of the system are examined. By balancing all forces, the relationships among the external force, joint torques, and tendon forces are developed.

Through the discussion of the fundamental kinematic and static equations, the criteria for the controllability of tendon-driven manipulators are then investigated. A methodology for determining an admissible transmission structure for a tendon-driven manipulator is derived. And finally, the basic equations for transmission structures with $n+1$ tendons will be addressed.

2.2 Planar Schematic Representation

First, we introduce a structural representation of a tendon-driven manipulator: the planar schematic representation. After assigning a positive direction of rotation to each joint in this representation, each joint axis is twisted so that all joint axes are parallel to each other and are pointed out of the paper. In this way, a tendon-driven manipulator can be represented in a planar format. Without losing the fundamental relationships between tendons and pulleys in this presentation, the routing of tendons can be clearly shown. Figure 2.1 shows the planar schematic of a general n-dof tendon-driven manipulator with m tendons (actuators). For the convenience of matrix operations, we have numbered the links and joints from 1 to n starting from the distal end.

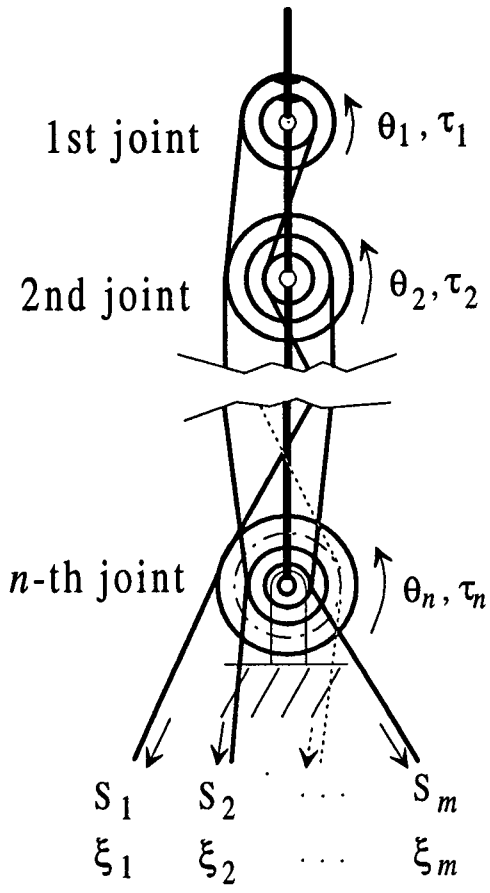

Figure 2.1: Planar schematic of an n-dof tendon-driven manipulator; whenever a tendon touches a pulley, it implies the tendon is routed around that pulley several times

2.3 General Assumptions

Before proceeding with the analysis of the mechanism, a tendon-driven manipulator in this study satisfies the following assumptions:

1. Tendons are always under tension so that the contact between tendons and pulleys is maintained, and the tension required to maintain such contact is neglected.
2. The elongation in a tendon due to tension is negligible.
3. Only the open-chain manipulator with revolute joints is considered.
4. All links are assumed to be rigid and each joint in the open-loop chain contributes to one degree of freedom.
5. The number of actuators is always larger than the degrees of freedom of a manipulator, i.e., no under-actuated mechanisms are allowed.

2.4 Fundamental Kinematic and Static Equations

In order to deal with the complexity of a tendon-driven manipulator, the description of the mechanism is divided into three different segments: (1) actuators (or tendons), (2) joints, and (3) the end-effector. Each segment is considered as a geometric space where its associated states are described. In actuator space,

the tendon input displacements and tendon forces are described. In joint space, the joint torques and joint angular displacements are traced, and in end-effector space, the end-effector position (or orientation) and an external force applied at the end-effector are of concern.

Hence, the study of kinematic and static equations of a tendon-driven manipulator is accomplished in three steps: first, the relationship between joint space and actuator space, i.e., the displacement and force functions between actuators and joints; secondly, the association between end-effector space and joint space which is characterized by the Jacobian matrix; and finally, the overall transformation between actuator space and end-effector space which is obtained by combining the results from the study of the first two steps.

2.4.1 Joint Space and Actuator Space

From Fig. 2.1, the relationship between tendon/actuator displacements and joint angles for a tendon-driven manipulator can be expressed as (Lee and Tsai, 1991b)

$$\underline{S} = \mathbf{A}\ \underline{\theta} \tag{2.1}$$

where $\underline{S} = [S_1, S_2, \cdots, S_m]^T$ denotes an $m \times 1$ linear displacement vector for the m tendons, $\underline{\theta} = [\theta_1, \theta_2, \cdots, \theta_n]^T$ denotes an $n \times 1$ joint angular displacement vector, and $\mathbf{A} = [a_{ij}]$ is an $m \times n$ matrix. Note that the links and joints are numbered sequentially from the distal end of the manipulator as shown in Fig. 2.1 and has been done to make the matrix operations in this work convenient. The elements a_{ij} of the matrix $\mathbf{A}$ are functions of tendon routings and pulley sizes. The absolute value of a_{ij} is equal to the radius of the pulley mounted on the jth

joint and routed by the ith tendon. And the sign of a_{ij} is positive if a positive displacement of tendon i produces a positive rotation of the pulley mounted on joint j, otherwise it is negative. The value of a_{ij} is equal to zero if tendon i is not routed about joint j. Figure 2.2 shows the definition of a_{ij} where the positive axis of rotation points out of the paper.

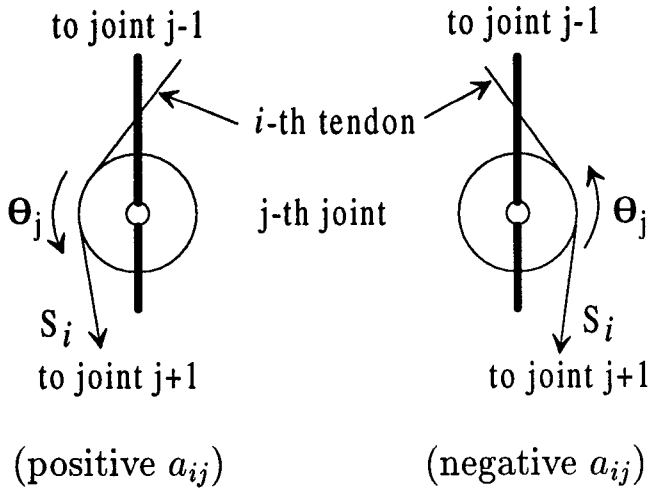

Figure 2.2: Sign convention for a_{ij}

Equation (2.1) is an over-determined problem for the $\underline{\theta}$ since $m \geq n+1$. Thus, only limit sets of tendon displacement vectors $\underline{S}$ are permissible, which make the implementation of direct control of tendon displacements impractical. Moreover, all tendons should be kept under tension while in operation. Therefore, it is necessary to implement a tension control system for the manipulator.

From eq. (2.1) and by using the principle of virtual work, the relationship between tendon forces and joint torques can be expressed as

$$\underline{\tau} = \mathbf{A}^T \underline{\xi} \tag{2.2}$$

where $\underline{\tau} = [\tau_1, \tau_2, \cdots, \tau_n]^T$ denotes an $n \times 1$ joint torque vector, $\underline{\xi} = [\xi_1, \xi_2, \cdots, \xi_m]^T$

denotes an $m \times 1$ tendon force vector, and $\mathbf{A}^T$, the transpose of $\mathbf{A}$, is called the structure matrix. Each column of the matrix $\mathbf{A}^T$ corresponds to one power "transmission line." When a unit actuator force is applied at the end of a tendon (a transmission line), the torque generated at each joint assumes the value of the corresponding element of the transmission line. Figure 2.3 shows one transmission line with its force relationship.

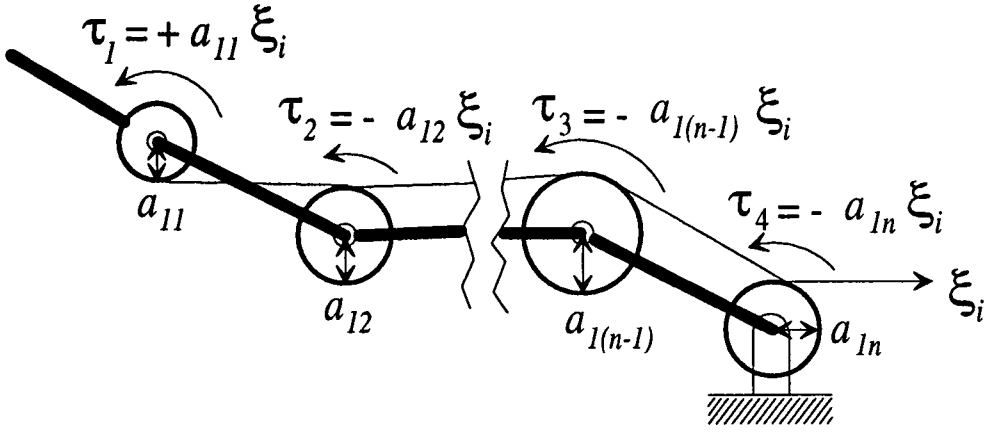

Figure 2.3: A transmission line of a tendon-driven manipulator

Equation (2.2) transforms tendon forces into joint torques. Given a set of tendon forces, the resultant joint torques are uniquely determined. Hence, to control all joint torques independently, $\mathbf{A}^T$ should be a full rank matrix. However, eq. (2.2) represents an under-determined linear system for the tendon forces. The inverse transformation of eq. (2.2) can thus be written as

$$\underline{\xi} = \mathbf{A}^{+T} \underline{\tau} + \mathbf{H} \underline{\lambda} \tag{2.3}$$

where $\mathbf{A}^{+T}$ is the pseudo-inverse of $\mathbf{A}^T$ (Ben-Israel and Greville, 1974; Strang, 1988), $\mathbf{H}$ is an $m \times (m-n)$ null space matrix with its column vectors spanning the null space of $\mathbf{A}^T$, and $\underline{\lambda}$ is an arbitrary $(m-n) \times 1$ vector. The first term

in the right-hand side of eq. (2.3) is known as the *particular solution* and the second term is the *homogeneous solution.* The homogeneous solution or the null space matrix satisfies

$$\mathbf{A}^T \mathbf{H} = \mathbf{0} \tag{2.4}$$

If the positive value of ξ_i $(i = 1, \cdots, m)$ represents tension and the negative value compression, then all the elements of $\underline{\xi}$ in eq. (2.3) should remain positive at all times. This uni-directional feature constrains the synthesis of transmission structures. In this regard, it appears to be sufficient that the column space of $\mathbf{H}$ should contain at least one m-dimensional vector with all positive elements. On the other hand, if there exists no such a positive vector in the column space of $\mathbf{H}$, then the particular solution space will contain vectors with all negative components. This is because the particular solution space is complementary to the homogenous solution space. Some tendon forces hence can not be adjusted into positive tensions. Therefore, the existence of such a positive vector is also a necessary condition for the structure matrix $\mathbf{A}^T$.

2.4.2 End-Effector Space and Joint Space

In many real-world tasks, it is necessary for a manipulator to touch parts, tools or surfaces. Such situations usually imply an external force acting at the end-effector. The ability of a manipulator to respond to such an external force is thus very important. Therefore, the kinematic and static relationships between end-effector space and joint space of a manipulator are reviewed in this section.

The Jacobian matrix of a manipulator maps the joint-rate vector $\dot{\underline{\theta}}$ to the generalized velocity vector $\dot{\underline{x}}$ of the end-effector (Fu, et al., 1987), i.e.,

$$\dot{\underline{x}} = \mathbf{J}\dot{\underline{\theta}} \tag{2.5}$$

where $\mathbf{J}$ is an $n \times n$ Jacobian matrix for a non-redundant degree-of-freedom manipulator.

It is well known that by neglecting the dynamic effect, the joint torques are related to an output force at the end-effector by the following equation (Salisbury and Craig, 1982):

$$\underline{\tau} = \mathbf{J}^T \underline{f} \tag{2.6}$$

where $\underline{f}$ is an $n \times 1$ output force vector at the end-effector. Generally speaking, as the configuration of a manipulator changes, so does the Jacobian matrix. Thus, the kinestatic performance of a manipulator varies as its end-effector assumes a new position.

Most researchers (Salisbury and Craig, 1982; Asada and Cro Granito, 1985; Gosselin and Angeles, 1988) have studied only the Jacobian matrix, which maps the joint space to the end-effector space; yet the transmission structure matrix, which maps the joint space to the actuator space, have not been considered. It is clear that their results are valid only for direct-drive manipulators. To design a tendon-driven manipulator, the overall transformation from the actuator space to the end-effector space should be examined.

2.4.3 End-effector Space and Actuator Space

Substituting eq. (2.6) into (2.3), yields

$$\underline{\xi} = \mathbf{A}^{+T}\mathbf{J}^{T}\underline{f} + \mathbf{H}\,\underline{\lambda} \tag{2.7}$$

The particular solution in eq. (2.7) is the minimum norm solution, which might contain infeasible negative forces. However, the homogeneous solution can be controlled, by adjusting $\underline{\lambda}$, to compensate for these negative forces so that tendon tensions are always positive. Both particular solution space (the column space of the matrix product $\mathbf{A}^{+T}\mathbf{J}^{T}$) and homogeneous solution space (the column space of the matrix $\mathbf{H}$) have significant effects on tendon forces. We may conclude that the configuration of the transmission structure (i.e. the matrix $\mathbf{A}$) is as important as that of the linkage structure (i.e. the matrix $\mathbf{J}$).

2.5 Admissible Transmission Structures

Based on the discussions in section 2.4.1, it is clear that a structure matrix with arbitrary pulley sizes and tendon routings might not be able to control each joint of a manipulator independently. The column vectors of $\mathbf{H}$ in eq. (2.3) form an $m - n$ dimensional null space for the matrix $\mathbf{A}^{T}$. An inspection of eq. (2.3) reveals that in order to maintain positive tensions in all tendons, there should exist at least one vector in the null space of $\mathbf{A}^{T}$ which contains all positive elements. We summarize the sufficient and necessary conditions for a feasible $n \times m$ transmission structure matrix as follows:

C1. The rank of $\mathbf{A}^T$ must be equal to n (Morecki, et al., 1980; Lee and Tsai, 1991a).

C2. There exists at least one vector with all positive elements in the null space of $\mathbf{A}^T$.

C3. Non-zero elements in each column of $\mathbf{A}^T$ must be consecutive since we assume that tendons are routed from joint to joint in a continuous manner.

Condition C1 ensures the existence of a non-trivial solution of $\underline{\xi}$ in eq. (2.3) for any given $\underline{\tau}$, while condition C2 makes it possible to adjust tendon forces in the positive direction. Together, they ensure that all tendons can maintain positive tensions. Condition C3 results from the physical limitation of tendon routing in an articulated mechanism.

Conditions C1 and C2 can be interpreted in terms of the elements of the structure matrix $\mathbf{A}^T$. According to C1, we can always rearrange the matrix $\mathbf{A}^T$ so that the determinant of the submatrix formed by the first n columns of matrix $\mathbf{A}^T$ is not zero. Let this determinant be d_{nn} and define

$$d_{ij} = \begin{vmatrix} & & & \text{col. } i & & \\ a_{11} & a_{21} & \cdots & a_{j1} & \cdots & a_{n1} \\ a_{12} & a_{22} & \cdots & a_{j2} & \cdots & a_{n2} \\ & \vdots & & \ddots & & \vdots \\ a_{1n} & a_{2n} & \cdots & a_{jn} & \cdots & a_{nn} \end{vmatrix}; \quad \begin{matrix} i = 1, \cdots, n \\ j = (n+1), \cdots, m \end{matrix} \tag{2.8}$$

where the i-th column of the square matrix formed by the first n columns of the matrix $\mathbf{A}^T$ is replaced by the j-th column of the matrix $\mathbf{A}^T$. By defining

$$h_{ij} = -\frac{d_{i(j+n)}}{d_{nn}}; \quad \begin{matrix} i = 1, \cdots, n \\ j = 1, \cdots, m-n \end{matrix} \tag{2.9}$$

from eq. (2.4), the null space matrix $\mathbf{H}$ of $\mathbf{A}^T$ can be obtained by using Cramer's rule as given below:

$$\mathbf{H} = \begin{bmatrix} h_{11} & h_{12} & \cdots & h_{1(m-n)} \\ h_{21} & h_{22} & \cdots & h_{2(m-n)} \\ \vdots & & & \vdots \\ h_{n1} & h_{n2} & \cdots & h_{n(m-n)} \\ 1 & 0 & \ddots & 0 \\ 0 & 1 & & \\ \vdots & 0 & \cdots & \vdots \\ & \vdots & & 0 \\ 0 & 0 & \ddots & 1 \end{bmatrix} \tag{2.10}$$

Since each column vector of the matrix $\mathbf{H}$ in eq. (2.10) is linearly independent, it forms a basis for the null space of the matrix $\mathbf{A}^T$. Equation (2.10) provides the symbolic form of the null space matrix $\mathbf{H}$. For numerical applications, the same form in eq. (2.10) can be obtained by first using the Gauss-Jordan reduction to derive the reduced row echelon form of the matrix $\mathbf{A}^T$ and then applying the reduced row echelon form to solve $\mathbf{A}^T\mathbf{H} = 0$ for $\mathbf{H}$.

Since any vector in the null space of $\mathbf{A}^T$ is the linear combination of the column vectors of $\mathbf{H}$ in eq. (2.10), condition C2 can then be interpreted as follows: There exists a vector $\underline{\lambda}$ such that $\mathbf{H}\underline{\lambda}$ contains all positive elements, i.e.,

from eq. (2.10),

$$\mathbf{H}' \underline{\lambda} > \underline{0}$$

$$\text{and} \quad \underline{\lambda} > \underline{0} \tag{2.11}$$

where

$$\mathbf{H}' = \begin{bmatrix} h_{11} & h_{12} & \cdots & h_{1(m-n)} \\ h_{21} & h_{22} & \cdots & h_{2(m-n)} \\ \vdots & & & \vdots \\ h_{n1} & h_{n2} & \cdots & h_{n(m-n)} \end{bmatrix} \tag{2.12}$$

and $\underline{\lambda} = (\lambda_1, \lambda_2, \cdots, \lambda_{m-n})^T$.

It can be seen when one column of the matrix $\mathbf{H}'$ contains all positive elements, then eqs. (2.11) and (2.12) can be satisfied and the corresponding transmission structure matrix is an admissible structure matrix. However, this is a sufficient but not a necessary condition.

To determine whether a structure matrix is admissible or not, we examine eq. (2.11). From a geometric point of view, each scalar inequality equation in eq. (2.11) represents a half space in the $(m-n)$-dimensional space. Since all of the half spaces intersect at the origin of the $(m-n)$-dimensional space, if a solution $\underline{\lambda}$ for eq. (2.11) exists, the solution domain is unbounded. Our objective is to determine whether a solution $\underline{\lambda}$ exists in eq. (2.11) for a given $\mathbf{H}'$. Therefore, eq. (2.11) can be changed into

$$\mathbf{H}' \underline{\lambda} \geq \underline{e}_1$$

$$\text{and} \quad \underline{\lambda} \geq \underline{e}_2 \tag{2.13}$$

where $\underline{e}_1$ is an $n \times 1$ vector with all positive elements and $\underline{e}_2$ is an $(m-n) \times 1$ vector with all positive elements. For ease of computation, in what follows, we let $\underline{e}_1 = [1, 1, \cdots, 1]$ and $\underline{e}_2 = [1, 1, \cdots, 1]$. By introducing the new variables $x_i = \lambda_i - 1$ $(i = 1, \cdots, m-n)$, eq. (2.13) can be rewritten as

$$\mathbf{H}' \ \underline{x} \geq (\underline{e}_1 - \mathbf{H}' \underline{e}_2)$$

$$\text{and} \quad \underline{x} \geq \underline{0} \tag{2.14}$$

Equation (2.14) represents the normal constraints of a linear programming problem. The existence of a "basic feasible solution" for eq. (2.14) hence can be determined efficiently through phase I of the simplex method (Press, et al., 1988). Thus, if and only if there exist feasible solutions $\underline{x}$ for the constraints in eq. (2.14), the corresponding structure matrix then satisfies condition C2.

2.6 Kinestatic Equations for $m = n+1$

As pointed out by early researchers (Morecki, et al., 1980; Salisbury and Craig, 1982), a minimum of $n+1$ tendons is necessary for the control of an n-dof manipulator. In this section, we shall focus only on those transmission structures that use the minimum number of tendons. For an n-dof system with $(n+1)$ tendons, eq. (2.3) can be rewritten as:

$$\underline{\xi} = \mathbf{A}^{+T} \underline{\tau} + \lambda \, \underline{h} \tag{2.15}$$

where $\underline{h}$ is a one-dimensional null vector of $\mathbf{A}^T$, and λ is an arbitrary constant.

Substituting eq. (2.6) into (2.15), we obtain the force relationship between

the actuator space and the end-effector space as

$$\underline{\xi} = \mathbf{A}^{+T}\mathbf{J}^T\underline{f} + \lambda\,\underline{h} \tag{2.16}$$

As we can see from eq. (2.16), to output a force $\underline{f}$, the required tendon force vector $\underline{\xi}$ consists of two components: a homogeneous solution $\lambda\underline{h}$ and a particular solution $\mathbf{A}^{+T}\mathbf{J}^T\underline{f}$. Since tendons can support only tensional forces, as mentioned before, all tendon forces must be positive.

Based on eq. (2.15), the condition C2 in Section 2.5 for an admissible $(n+1)\times n$ transmission structure matrix can be simplified as

C2. Each element in the null vector of $\mathbf{A}^T$ must be of the same sign and not equal to zero.

This simplified condition C2 can be interpreted as requiring all elements of $\underline{h}$ to be positive. Using Cramer's rule, the null vector can be written as

$$\underline{h} = \left[-d_1, d_2, \cdots, (-1)^i d_i, \cdots, (-1)^{n+1} d_{n+1}\right]^T \tag{2.17}$$

where d_i is the determinant of the matrix formed by deleting the ith column of $\mathbf{A}^T$. Note that eq. (2.17) also can be obtained by using the Gauss-Jordan reduction as discussed in Section 2.5. Since $d_i \neq 0$, for $i = 1, \cdots, n+1$, implies that matrix $\mathbf{A}$ is of rank n, conditions C1 and C2 can be combined into a single condition as

$$(-1)^i d_i > 0, \quad for \;\; i = 1, .., n+1 \tag{2.18}$$

Using eq. (2.18) and condition C3 in Section 2.5 as the constraints, all admissible $n+1$ tendon routings can be enumerated.

Based on the assumption that all pulleys mounted on the same joint axis are of the same size, Lee and Tsai (1991a) enumerated all and limited numbered admissible tendon routings. In many applications, pulley sizes can be different, thus their result is a subset of what can be enumerated by using condition C3 and eq. (2.18). From eq. (2.18) and C3, we can see that, even with the minimum number of tendons, the selection of transmission structures is unlimited.

2.7 Summary

The kinestatic relationship between joint space and actuator space of a tendon-driven manipulator depends on its transmission structure matrix $\mathbf{A}^T$. Due to the feature of the uni-directional tension, the transformation between both spaces is not a one-to-one mapping. Thus, there exist special constraints for the synthesis of the power transmission structure. Through the study of the kinestatic equations between the joint space and the actuator space, these constraints are outlined in three conditions in terms of the transmission structure matrix $\mathbf{A}^T$. In return, by examining a transmission structure matrix $\mathbf{A}^T$, a feasible transmission structure can be determined.

The kinestatic relationship between end-effector space and joint space depends on its Jacobian matrix $\mathbf{J}$, which varies as the configuration of the manipulator changes. When the end-effector moves to a singular point, the manipulator loses one or more degrees of freedom. Both transmission structure matrix $\mathbf{A}^T$ and Jacobian matrix $\mathbf{J}$ hence play an important role in the kinestatic performance of a manipulator.

As mentioned in the previous section, there are unlimited selection of admissible transmission structures, it is necessary to develop methodologies for choosing a physical dimension and tendon routings from possible structures to achieve optimum performance. This is the subject of study of the next chapters.

Chapter 3

Manipulators with Isotropic Transmission Characteristics

3.1 Introduction

Tendons feature the capability of supporting tension but not compression. Thus tendon-driven manipulators inherit and exhibit this unique nature in its transmission structure. Due to this distinct characteristic, as pointed out by early researchers (Morecki, et al., 1980; Salisbury, 1982; Salisbury and Craig, 1982), a minimum of $n+1$ tendons is necessary to gain a full control of an n-dof (degree-of-freedom) manipulator. A literature survey reveals that tendon-driven manipulators are primarily made up of two types of transmission structures. The first type employs $n+1$ tendons to drive an n-dof manipulator. Examples include the six-dof, seven-tendon manipulator designed by Morecki, et al. (1980) and the

three-fingered Stanford/JPL hand by Salisbury (1982). The second type uses $2n$ tendons. One such example is the Utah/MIT dexterous hand designed by Jacobsen, et al. (1984). Although other types of construction, such as using $n+2$ tendons to control an n-dof manipulator, are possible, no practical designs have been found in the literature.

Most of the previous studies on tendon-driven manipulators have focused on the mechanics of manipulation and control of specific designs. The construction of actuation systems seems to rely on the designer's intuition. Those ad hoc approaches often fail to achieve an optimal implementation of tendons for power transmission. This chapter aims at improving this limitation by developing a theory for arriving at a local optimal design of power transmission in a tendon-driven manipulator.

Salisbury (1982) first applied linear force error analysis to the Stanford/JPL hand and defined those end-effector points where the Jacobian matrix has a unity condition number as the isotropic points. Asada and Cro Granito (1985) used the generalized velocity ratios and the mobility ellipsoid as a measure of kinematic performance. When the maximal generalized velocity ratio is equal to the minimal ratio, the manipulator is referred to as having an isotropic mobility at the given posture. Yoshikawa (1985) developed the manipulability ellipsoid and defined an index, the reciprocal of the condition number of the Jacobian matrix, for the directional uniformity of the ellipsoid. Klein and Blaho (1987) used the condition number of the Jacobian matrix as one of the dexterity measures to determine optimal postures for redundant manipulator design. Gosselin and Angeles (1988) defined an index based on the condition number of the Ja-

cobian matrix for kinematic optimization of manipulators. Angeles (1992) then extended the isotropic conditions to the kinematic design of redundant manipulators.

The aforementioned condition number is defined as the ratio of the maximal singular value to the minimal singular value of the Jacobian matrix which only relates the static force (or velocity) transformation between joint space and end-effector space. This definition does not consider the effect of mechanical power transmission mechanism. Lee and Tsai (1991a) first considered the transformation between actuator space and joint space for an n-dof manipulator with $n+1$ tendons. Lee (1991) defined the condition number of a tendon transmission structure as the ratio of the maximal singular value to the minimal singular value of the structure matrix. The transformation between joint space and actuator/tendon space is said to be isotropic, if the condition number of the structure matrix is equal to one. When the condition number of the Jacobian matrix and that of the structure matrix are both equal to one, an isotropic transformation is obtained for the overall system.

The above two approaches can only achieve partial or limited results. To make the theory complete, Chen and Tsai (1993) then considered the overall transformation from actuator space to end-effector space and derived isotropic transmission conditions for geared robotic mechanisms. They defined the isotropic transformation as one that has the unity condition number for the overall transformation matrix. It does not require that both the condition numbers of the Jacobian matrix and the structure matrix to be equal to one. Therefore, it gives more flexibility for the synthesis of manipulators. However, their results are not

directly applicable to tendon-driven manipulators. In this chapter, the synthesis of a general n-dof tendon-driven manipulator with m tendons based on the similar concept of isotropic transmission, where $m \geq n+1$, will be discussed.

3.2 Isotropic Condition

The condition number indicates the error sensitivity in a linear transformation system (Strang, 1988). The Jacobian matrix of a manipulator maps the joint-rate vector $\underline{\dot{\theta}}$ to the generalized velocity vector $\underline{\dot{x}}$ of the end-effector, i.e.

$$\underline{\dot{x}} = \mathbf{J}\underline{\dot{\theta}} \tag{3.1}$$

When the generalized velocity vector $\underline{\dot{x}}$ contains inhomogeneous quantities, for instance linear velocity and angular velocity, the condition number of the Jacobian matrix becomes meaningless. Thus the norm of $\underline{\dot{x}}$ is defined as

$$\|\underline{\dot{x}}\| = \underline{\dot{x}}^T\mathbf{W}\underline{\dot{x}} = \underline{\dot{\theta}}^T\mathbf{J}^T\mathbf{W}\mathbf{J}\underline{\dot{\theta}} \tag{3.2}$$

where $\mathbf{W}$ is a positive definite weighting matrix and is defined so that the norm in eq. (3.2) is frame invariant. By using Cholesky factorization, one can write

$$\mathbf{W} = \mathbf{L}^T\mathbf{L} \tag{3.3}$$

Hence, when the generalized velocity vector contains inhomogeneous quantities, the condition number of the matrix product $\mathbf{LJ}$ will be used as a measure of the error sensitivity for the system described by eq. (3.1). When the condition number is equal to one, one can show that

$$\mathbf{L}\mathbf{J}\mathbf{J}^T\mathbf{L}^T = \mu^2\mathbf{I}_n \tag{3.4}$$

where μ is an arbitrary non-zero constant and $\mathbf{I}_n$ is an identity matrix of dimension n. From eq. (2.6), a Jacobian matrix satisfying eq. (3.4) maps a unit hypersphere in the n-dimensional end-effector force space into a scaled n-dimensional hypersphere in the joint torque space.

For a tendon-driven manipulator, the feasible domain of actuator forces contains only the positive hyperquadrant of an m-dimensional space. In eq. (2.7), the particular solution is obtained as a linear transformation of the output force $\underline{f}$. Thus a unit hypersphere in the n-dimensional end-effector force space maps into an n-dimensional ellipsoid in the m-dimensional actuator force space. The space occupied by this n-dimensional ellipsoid is called the n-dimensional particular solution subspace. The superposition of the particular solution with the homogeneous solution then translates the n-dimensional ellipsoid into the positive hyperquadrant of the m-dimensional actuator force space by adjusting $\underline{\lambda}$. Therefore, an isotropic transmission structure can be characterized by the following two conditions.

3.2.1 Unity Condition Number

The condition number of $\mathbf{A}^{+T}\mathbf{J}^T$ should be equal to one so that a unit hypersphere in the end-effector force space can be mapped into a scaled hypersphere in the particular solution space. This leads to

$$\mathbf{L}\mathbf{J}\mathbf{A}^{+}\mathbf{A}^{+T}\mathbf{J}^T\mathbf{L}^T = \mu^2\mathbf{I}_n \tag{3.5}$$

Using $\mathbf{A}^+ = (\mathbf{A}^T\mathbf{A})^{-1}\mathbf{A}^T$ and $(\mathbf{A}^T\mathbf{A})^{-T} = (\mathbf{A}^T\mathbf{A})^{-1}$, eq. (3.5) can be simplified as

$$\mathbf{LJ}(\mathbf{A}^T\mathbf{A})^{-1}\mathbf{A}^T\mathbf{A}(\mathbf{A}^T\mathbf{A})^{-1}\mathbf{J}^T\mathbf{L}^T = \mu^2\mathbf{I}_n \tag{3.6}$$

or

$$\mathbf{LJ}(\mathbf{A}^T\mathbf{A})^{-1}\mathbf{J}^T\mathbf{L}^T = \mu^2\mathbf{I}_n \tag{3.7}$$

Pre-multiplying $(\mathbf{LJ})^T$ to both sides of eq. (3.7), we obtain

$$\mathbf{J}^T\mathbf{WJ}(\mathbf{A}^T\mathbf{A})^{-1}(\mathbf{LJ})^T = \mu^2(\mathbf{LJ})^T \tag{3.8}$$

Since eq. (3.8) is valid for any matrix $(\mathbf{LJ})^T$, we conclude that

$$\mathbf{J}^T\mathbf{WJ}(\mathbf{A}^T\mathbf{A})^{-1} = \mu^2\mathbf{I}_n \tag{3.9}$$

Post-multiplying eq. (3.9) by $(\mathbf{A}^T\mathbf{A})$, we obtain

$$\mathbf{A}^T\mathbf{A} = \frac{1}{\mu^2}(\mathbf{J}^T\mathbf{WJ}) \tag{3.10}$$

Equation (3.10) is the necessary and sufficient condition for the condition number of $\mathbf{A}^{+T}\mathbf{J}^T$ to be equal to one. Since $\mathbf{A}$ is a matrix of rank n, eq. (3.10) can only be satisfied at those positions where the Jacobian matrix $\mathbf{J}$ is of rank n. Since the Jacobian matrix is position dependent, the condition number is also position dependent. Therefore, the unity condition number can be achieved only at a specified manipulator posture.

3.2.2 Isotropic Particular Solution Subspace

Equation (3.10) involves only the mapping from the end-effector space to the particular solution subspace. The transformation from the particular solution

subspace to the positive hyperquadrant of the actuator space depends on the selection of $\underline{\lambda}$ and the orthogonal projection (Coxeter, 1973) of the positive hyperquadrant of the m-dimensional actuator space onto the n-dimensional particular solution subspace. The value of $\underline{\lambda}$ is chosen such that the resulting tendon forces are all positive. The projection of the positive hyperquadrant of the actuator space onto the particular solution subspace depends on the arrangement of tendons and pulley sizes. Therefore, it is equally important to consider the transformation of the coordinate axes of the actuator space to the particular solution subspace.

Since each positive Cartesian axis of the m-dimensional actuator space represents a tendon force, the particular solution subspace needs to be in a special subspace so that the orthogonal projection of the positive hyperquadrant of the actuator space onto the particular subspace remains centrally symmetrical. Here the phrase central symmetry means that when both origins of the n-dimensional particular solution subspace and the m-dimensional actuator force space coincide, orthogonally projected vectors of the positive Cartesian axes of the m-dimensional actuator space are evenly-distributed in the n-dimensional particular solution subspace. In such a way, the particular solution space is divided into several equal portions. A particular solution in each portion is always the resultant of an equal number of actuators. We called this special subspace "an isotropic subspace." Note that the magnitudes of the projected vectors are not necessarily equal to one another even though they are projected from the Cartesian axes of the same length. Figure 3.1 shows all 3-D positive Cartesian axes being projected orthogonally onto a 2-D particular solution subspace where all the projected vectors are 120 degrees apart.

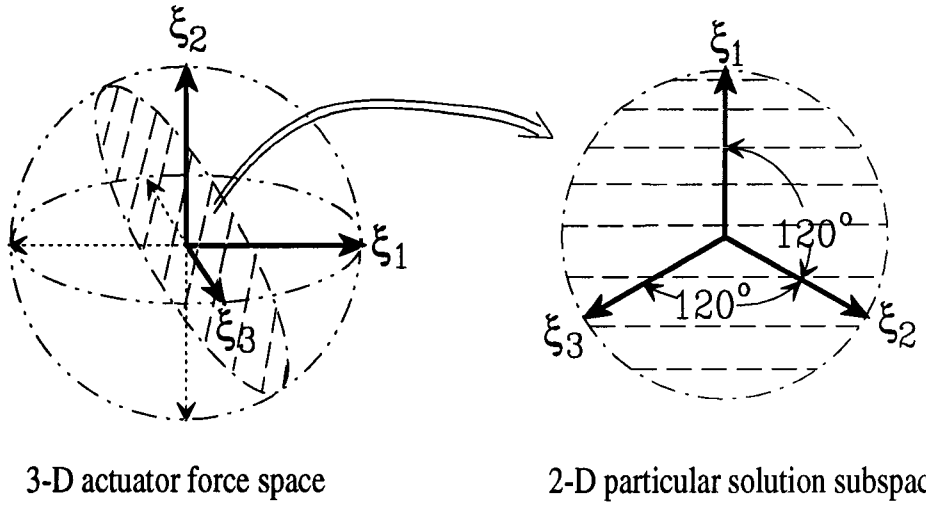

Figure 3.1: The orthogonal projection of a 3-D positive actuator quadrant onto a 2-D particular solution subspace

It is not always possible to distribute all m orthogonally projected vectors symmetrically in an n-dimensional subspace. In fact, by connecting the apexes of all m symmetrically projected unit vectors, an n-dimensional regular convex polytope is formed. In the 2-D space, a regular m-polygon is formed for any m greater than two. In the 3-D space, there exists only five regular polyhedra (i.e. five Platonic solids). They are the tetrahedron, octahedron, cube, icosahedron, and dodecahedron. Each of them has 4, 6, 8, 12, and 20 apexes, respectively. Figure (3.2) shows three of the five solids. In the n-D space, a possible regular polytope contains $n+1$, or $2n$, or 2^n, $\cdots$, apexes (Coxeter, 1973). Since each apex represents an actuator/tendon, we conclude that kinematic isotropy is possible only for certain numbers of tendons. For 2-dof manipulators, any number of tendons ($m \geq 2$) can be routed to possess isotropic transmission characteristics. While for 3-dof manipulators, the feasible number of tendons can only be 4, 6, 8,

Tetrahedron

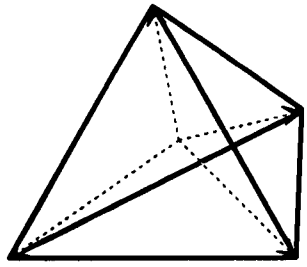

Octahedron

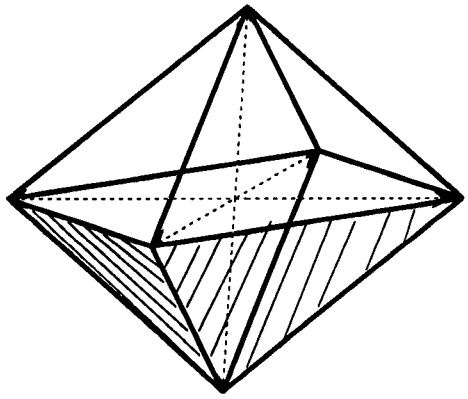

Cube (Hexahedron)

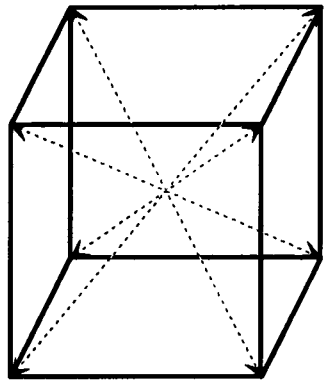

Figure 3.2: the tetrahedron, octahedron and cube of five Platonic solids

12, or 20. For n-dof manipulators ($n \geq 2$), the feasible numbers of tendons are $n+1$, $2n$, 2^n, $\cdots$, etc. In general, when m is larger than $2n$, tendon routings will be unnecessarily complex and inefficient. Hence, only manipulators with $n+1$ and $2n$ tendons are considered to be practical.

In the n-dimensional space, a regular simplex polytope has $n+1$ apexes. Each edge connects two apexes. The angle subtended by an edge at the center of the polytope is $Cos^{-1}(-1/n)$. Let the coordinates of an apex be represented by a column vector. Also let the origin of the Cartesian frame be located at the center of the regular simplex, and the distance from the origin to each apex be one unit length. Then we can locate the first apex at $(0, \cdots, 0, -1)^T$, and the second at $(0, \cdots, 0, a2, a1)^T$, where $a1$ and $a2$ can be computed from the angle relationship with the first apex and the requirement of one unit length of the second vector. Similarly, the third apex can be located at $(0, ..., 0, b3, b2, b1)^T$, where $b3$, $b2$, and $b1$ can be calculated from its angle relationship with the first and the second apexes. Following the same procedure, the coordinates of all apexes can be obtained and expressed in an $n \times (n+1)$ pseudo-triangular matrix form:

$$\tilde{\mathbf{P}}_{n+1} = \sqrt{\frac{n+1}{2n}} \begin{bmatrix} 1 & -1 & 0 & \cdots & \cdots & 0 \\ 1/\sqrt{3} & 1/\sqrt{3} & -2/\sqrt{3} & 0 & \cdots & 0 \\ 1/\sqrt{6} & 1/\sqrt{6} & 1/\sqrt{6} & -3/\sqrt{6} & 0\cdots & 0 \\ & \cdots & & \cdots & & \\ \sqrt{\frac{2}{(n^2+n)}} & & \cdots & & \sqrt{\frac{2}{(n^2+n)}} & -\sqrt{\frac{2n^2}{(n^2+n)}} \end{bmatrix} \quad (3.11)$$

where each column vector of the matrix $\tilde{\mathbf{P}}_{n+1}$ corresponds to one apex. Hence, the dot product of any two column vectors is equal to (-1/n). Note that the coordinates of all apex of a regular simplex polytope can be represented by $2^n - 1$

different pseudo-triangular matrices, which can be obtained by multiplying any row or combination of rows of the matrix $\tilde{\mathbf{P}}_{n+1}$ in eq. (3.11) by "-1'. We note that the row vectors of the matrix $\tilde{\mathbf{P}}_{n+1}$ are orthogonal to each other and they span an isotropic subspace.

The null space of matrix $\tilde{\mathbf{P}}_{n+1}$ can be derived as

$$\tilde{\mathbf{H}}_{n+1} = [1, 1, \cdots, 1]^T \tag{3.12}$$

A regular cross polytope has $2n$ apexes, and the angle subtended by an edge at the center of the polytope is equal to 90°. Let the coordinates of each apex be represented by a column vector. Then the coordinates of the $2n$ apexes with the center of the polytope located at the origin of a Cartesian frame, and the distance from the origin to each apex be one unit length, can be expressed by an $n \times 2n$ matrix as

$$\tilde{\mathbf{P}}_{2n} = \begin{bmatrix} 1 & -1 & 0 & 0 & 0 & \cdots & 0 & 0 \\ 0 & 0 & 1 & -1 & 0 & \cdots & 0 & 0 \\ \vdots & \vdots & & & \ddots & \ddots & \vdots & \vdots \\ 0 & 0 & 0 & 0 & \cdots & 0 & 1 & -1 \end{bmatrix} \tag{3.13}$$

In this case, the dot product of any two column vectors is equal to zero or minus one and the row vectors are orthogonal to each other and span an isotropic subspace.

The null space of matrix $\tilde{\mathbf{P}}_{2n}$ can be derived as a $2n \times n$ matrix:

$$\tilde{\mathbf{H}}_{2n} = \begin{bmatrix} 1 & 0 & \cdots & 0 \\ 1 & 0 & \cdots & 0 \\ 0 & 1 & \cdots & \vdots \\ 0 & 1 & \cdots & \vdots \\ \vdots & \vdots & \cdots & 0 \\ 0 & 0 & \cdots & 1 \\ 0 & 0 & \cdots & 1 \end{bmatrix} \tag{3.14}$$

Note that $\tilde{\mathbf{P}}_{2n}$ contains two opposing column vectors (apexes) located on each axis of the n-dimensional Cartesian space. Although the null space of the matrix obtained by exchanging any two columns of $\tilde{\mathbf{P}}_{2n}$ is different from that of the matrix $\tilde{\mathbf{P}}_{2n}$ itself, they represent a permutation of the order of the apexes and, hence, are isomorphic to each other.

Equations (3.11) and (3.13) represent a regular simplex polytope and a regular cross polytope in a special orientation. By rotating a regular polytope with respect to the Cartesian frame, the matrices shown in eqs. (3.11) and (3.13) can be changed to

$$\mathbf{P}_m = \mathbf{U}\tilde{\mathbf{P}}_m \tag{3.15}$$

where m=n+1 or $2n$, and $\mathbf{U}$ is an $n \times n$ orthogonal rotation matrix which rotates all coordinates by the same angle. Since the row vectors of matrix $\tilde{\mathbf{P}}_m$ are orthogonal and span an isotropic subspace, we have

$$\mathbf{P}_m\mathbf{P}_m^T = \alpha_m^2\mathbf{I}_n \tag{3.16}$$

where $\alpha_{n+1}^2 = (n+1)/n$ and $\alpha_{2n}^2 = 2$.

Since the complementary space of the column space of $\tilde{\mathbf{H}}_m$ ($m = n+1$ or $2n$) is the row space of $\mathbf{P}_m$, any matrix with the null space of the form of eq. (3.12) or (3.14) spans the same row space as $\mathbf{P}_m$. Therefore, an isotropic transmission structure matrix, whose row vectors span an isotropic subspace, should satisfy

$$\mathbf{A}^T\tilde{\mathbf{H}}_m = 0, \text{ for } m = n+1 \text{ or } 2n \tag{3.17}$$

From the above derivations, we arrive at the following theorem:

Theorem:

An n-dof tendon-driven manipulator can possess the isotropic transmission characteristics at a given posture if it is constructed by $n+1$ or $2n$ tendons and if its structure matrix $\mathbf{A}^T$ and Jacobian matrix $\mathbf{J}$ satisfy eqs. (3.10) and (3.17).

3.2.3 Isotropic Transmission

A manipulator is said to possess *isotropic transmission* characteristics if its overall transformation matrix $\mathbf{A}^{+T}\mathbf{J}^T$ has a unity condition number and if the row vectors of $\mathbf{A}^T$ span an isotropic subspace.

Equation (3.10) assures that $\mathbf{A}^T$ is a matrix of rank n and eq. (3.17) indicates that the row vectors of matrix $\mathbf{A}^T$ span an isotropic subspace. We call a structure matrix, which satisfies eqs. (3.10), (3.17), and condition C3 in Chapter 2, an isotropic transmission structure (ITS).

Equation (3.10) contains $n(n+1)/2$ quadratic equations while eq. (3.17) contains $(m-n)\times n$ linear equations. Thus, there are a total of $n(2m-n+1)/2$ equations of constraint imposed on the elements of $\mathbf{A}^T$.

Since eq. (3.10) contains an arbitrary constant μ, we conclude that once a kinematical isotropic transmission arrangement is found, the pulley sizes can be proportionally increased (or decreased) without affecting its isotropic transmission characteristics. The proportional constant, however, does have an effect on the pulley sizes and, therefore, on the resulting tensions in the tendons.

3.3 Design Equations

In what follows, we shall assume that the dimensions of the links such as the offset distances and twist angles of a manipulator are known. Thus, once the posture of a manipulator is specified, the Jacobian matrix is completely known. Our objective is to apply eqs. (3.10) and (3.17) to find appropriate tendon routings and pulley sizes, which yield isotropic transmission characteristics for the manipulator at a specified posture of interest.

First, we apply the "skinny" QR factorization (Golub and Van Loan, 1983) to matrix $\mathbf{A}$, i.e.,

$$\mathbf{A} = \mathbf{Q}_1\mathbf{R}_1 \tag{3.18}$$

where $\mathbf{Q}_1$ is an $m \times n$ matrix with orthonormal columns and $\mathbf{R}_1$ is an $n \times n$ upper triangular matrix with positive diagonal entries so that the factorization is unique. Substituting eq. (3.18) into (3.10), and using the fact $\mathbf{Q}_1^T\mathbf{Q}_1 = \mathbf{I}_n$, we obtain

$$\mathbf{R}_1^T\mathbf{R}_1 = \frac{1}{\mu^2}(\mathbf{J}^T\mathbf{W}\mathbf{J}) = \frac{1}{\mu^2}(\mathbf{J}^T\mathbf{L}^T\mathbf{L}\mathbf{J}) \tag{3.19}$$

Since $\mathbf{LJ}$ is a full rank matrix, its QR factorization can be written as

$$\mathbf{LJ} = \mathbf{QR} \tag{3.20}$$

where $\mathbf{Q}$ is an $n \times n$ orthonormal matrix and $\mathbf{R}$ is an $n \times n$ upper triangular matrix with positive diagonal entries. Substituting eq. (3.20) into (3.19), we obtain

$$\mathbf{R}_1^T\mathbf{R}_1 = \frac{1}{\mu^2}\mathbf{R}^T\mathbf{R} \tag{3.21}$$

Since both side of eq. (3.21) are in the form of Cholesky factorization, we conclude that

$$\mathbf{R}_1 = \frac{1}{\mu}\mathbf{R} \tag{3.22}$$

Substituting eq. (3.18) into (3.17), yields

$$\mathbf{R}_1^T\mathbf{Q}_1^T\tilde{\mathbf{H}}_m = \underline{0} \tag{3.23}$$

Since $\mathbf{R}_1^T$ is a full rank matrix, its null space is empty. Hence, eq. (3.23) can be reduced to

$$\mathbf{Q}_1^T\tilde{\mathbf{H}}_m = \underline{0} \tag{3.24}$$

Comparing eq. (3.24) with (3.17) and using eq. (3.16), it can be shown that

$$\mathbf{Q}_1^T = \frac{1}{\alpha_m}\mathbf{P}_m \tag{3.25}$$

Taking the transpose of eq. (3.18), and substituting eqs. (3.22) and (3.25) into the resulting equation, yields

$$\mathbf{A}^T = c_m\mathbf{R}^T\mathbf{P}_m \tag{3.26}$$

where c_m=$1/\mu\alpha_m$. Since we may include $\mathbf{Q}$ as part of the rotation matrix $\mathbf{U}$, using eqs. (3.20) and (3.22), eq. (3.26) can be rewritten as

$$\mathbf{A}^T = c_m\mathbf{J}^T\mathbf{L}^T\mathbf{P}_m = c_m\mathbf{J}^T\mathbf{L}^T\mathbf{U}\tilde{\mathbf{P}}_m \tag{3.27}$$

Equations (3.26) and (3.27) provides a method for generating a general structure matrix with isotropic transmission characteristics. However the matrix $\mathbf{A}^T$ may not necessarily satisfy condition C3; that is, non-zero elements in the columns of $\mathbf{A}^T$ may not necessarily be consecutive. In general, $\mathbf{A}^T$ derived from eq. (3.26) has the same form as $\mathbf{P}_m$, i.e., the positions of zero elements remain the same. Thus, a particular form of $\mathbf{A}^T$ can be obtained by selecting $\mathbf{P}_m$.

A structure matrix satisfying eqs. (3.10) and (3.17) automatically satisfies constraints C1 and C2, but not necessarily C3. If the isotropic point is chosen at a location where the condition number of $\mathbf{LJ}$ is equal to one and $\mathbf{U}$ is an identity matrix, then the structure matrix is given by $\tilde{\mathbf{P}}_{n+1}$ or $\tilde{\mathbf{P}}_{2n}$. Both $\tilde{\mathbf{P}}_{n+1}$ and $\tilde{\mathbf{P}}_{2n}$ satisfy constraint C3. Since $\tilde{\mathbf{P}}_{n+1}$ is already in a pseudo-triangular form, it permits all actuators to be base mounted. However, $\tilde{\mathbf{P}}_{2n}$ is in a bi-diagonal form, and, therefore, does not permit all actuators to be base mounted.

Pre-multiplying $\tilde{\mathbf{P}}_{2n}$ by a rotation matrix $\mathbf{U}$ as shown in eq. (3.15) changes $\tilde{\mathbf{P}}_{2n}$ into $\mathbf{P}_{2n}$. Therefore, by choosing a proper rotation matrix, it is possible to obtain a matrix $\mathbf{P}_{2n}$ such that all the actuators can be base mounted. In the next two sections, we will discuss those ITSs which permit all actuators to be base mounted and their representative matrices with the minimum number of non-zero elements.

3.4 Manipulators with n+1 Tendons Arranged in a Pseudo-triangular Form

When m is equal to n+1, eqs. (3.10) and (3.17) impose $n(n+3)/2$ equations of constraint on the elements of $\mathbf{A}^T$. If we require all actuators to be installed on the ground and seek a tendon routing method with the minimal number of pulleys, then the elements of $\mathbf{A}^T$ can be arranged into a pseudo-triangular form as shown below (Morecki, et al., 1980):

$$\mathbf{A}^T = \begin{bmatrix} a_{11} & a_{21} & 0 & \cdots & \cdots & 0 \\ a_{12} & a_{22} & a_{32} & 0 & \cdots & 0 \\ & \vdots & & & \ddots & \vdots \\ a_{1,n-1} & a_{2,n-1} & \cdots & \cdots & a_{n,n-1} & 0 \\ a_{1,n} & a_{2,n} & \cdots & \cdots & a_{n,n} & a_{n+1,n} \end{bmatrix} \tag{3.28}$$

where $a_{ij} \neq 0$. Note that the number of elements in a pseudo-triangular structure matrix is exactly equal to the number of constraints. Hence, all elements can be determined uniquely. Alternately, we can also use eq. (3.26) to find $\mathbf{A}_{n+1}^T$ as follows.

If the desired isotropic point is located at a special manipulator posture where the condition number of its Jacobian matrix is equal to one, i.e.,

$$\mathbf{J}^T\mathbf{W}\mathbf{J} = \beta^2\mathbf{I}_n \tag{3.29}$$

where β is an arbitrary constant, then both $\mathbf{R}_1$ and $\mathbf{R}$ are proportional to the identity matrix, and the isotropic transmission structure in eq. (3.26) reduces to

$$\mathbf{A}^T = \beta c_{n+1}\tilde{\mathbf{P}}_{n+1} \tag{3.30}$$

Now consider a general case for which the condition number of its Jacobian matrix $\mathbf{J}$ at the position of interest is not equal to one. Since $\mathbf{R}$ is an $n \times n$ upper-triangular matrix, we conclude from eq. (3.26) that for the matrix $\mathbf{A}^T$ to be in a pseudo-triangular form, $\mathbf{P}_{n+1}$ must also be a pseudo-triangular matrix. Since $\tilde{\mathbf{P}}_{n+1}$ is a pseudo-triangular matrix, we also conclude that for $\mathbf{P}_{n+1}$ to be in a pseudo-triangular form, the rotation matrix $\mathbf{U}$ in eq. (3.15) must be an identity matrix. Hence, eq. (3.26) reduces to

$$\mathbf{A}^T = c_{n+1}\mathbf{R}^T\tilde{\mathbf{P}}_{n+1} \tag{3.31}$$

Since matrix $\mathbf{R}$ is uniquely determined from eq. (3.20), we conclude that eq. (3.31) is the only pseudo-triangular structure matrix which yields an isotropic transmission structure.

3.5 Manipulators with $2n$ Tendons Arranged in a $2n$ Pseudo-Triangular Form

Each column of $\mathbf{A}^T$ represents a power transmission line contributed by a tendon. Since an ITS matrix satisfies eqs. (3.17) and (3.14), corresponding to each transmission line of an ITS matrix $\mathbf{A}_{2n}^T$ there exists an opposing transmission line. That is, the corresponding elements of two opposing transmission lines are equal in magnitude but negative to each other. We call these two opposing transmission lines a "dual transmission line" and the two opposing column vectors a "dual vector". Thus the simplest routing of an ITS with all the actuators

base mounted takes the following form:

$$\mathbf{A}_{2n}^T = \begin{bmatrix} a_1 & -a_1 & 0 & 0 & \cdots & 0 & 0 \\ a_2 & -a_2 & b_2 & -b_2 & \cdots & 0 & 0 \\ \vdots & \vdots & \vdots & \vdots & \vdots & \vdots & \\ a_{n-1} & -a_{n-1} & b_{n-1} & -b_{n-1} & \cdots & 0 & 0 \\ a_n & -a_n & b_n & -b_n & \cdots & e_n & -e_n \end{bmatrix} \tag{3.32}$$

A matrix of this form is called an "$n \times 2n$ pseudo-triangular" matrix. Note that there are $n(n+1)/2$ unknown variables in the matrix of eq. (3.32). When m is equal to $2n$, eqs. (3.10) and (3.17) impose $n(3n+1)/2$ equations of constraint on the elements of $\mathbf{A}_{2n}^T$. A matrix $\mathbf{A}_{2n}^T$ with properly arranged n dual vectors as in eq. (3.32) satisfies the n^2 linear constraint equations imposed by eq. (3.17) automatically. Hence, there are $n(n+1)/2$ quadratic equations in eq. (3.10) left to be satisfied by an ITS matrix. Hence, we can solve eq. (3.10) for the elements of $\mathbf{A}_{2n}^T$ in eq. (3.32). Alternately, we can also find $\mathbf{A}_{2n}^T$ from eq. (3.26).

In general, the $\mathbf{P}_m$ obtained from eq. (3.15) will have non-zero elements distributed in the upper-right and lower-left corners of the matrix, unless $\mathbf{U}$ is an identity matrix. Since the matrix $\mathbf{R}$ in eq. (3.26) is an upper triangular matrix, we conclude that for $\mathbf{A}_{2n}^T$ to be a pseudo-triangular matrix, $\mathbf{U}$ must be an identity matrix and all the elements in the upper triangle of $\mathbf{R}$ must be non-zero. This implies that whether a pseudo-triangular structure matrix can be achieved or not depends on the matrix $\mathbf{R}$, i.e., the choice of the end-effector position. This also implies that the isotropic point can not be located at the position where the condition number of $\mathbf{LJ}$ is equal to one.

3.6 Summary

A general theory for the synthesis of the mechanical power transmission structure in tendon-driven manipulators has been developed. Based on the static force analysis, the conditions for the kinematic structure of a manipulator to possess isotropic transmission characteristics are developed. It is shown that isotropic transmission characteristics can be achieved only if the manipulator is driven by either $n+1$ or $2n$ tendons. This result matches the two existing types of tendon-driven manipulators and helps to explain the oddness of the other types. However, as far as we understand both the Stanford/JPL and the Utah/MIT hands were not designed to have isotropic transmission characteristics. However, the structure matrix of the Utah/MIT hand's finger does satisfy eq. (3.17), but not eq. (3.10).

Chapter 4

Numerical Examples

4.1 Introduction

The theory for designing a manipulator with isotropic transmission characteristics has been investigated in the previous chapter. Based on the theory, only those transmission structures with $n+1$ or $2n$ tendons can possess these characteristics. In this chapter, examples of two manipulators with different transmission structures will be examined to demonstrate the features of isotropic transmission characteristics. The two manipulators considered are: (1) a two-dof planar manipulator and (2) a three-dof spatial manipulator. In each example, transmission structures with $n+1$ tendons are presented first. This is followed by transmission structures with $2n$ tendons. For simplicity, an algorithm that controls the sum of actuator forces to a minimum is applied to all the examples to regulate the vector $\underline{\lambda}$ in eq. (2.7) and to maintain non-negative tensions.

4.2 Example 1: Two-dof Manipulator

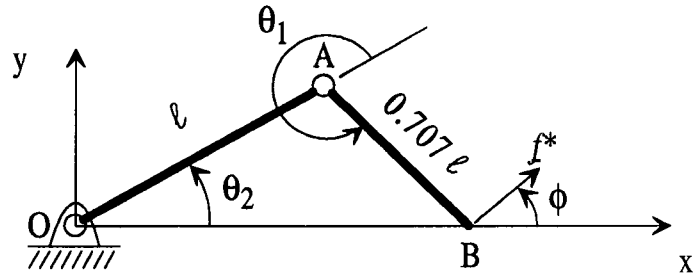

Figure 4.1: A two-dof planar manipulator

A two-dof planar manipulator, with its link lengths proportional to $1/\sqrt{2}:1$ as shown in Fig. 4.1, is selected for the purpose of demonstration. The Jacobian matrix for this manipulator is given by

$$\mathbf{J} = \ell \begin{bmatrix} -S_{12}/\sqrt{2} & -S_2 - S_{12}/\sqrt{2} \\ C_{12}/\sqrt{2} & C_2 + C_{12}/\sqrt{2} \end{bmatrix} \tag{4.1}$$

where $C_2 = Cos(\theta_2), S_2 = Sin(\theta_2), C_{12} = Cos(\theta_1 + \theta_2), S_{12} = Sin(\theta_1 + \theta_2)$ and ℓ is the second link length. In what follows, we let $\ell = 1$ unit for simplicity. Note that the link lengths has been proportioned in such a way that its Jacobian matrix, **J**, has a unity condition number when the manipulator assumes the position for which $\theta_1 = 225°$. Also note that the links and joints are numbered sequentially from the distal end.

4.2.1 Transmission Structures with Three Tendons

Three different 2×3 pseudo-triangular structure matrices shown in Table 4.1 are synthesized for the purposes of comparison. All three structure matrices

Transmission Structure	$\mathbf{A}^T$	κ	$\underline{\xi}_h$	Cond($\mathbf{A}^T$)
(a)	$\kappa \begin{bmatrix} 1 & -1 & 0 \\ \frac{1}{\sqrt{3}} & \frac{1}{\sqrt{3}} & \frac{-2}{\sqrt{3}} \end{bmatrix}$	0.7071	$\begin{bmatrix} 1 \\ 1 \\ 1 \end{bmatrix}$	1
(b)	$\kappa \begin{bmatrix} 1 & -1 & 0 \\ 1 & 1 & -1 \end{bmatrix}$	0.6389	$\begin{bmatrix} 1 \\ 1 \\ 2 \end{bmatrix}$	1.225
(c)	$\kappa \begin{bmatrix} 1 & -1 & 0 \\ 1.264 & 0.264 & -1.528 \end{bmatrix}$	0.6148	$\begin{bmatrix} 1 \\ 1 \\ 1 \end{bmatrix}$	1.668

Table 4.1: Three transmission structures and their kinematic properties

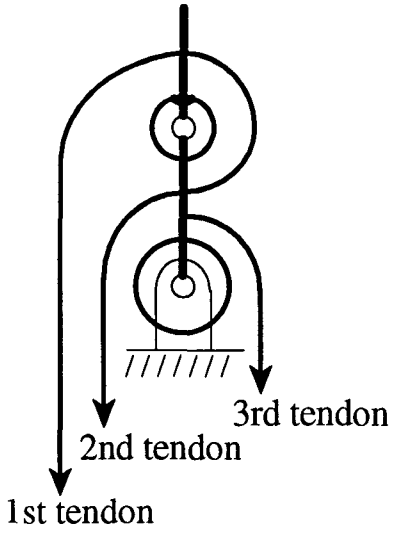

Figure 4.2: Tendon routings of the two-dof manipulator

share the same tendon routing as shown in Fig. 4.2. However, their pulley sizes are different from one another. Structure (a) is a structure matrix derived from eq. (3.11). Hence, structure (a) will possess isotropic transmission characteristics when its end-effector is positioned at x = $\ell/\sqrt{2}$ and y = 0. Structure (b) uses equal size pulleys. It does not possess isotropic transmission characteristics. Structure (c) is calculated from eq. (3.31) based on the condition that the manipulator will possess isotropic transmission characteristics when the end-effector is positioned at the x = ℓ and y = 0. The homogeneous solutions and the condition numbers of the structure matrices, $\mathbf{A}^T$, are also listed in Table 4.1. We note that the null vectors of structures (a) and (c) both point in the isotropic direction.

For these two-dof systems, if we confine the joint torque vector, $\underline{\tau}$, to be bounded on a unit circle, then the particular solution ξ_p lies on an ellipse (Lee, 1991). To achieve a fair comparison, the values of κ in Table 4.1 are chosen so that the areas bounded by the ellipses in the ξ_p-space are all equal to π.

Figure 4.3 shows the variation of condition numbers of $\mathbf{A}^{+T}\mathbf{J}^T$ as functions of the end-effector position. Structure (a) has a unity condition number at the x = $\ell/\sqrt{2}$ and y = 0 ($\theta_1 = 225°$) position. The condition number of structure (b) is fairly close to that of structure (a) due to the fact that the two structure matrices differ from each other by a small amount. Structure (c) has a unity condition number at the x = ℓ and y = 0 ($\theta_1 = 249.3°$) position. Comparing structure (a) with (c), structure (c) seems to be better than structure (a) because the condition number of structure (c) is closer to 1.0 over a greater range of the workspace.

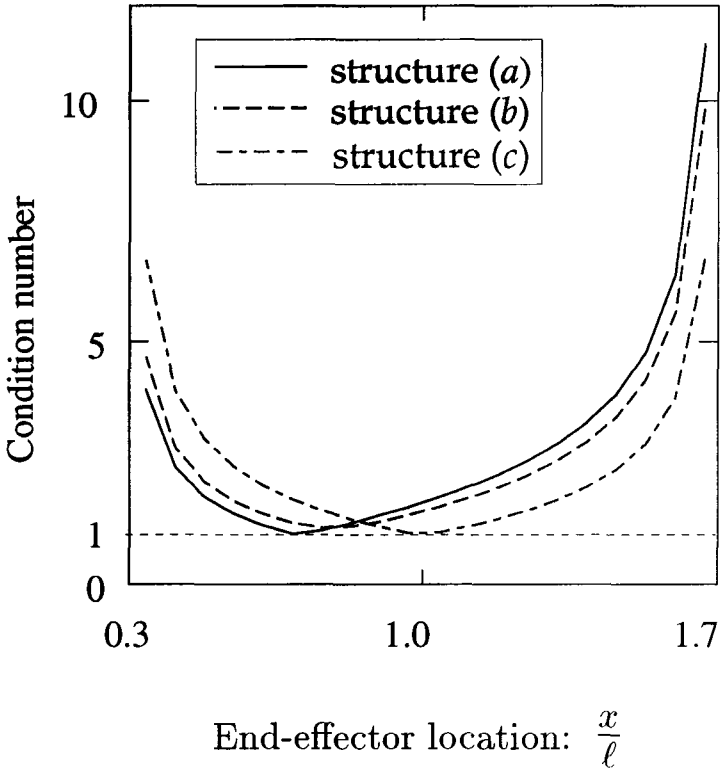

Figure 4.3: Condition number versus end-effector location for three transmission structures

Two manipulator postures are chosen for evaluation. Position 1 is at x = ℓ, y = 0, and position 2 is at x = $\ell/\sqrt{2}$, y = 0. Let a unity force $\underline{f}^*$ (= -$\underline{f}$) be applied to the end-effector as shown in Fig. 4.1. Using eq. (2.16), the required tensions for each structure are calculated for every given direction, ϕ, of the applied force. For the purpose of comparison, we adjust the value of λ in eq. (2.16) such that one of the tendons will have zero tension while the other two have nonnegative tensions. Note that the tendon whose force is set to zero by adding a scalar multiple of the homogeneous solution, must be chosen from the one which corresponds to the largest negative component in the particular solution vector. Otherwise negative tensions may occur in some other tendons. As ϕ varies from 0 to 2π, the locus of each tendon force forms a closed curve.

Figure 4.4 shows the polar plots of the three tendon forces for transmission structures (a), (b), and (c), respectively. In a polar plot, the radial distance represents the magnitude of tendon force while the phase angle represents the direction of the applied force. From Fig. 4.4a-(ii), we note that the shapes of the three tendon forces are identical except for a shift in the phase angle. When the external force is applied along the ϕ = 210°, 330° and 90° directions, only one tendon is under tension. Under these situations, the resultant torques produced by one tendon are sufficient to work against the external force. We call these directions the "solo directions." At any other directions, only one tendon will have zero tension. To calculate the solo directions at a given posture where the Jacobian matrix **J** is invertible, from eqs. (2.2) and (2.6), we have

$$\mathbf{J}^T \underline{f} = \mathbf{A}^T \underline{\xi} \tag{4.2}$$

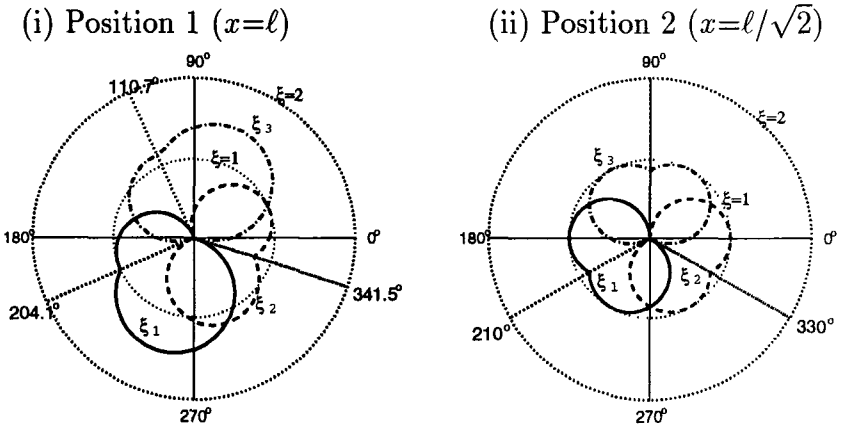

a. Transmission structure (a)

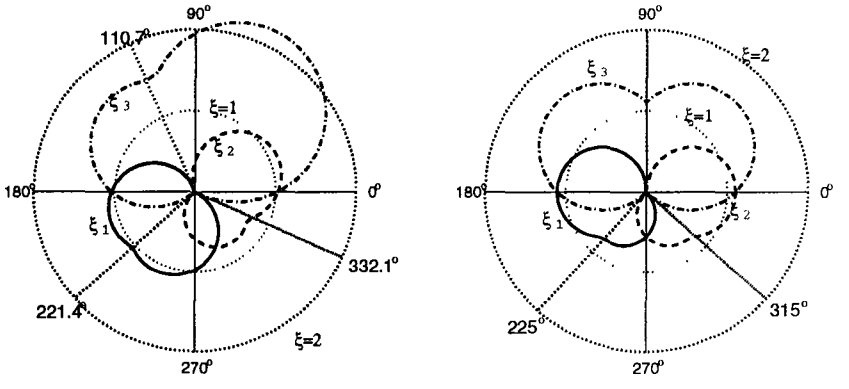

b. Transmission structure (b)

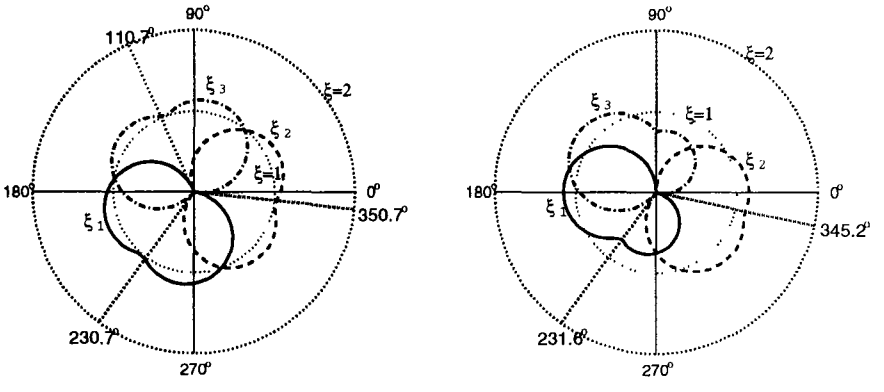

c. Transmission structure (c)

Figure 4.4: Polar plots of tendon forces versus the direction of applied force for structure (a) and (b). The radial distance represents the tendon force and the phase angle represents the direction of applied force

Pre-multiplying $\mathbf{J}^{-T}$ to both sides of eq. (4.2), we obtain

$$\underline{f} = \mathbf{J}^{-T}\mathbf{A}^{T}\underline{\xi} \tag{4.3}$$

Therefore, the solo direction for tendon i ($i = 1, \cdots, m$) can be calculated by substituting $\underline{\xi}_i$ into eq. (4.3), where $\underline{\xi}_i$ is a unit vector along the ith axis of the actuator space.

Since structure (a) possesses isotropic transmission characteristics at the second position, the distribution of tensions becomes distorted as the end-effector moves to position 1 (see Fig. 4.4a-(i)). The corresponding solo directions, as shown in Fig. 4.4a-(i), also change their locations and become unevenly spaced.

Although the condition number of structure (b) is fairly close to that of structure (a), the tension distribution of structure (b) is quite different from that of structure (a) as can be seen in Fig. 4.4b. We note that tension exerted on the third tendon is much larger than that on the other two. This is due to the fact that its null vector, $[1, 1, 2]^T$, points away from the isotropic direction. As shown in Fig. 4.4c-(i), structure (c) has isotropic transmission characteristics at position 1. Again, at the isotropic point, position 1, the solo directions, ϕ=230.7°, 350.7°, and 110.7°, are evenly spaced. Both structures (a) and (c) are equally good in tension distribution. The only difference seems to be that structure (c) has higher tendon forces than that of structure (a). However, this difference can be corrected by adjusting the value of κ, i.e. the pulley sizes.

Table 4.2 lists the maximum value of each tendon force plotted in Fig. 4.4 and their ratios. The corresponding condition numbers of $\mathbf{A}^{+T}\mathbf{J}^{T}$ for the manipulator at the two specified positions are also listed. It can be seen that structure (c)

Structure		(a)	(b)	(c)
position 1	max. tensions	$\begin{bmatrix} 1.478 \\ 1.148 \\ 1.478 \end{bmatrix}$	$\begin{bmatrix} 1.107 \\ 1.107 \\ 2.213 \end{bmatrix}$	$\begin{bmatrix} 1.15 \\ 1.15 \\ 1.15 \end{bmatrix}$
	ratio	1.287:1:1.287	1:1:2	1:1:1
	solo directions ϕ (deg)	$\begin{bmatrix} 204.1 \\ 341.5 \\ 110.7 \end{bmatrix}$	$\begin{bmatrix} 221.4 \\ 332.1 \\ 110.7 \end{bmatrix}$	$\begin{bmatrix} 230.7 \\ 350.7 \\ 110.7 \end{bmatrix}$
	Cond($\mathbf{A}^{+T}\mathbf{J}^T$)	1.668	1.488	1
position 2	max. tensions	$\begin{bmatrix} 1 \\ 1 \\ 1 \end{bmatrix}$	$\begin{bmatrix} 1.107 \\ 1.107 \\ 1.565 \end{bmatrix}$	$\begin{bmatrix} 1.15 \\ 1.213 \\ 1.213 \end{bmatrix}$
	ratio	1:1:1	1:1:1.414	1:1.055:1.055
	solo directions ϕ (deg)	$\begin{bmatrix} 210 \\ 330 \\ 90 \end{bmatrix}$	$\begin{bmatrix} 225 \\ 315 \\ 90 \end{bmatrix}$	$\begin{bmatrix} 231.6 \\ 345.2 \\ 90 \end{bmatrix}$
	Cond($\mathbf{A}^{+T}\mathbf{J}^T$)	1	1.225	1.668

Table 4.2: Maximum tensions, their ratios, solo directions and the condition numbers of the three structures

has the best distribution of tensions. It has a nearly $1:1:1$ maximum tendon force ratio between positions 1 and 2. It can be concluded that the selection of the isotropic position can have great influence on the tendon force ratios, and that careful consideration should be given to the selection of this position.

Transmission Structure	$\mathbf{A}^T$	κ	$\mathbf{H}$	$\text{Cond}(\mathbf{A}^T)$
(a)	$\kappa \begin{bmatrix} 1 & -1 & 0 & 0 \\ 1 & -1 & 1 & -1 \end{bmatrix}$	0.7071	$\begin{bmatrix} 1 & 0 \\ 1 & 0 \\ 0 & 1 \\ 0 & 1 \end{bmatrix}$	2.6180
(b)	$\kappa \begin{bmatrix} 1 & -1 & 0 & 0 \\ 0.5 & -0.5 & 1.33 & -1.33 \end{bmatrix}$	0.8695	$\begin{bmatrix} 1 & 0 \\ 1 & 0 \\ 0 & 1 \\ 0 & 1 \end{bmatrix}$	1.6685

Table 4.3: Two transmission structures and their kinematic properties for the two-dof manipulator shown in Fig. 4.1

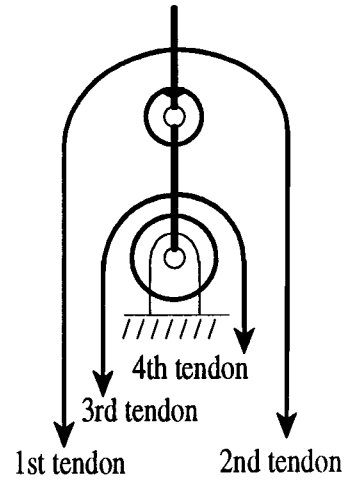

Figure 4.5: Tendon routings for the two-dof manipulator shown in Fig. 4.1

4.2.2 Transmission Structures with Four Tendons

Two different 2×4 pseudo-triangular structure matrices shown in Table 4.3 are synthesized and compared. Both two structures share the same tendon routing shown in Fig. 4.5, where each positive joint axis points out of the paper. However, their pulley sizes are different from each other. Structure (b) is a structure matrix derived from eq. (3.26) based on the condition that the manipulator will possess isotropic transmission characteristics when the end-effector is positioned at the x=ℓ, y=0. Structure (a) uses equal size pulleys. It does not possess isotropic transmission characteristics when the end-effector is positioned at the same point. The homogeneous solutions and the condition numbers of the structure matrix, $\mathbf{A}^T$, are also listed in Table 4.3. The null spaces of both structures are the same. To achieve a fair comparison, the values of κ in Table 4.3 are chosen so that the product of the two singular values of each $\mathbf{A}^T$ is equal to one.

Figure 4.6 shows the variation of the condition number of $\mathbf{A}^{+T}\mathbf{J}^T$ as a function of the end-effector position. We note that the condition number of the Jacobian matrix is equal to one at x=$\ell/\sqrt{2}$, and y=0 for both cases. The condition number of $\mathbf{A}^{+T}\mathbf{J}^T$ for case (a) is not equal to one within the entire workspace, while the condition number of $\mathbf{A}^{+T}\mathbf{J}^T$ for case (b) is equal to one at the x=ℓ, y=0 position. Comparing structure (a) with (b), structure (b) is better than structure (a) because the condition number of structure (b) is closer to 1.0 over a larger range of the workspace.

The same two manipulator postures are chosen for evaluation. Position 1 is at x=ℓ and y=0; and position 2 is at x=$\ell/\sqrt{2}$ and y=0. Similar to the example

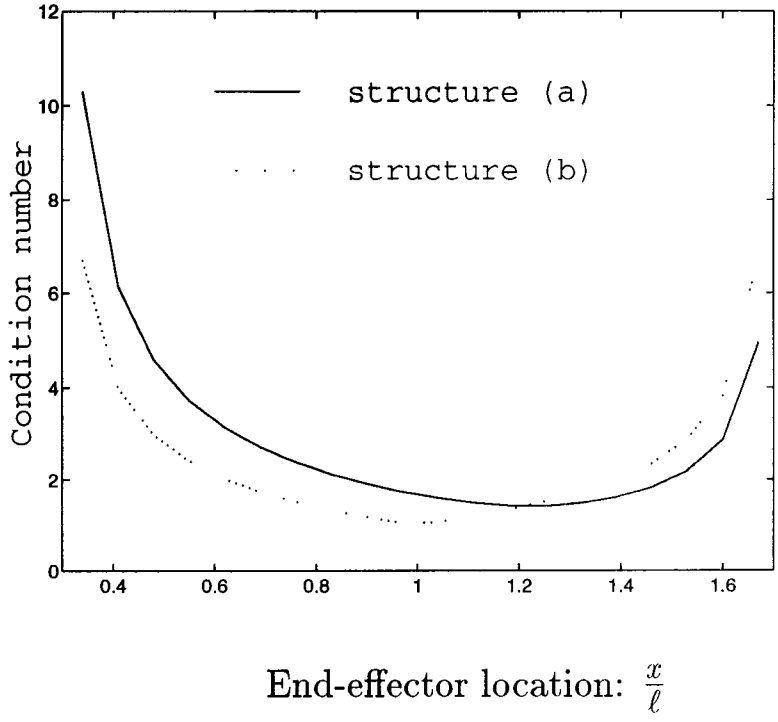

Figure 4.6: Condition number of $\mathbf{A}^{+T}\mathbf{J}^T$ versus end-effector location for two transmission structures

with three tendons, let a unity force $\underline{f}^*$ (=-$\underline{f}$) be applied to the end-effector as shown in Fig. 4.1, where ϕ represents the direction of the applied force. Using eq. (2.7), the required tensions for each structure are calculated for every given direction, ϕ, of the applied force. As ϕ varies from 0 to 2π, the locus of each tendon force forms a closed curve in a polar plot.

Figure 4.7 shows the polar plots of the four tendon forces for both transmission structures evaluated at these two positions. When the external force is applied along a solo direction, only one tendon is sufficient to work against the external force. At other directions two tendons are needed to work against the external force.

Both structure matrices (a) and (b) contain two pairs of dual vectors. Therefore, their tendon force plots contain two pairs of opposing solo directions. Furthermore, each tendon force has nonzero values over exactly a 180° range. Since tendons 3 and 4 of both structures are routed only through the base pulleys, the corresponding solo directions occur when the applied force is parallel to the line AB shown in Fig. 4.1. Due to equal size pulleys in structure (a), the corresponding solo directions of tendons 1 and 2 of structure (a) occur when the applied force is parallel to the line OA shown in Fig. 4.1. Also since the matrix **J** at position 2 is equal to a scaled identity matrix, from eq. (4.3), each column vector of the structure matrix $\mathbf{A}^T$ defines one solo direction.

From Fig. 4.7b-(i), we note that the shapes of the four tendon forces are identical to one another except for a shift in the phase angle. The two dual solo directions are perpendicular to each other. Since structure (b) is designed

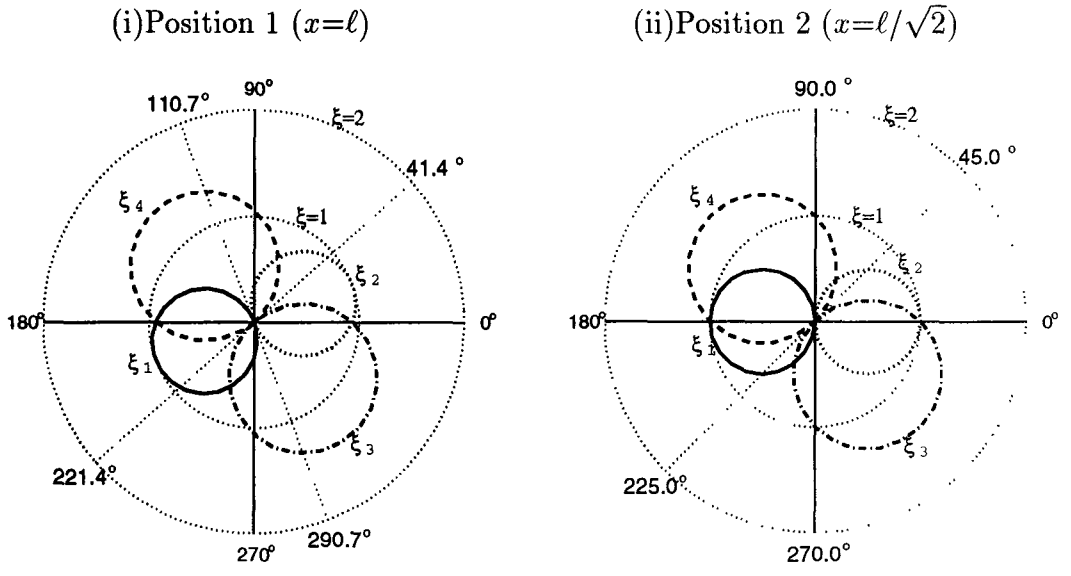

a. Transmission structure (a)

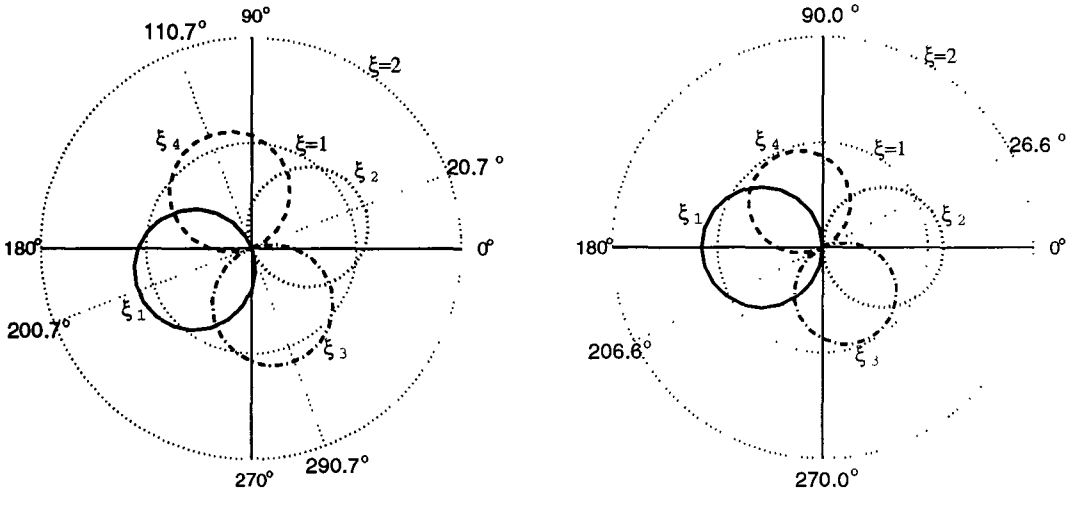

b. Transmission structure (b)

Figure 4.7: Polar plot of tendon forces versus the direction of applied force where the radial distance represents the tendon force and the phase angle represents the direction of applied force

to possess isotropic transmission characteristics at position 1, the distribution of tensions becomes distorted as the end-effector moves to position 2, as shown in Fig. 4.7b-(ii). The corresponding solo directions shown in Fig. 4.7b-(ii) also change their locations and become unevenly spaced.

Structure		(a)	(b)
position 1	max. tensions	$\begin{bmatrix} 1 \\ 1 \\ 1.414 \\ 1.414 \end{bmatrix}$	$\begin{bmatrix} 1.150 \\ 1.150 \\ 1.150 \\ 1.150 \end{bmatrix}$
	ratio	1 : 1 : 1.4 : 1.4	1 : 1 : 1 : 1 : 1
	solo directions ϕ (deg)	$\begin{bmatrix} 221.4 \\ 41.4 \\ 290.7 \\ 110.7 \end{bmatrix}$	$\begin{bmatrix} 200.7 \\ 20.7 \\ 290.7 \\ 110.7 \end{bmatrix}$
	Cond($\mathbf{A}^{+T}\mathbf{J}^T$)	1.6684	1
position 2	max. tensions	$\begin{bmatrix} 1 \\ 1 \\ 1.414 \\ 1.414 \end{bmatrix}$	$\begin{bmatrix} 1.150 \\ 1.150 \\ 0.972 \\ 0.972 \end{bmatrix}$
	ratio	1 : 1 : 1.4 : 1.4	1.2 : 1.2 : 1 : 1
	solo directions ϕ (deg)	$\begin{bmatrix} 225 \\ 45 \\ 270 \\ 90 \end{bmatrix}$	$\begin{bmatrix} 206.6 \\ 26.6 \\ 270 \\ 90 \end{bmatrix}$
	Cond($\mathbf{A}^{+T}\mathbf{J}^T$)	2.6180	1.6685

Table 4.4: List of maximum tensions, their ratios, solo directions and the condition numbers for structures (a) and (b), each at two positions

Table 4.4 lists the maximum value of each tendon force plotted in Fig. 4.7 and their ratios. The corresponding solo directions and condition numbers of $\mathbf{A}^{+T}\mathbf{J}^T$ are also listed. It can be seen that structure (b) has better distribution

of tensions. It has a nearly 1 : 1 : 1 : 1 maximum tendon force ratios between positions 1 and 2.

4.3 Example 2: Three-dof Manipulator

A two-dof planar manipulator was investigated in the previous section. In this section, we explore a three-dof spatial manipulator with different transmission structures.

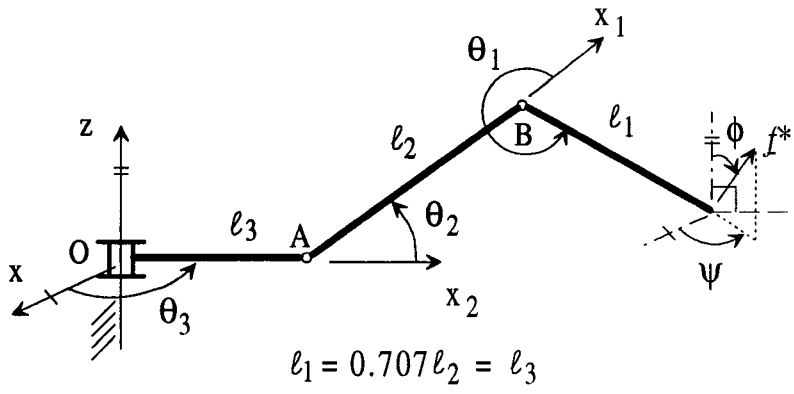

Figure 4.8: Link proportions of the three-dof manipulator

The spatial three-dof manipulator shown in Fig. 4.8 is used to compare the effect of different transmission structures. The joint axes are arranged such that, starting from the distal joint (first joint), the second joint axis is parallel to the first while the third is perpendicular to the second. The link lengths are proportional to $1/\sqrt{2} : 1 : 1/\sqrt{2}$. A unity force acting on the end-effector is assumed, and as shown in Fig. 4.8 ϕ is the angle the external force makes with the z-axis and ψ is the angle the projected vector of the external force in x-y

plane makes with the x-axis. The unity force can be expressed as

$$\underline{f}^* = [sin(\phi)cos(\psi), sin(\phi)sin(\psi), cos(\phi)]^T \tag{4.4}$$

where ϕ varies from 0 to π and ψ varies from 0 to 2π. Without loosing generality, we let $\theta_3 = 90°$ and the Jacobian matrix for the manipulator shown in Fig. 4.8 is given by

$$\mathbf{J} = \ell \begin{bmatrix} 0 & 0 & -(C_2 + (1 + C_{12})/\sqrt{2}) \\ -S_{12}/\sqrt{2} & -S_2 - S_{12}/\sqrt{2} & 0 \\ C_{12}/\sqrt{2} & C_2 + C_{12}/\sqrt{2} & 0 \end{bmatrix} \tag{4.5}$$

where $C_2 = Cos(\theta_2), S_2 = Sin(\theta_2), C_{12} = Cos(\theta_1 + \theta_2), S_{12} = Sin(\theta_1 + \theta_2)$, and ℓ is the length of the second link. In what follows, we let $\ell = 1$ for simplicity. For this manipulator, it can be shown that the condition number of the Jacobian matrix is equal to one when θ_1=135° and θ_2=45°, and that when $x = 0, y = z = 1/\sqrt{2}$, we have one such point on the locus.

4.3.1 Transmission Structures with Four Tendons

To compare the influence of different pulley sizes, the same tendon routing shown in Fig. 4.9 is adapted. Table 4.5 lists two different transmission structures, their corresponding homogeneous solutions, and the condition number of $\mathbf{A}^T$. Structure (a) has its null vector pointed 31.4° away from the isotropic direction. Structure (b) has its null vector pointed in the isotropic direction. Structure (a) is designed with equal size pulleys while structure (b) is a transmission structure derived from eq. (3.11). Similar to that of two-dof manipulator, with $\underline{\tau}$ bounded on a unit sphere, the values of κ in Table 4.5 are calculated by equating the

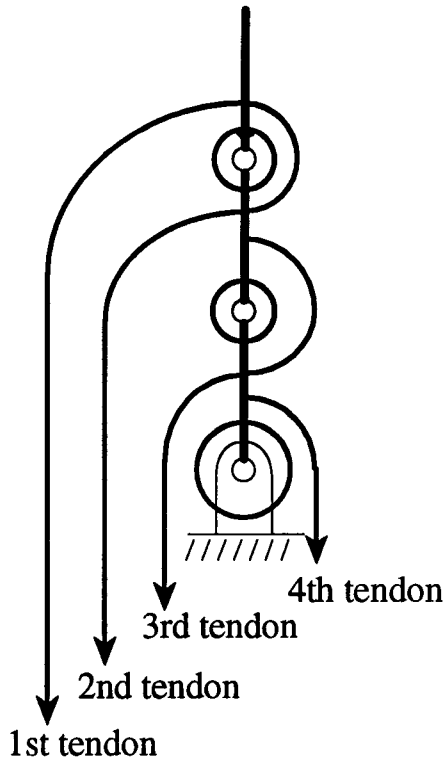

Figure 4.9: Tendon routings of the three-dof manipulator

Transmission Structure	$\mathbf{A}^T$	κ	$\underline{\xi}_h$	Cond($\mathbf{A}^T$)
(a)	$\kappa \begin{bmatrix} 1 & -1 & 0 & 0 \\ 1 & 1 & -1 & 0 \\ 1 & 1 & 1 & -1 \end{bmatrix}$	0.5974	$\begin{bmatrix} 1 \\ 1 \\ 2 \\ 4 \end{bmatrix}$	1.520
(b)	$\kappa \begin{bmatrix} 1 & -1 & 0 & 0 \\ \frac{1}{\sqrt{3}} & \frac{1}{\sqrt{3}} & \frac{-2}{\sqrt{3}} & 0 \\ \frac{1}{\sqrt{6}} & \frac{1}{\sqrt{6}} & \frac{1}{\sqrt{6}} & \frac{-2}{\sqrt{6}} \end{bmatrix}$	0.7071	$\begin{bmatrix} 1 \\ 1 \\ 1 \\ 1 \end{bmatrix}$	1

Table 4.5: Two transmission structures and their kinematic properties

volume enclosed by $\underline{\xi}_p$ in the particular solution space to $4\pi/3$. Two positions are chosen for evaluation. At position 1: x = 0, y = z = $\ell/\sqrt{2}$; and at position 2: x = 0, y = $\ell + \ell/\sqrt{2}$, z = 0. As the applied force, $\underline{f}^*$, varies its direction, the tension experienced by each tendon varies accordingly.

Figures 4.10 shows the spherical plots of the tensions for structure (a) when the end-effector is located at position 1. In a spherical plot, the radial distance represents the tension, and the direction represents the direction of the applied force. The dotted line in each tendon force plot indicates the corresponding solo direction. Note that these four figures are different from one another since structure (a) doesn't possess isotropic transmission characteristics. Figure 4.11 shows the spherical plots of the tensions in tendons 1, 2, 3, and 4, respectively, for structure (b) with the end-effector located at position 1. Since position 1 is an isotropic point for structure (b), the four plots are identical in shape with one another except for a shift in orientation, i.e., Figs. 4.11b through 4.11d will look like Fig. 4.11a when they are viewed from some appropriate angle. The solo directions for the four tendons are evenly distributed, and are given by (ϕ= 144.7°, ψ= 54.7°), (ϕ= 35.3°, ψ= 54.7°), (ϕ= 90°, ψ= 289.5°), and (ϕ= 90°, ψ= 180°), respectively. The separation angle between every two solo directions is 109.5°. Figures 4.12 and 4.13 are the spherical plots of the tensions for structures (a) and (b), respectively, when the end-effector is located at position 2. Table 4.6 lists the maximum tensions, their ratios, solo directions and the condition numbers of $\mathbf{A}^{+T}\mathbf{J}^T$ of the manipulator at the two specified positions.

The overall condition number depends on the linkage structure and the transmission structure of a manipulator. It is strongly position dependent. Yet, it can

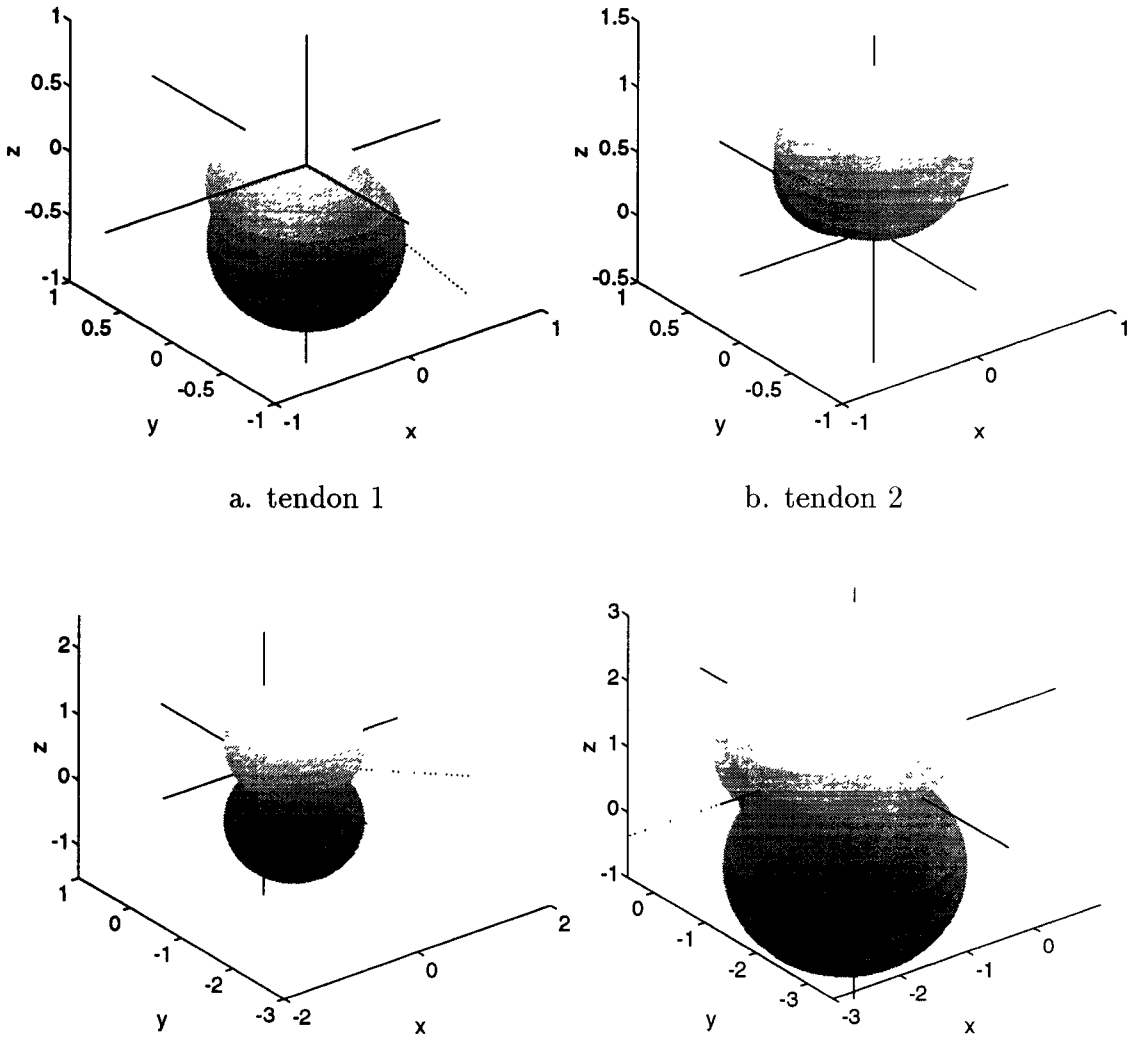

a. tendon 1

b. tendon 2

c. tendon 3

d. tendon 4

Figure 4.10: Spherical plots of tendon force versus direction of applied force for structure (a) evaluated at position 1. The radial distance represents the tendon force and the phase angle represents the direction of applied force.

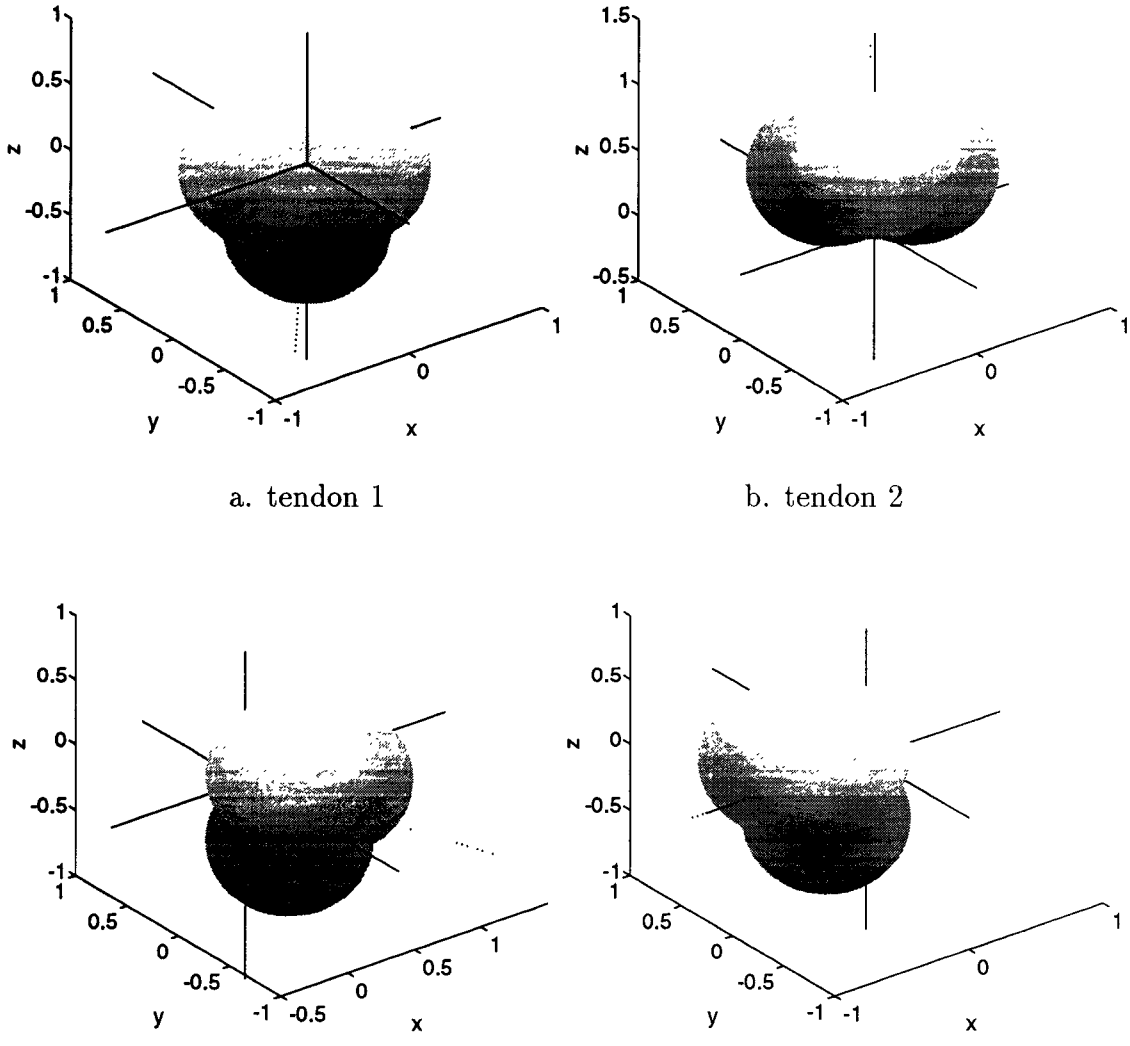

a. tendon 1

b. tendon 2

c. tendon 3

d. tendon 4

Figure 4.11: Spherical plots of tendon force versus direction of applied force for structure (*b*) evaluated at position 1. The radial distance represents the tendon force and the phase angle represents the direction of applied force.

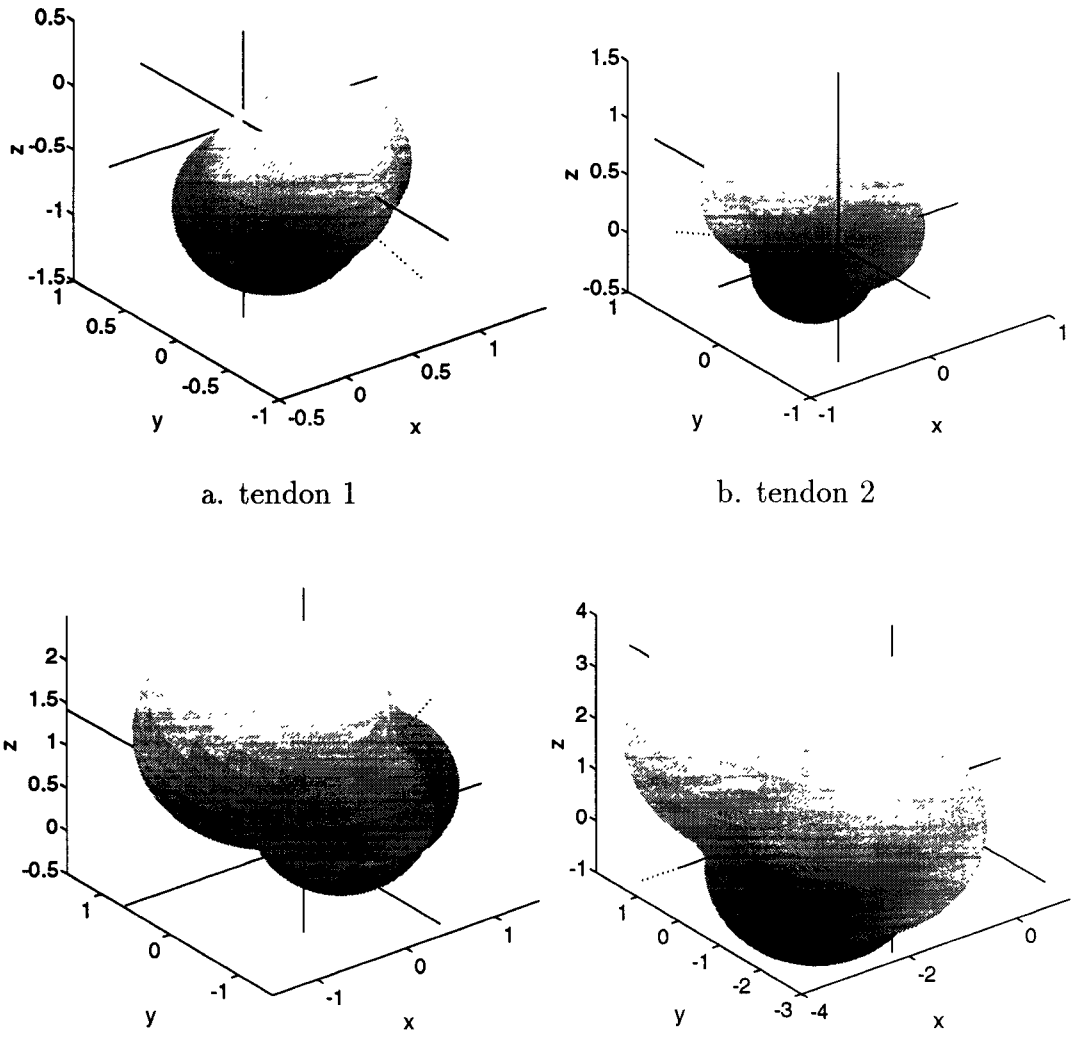

a. tendon 1

b. tendon 2

c. tendon 3

d. tendon 4

Figure 4.12: Spherical plots of tendon force versus direction of applied force for structure (a) evaluated at position 2. The radial distance represents the tendon force and the phase angle represents the direction of applied force.

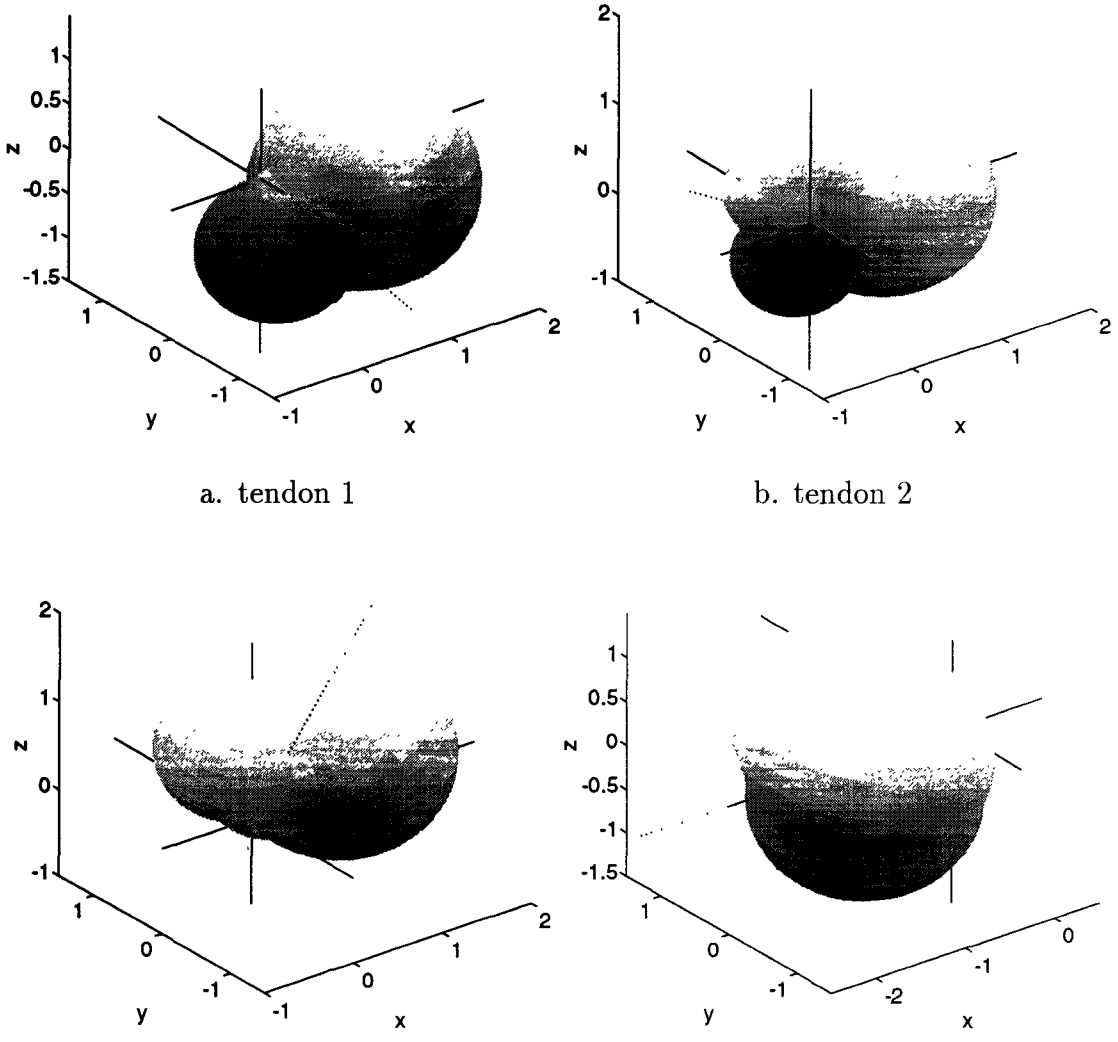

Figure 4.13: Spherical plots of tendon force versus direction of applied force for structure (b) evaluated at position 2. The radial distance represents the tendon force and the phase angle represents the direction of applied force.

Structure		(a)	(b)
position 1	max. tensions	$\begin{bmatrix} 1.184 \\ 1.184 \\ 1.674 \\ 2.899 \end{bmatrix}$	$\begin{bmatrix} 1 \\ 1 \\ 1 \\ 1 \end{bmatrix}$
	ratio	1:1:1.414:2.449	1:1:1:1
	solo angles ϕ, ψ (deg)	$\begin{bmatrix} 125.3 & 45 \\ 54.7 & 45 \\ 90 & 315 \\ 90 & 180 \end{bmatrix}$	$\begin{bmatrix} 144.7 & 54.7 \\ 35.3 & 54.7 \\ 90 & 289.5 \\ 90 & 180 \end{bmatrix}$
	Cond($\mathbf{A}^{+T}\mathbf{J}^T$)	1.520	1
position 2	max. tensions	$\begin{bmatrix} 1.184 \\ 1.184 \\ 2.367 \\ 4.402 \end{bmatrix}$	$\begin{bmatrix} 2.109 \\ 2.039 \\ 2.134 \\ 2.134 \end{bmatrix}$
	ratio	1:1:2:3.719	1.034:1:1.046:1.046
	solo angles ϕ, ψ (deg)	$\begin{bmatrix} 128.1 & 297.3 \\ 116.8 & 72.8 \\ 34.9 & 327.2 \\ 90 & 180 \end{bmatrix}$	$\begin{bmatrix} 113.7 & 280.5 \\ 108.3 & 82.1 \\ 23.3 & 298.7 \\ 90 & 180 \end{bmatrix}$
	Cond($\mathbf{A}^{+T}\mathbf{J}^T$)	2.173	2.711

Table 4.6: Maximum tensions, their ratios and the condition numbers of the three-dof manipulator

be seen from Table 4.6 that, even the condition number of structure (b) is worse than that of structure (a) at position 2, structure (b) still has better maximum tension ratios than that of structure (a), 1.034 : 1 : 1.046 : 1.046 compared with 1 : 1 : 2 : 3.719. Also, the largest maximum tension in structure (b) is far less than that of structure (a). This is because the null vector of structure (b) points in the isotropic direction while that of structure (a) points in the $[1,1,2,4]^T$ direction.

4.3.2 Transmission Structures with Six Tendons

The upper-triangular matrix **R** from the QR factorization of the Jacobian matrix in eq. (4.5) contains zero elements in its upper-triangle. Therefore an isotropic transmission structure matrix of the pseudo-triangular form is infeasible. In what follows, we seek a non-pseudo-triangular form of the tendon routing.

Table 4.7 lists two different structure matrices, their corresponding homogeneous solutions, and the condition numbers of $\mathbf{A}^T$. Structure (a) is designed with equal size pulleys. Structure (b) is a transmission structure derived from eq. (3.15) using the following rotation matrix:

$$\mathbf{U} = \begin{bmatrix} 1 & 0 & 0 \\ 0 & Cos(\frac{3\pi}{4}) & Sin(\frac{3\pi}{4}) \\ 0 & -Sin(\frac{3\pi}{4}) & Cos(\frac{3\pi}{4}) \end{bmatrix} \begin{bmatrix} Cos(\frac{-\pi}{4}) & Sin(\frac{-\pi}{4}) & 0 \\ -Sin(\frac{-\pi}{4}) & Cos(\frac{-\pi}{4}) & 0 \\ 0 & 0 & 1 \end{bmatrix} \tag{4.6}$$

The designated isotropic point for structure (b) occurs at the position x=0, y=z=$\ell/\sqrt{2}$, where the condition number of the Jacobian matrix is equal to one.

The routings of structures (a) and (b) are shown in Figs. 4.14 and 4.15,

Transmission Structure	$\mathbf{A}^T$	κ	$\mathbf{H}$	Cond($\mathbf{A}^T$)
(a)	$\kappa \begin{bmatrix} 1 & -1 & 0 & 0 & 0 & 0 \\ 1 & -1 & 1 & -1 & 0 & 0 \\ 1 & -1 & 1 & -1 & 1 & -1 \end{bmatrix}$	0.7071	$\begin{bmatrix} 1 & 0 & 0 \\ 1 & 0 & 0 \\ 0 & 1 & 0 \\ 0 & 1 & 0 \\ 0 & 0 & 1 \\ 0 & 0 & 1 \end{bmatrix}$	4.0489
(b)	$\kappa \begin{bmatrix} 1 & -1 & 1 & -1 & 0 & 0 \\ \frac{1}{\sqrt{2}} & \frac{-1}{\sqrt{2}} & \frac{-1}{\sqrt{2}} & \frac{1}{\sqrt{2}} & 1 & -1 \\ \frac{1}{\sqrt{2}} & \frac{-1}{\sqrt{2}} & \frac{-1}{\sqrt{2}} & \frac{1}{\sqrt{2}} & -1 & 1 \end{bmatrix}$	0.500	$\begin{bmatrix} 1 & 0 & 0 \\ 1 & 0 & 0 \\ 0 & 1 & 0 \\ 0 & 1 & 0 \\ 0 & 0 & 1 \\ 0 & 0 & 1 \end{bmatrix}$	1

Table 4.7: Two transmission structures and their kinematic properties for the three-dof manipulator shown in Fig. 4.8

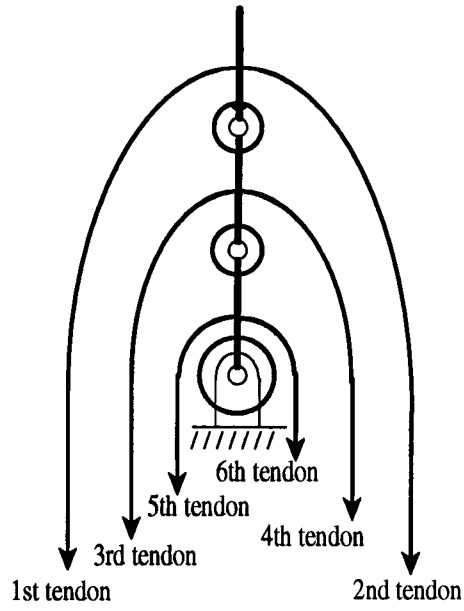

Figure 4.14: Tendon routings for transmission structure (a) shown in Table 4.7

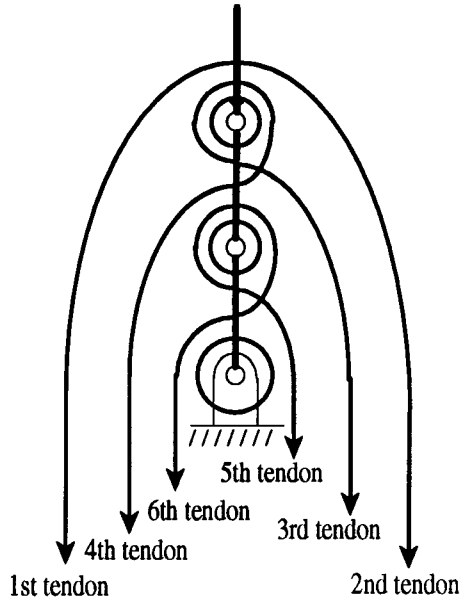

Figure 4.15: Tendon routings for transmission structure (b) shown in Table 4.7

respectively, where each positive joint axis points out of the paper. Similar to the example of a two-dof manipulator with four tendons, the values of κ shown in Table 4.7 are calculated so that the product of the three singular values of each $\mathbf{A}^T$ is equal to one. The same two positions are chosen for evaluation. At position 1 x=0, y=z=$\ell/\sqrt{2}$, and at position 2 x=0, y=$\ell+\ell/\sqrt{2}$, z=0.

Figures 4.16 and 4.17 are the spherical plots of the six tendon forces for transmission structures (a) and (b) evaluated at position 1, respectively. Since both structures (a) and (b) contain three pairs of dual vectors, there are three pairs of solo directions. Hence, each tendon force has zero value over one half of the end-effector space. Also tendons 5 and 6 of the transmission structure (a) are routed only through the base pulleys, and the corresponding solo directions are always perpendicular to the plane of the manipulator. Since the condition number of the Jacobian matrix at position 1 is equal to one, each solo direction at position 1 is pointing along one column vector of the corresponding transmission structure matrix $\mathbf{A}^T$. At position 1, the angle between any two solo directions of structure (b) is either 90° or 180°, whereas that of structure (a) is irregular. Since position 1 is an isotropic point for structure (b), the six tendon force plots in Fig. 4.17 are identical in shape with one another, whereas the tendon force plots in Fig. 4.16 contain shapes with different sizes. Figures 4.18 and 4.19 are the spherical plots of the six tendon forces for the transmission structures evaluated at position 2. Note that there are at most three tendons under tension at all times for both cases and both positions. This is because of the particular tendon routings chosen for the design, which results in a decoupled form of the null matrix $\mathbf{H}$ shown in Table 4.7.

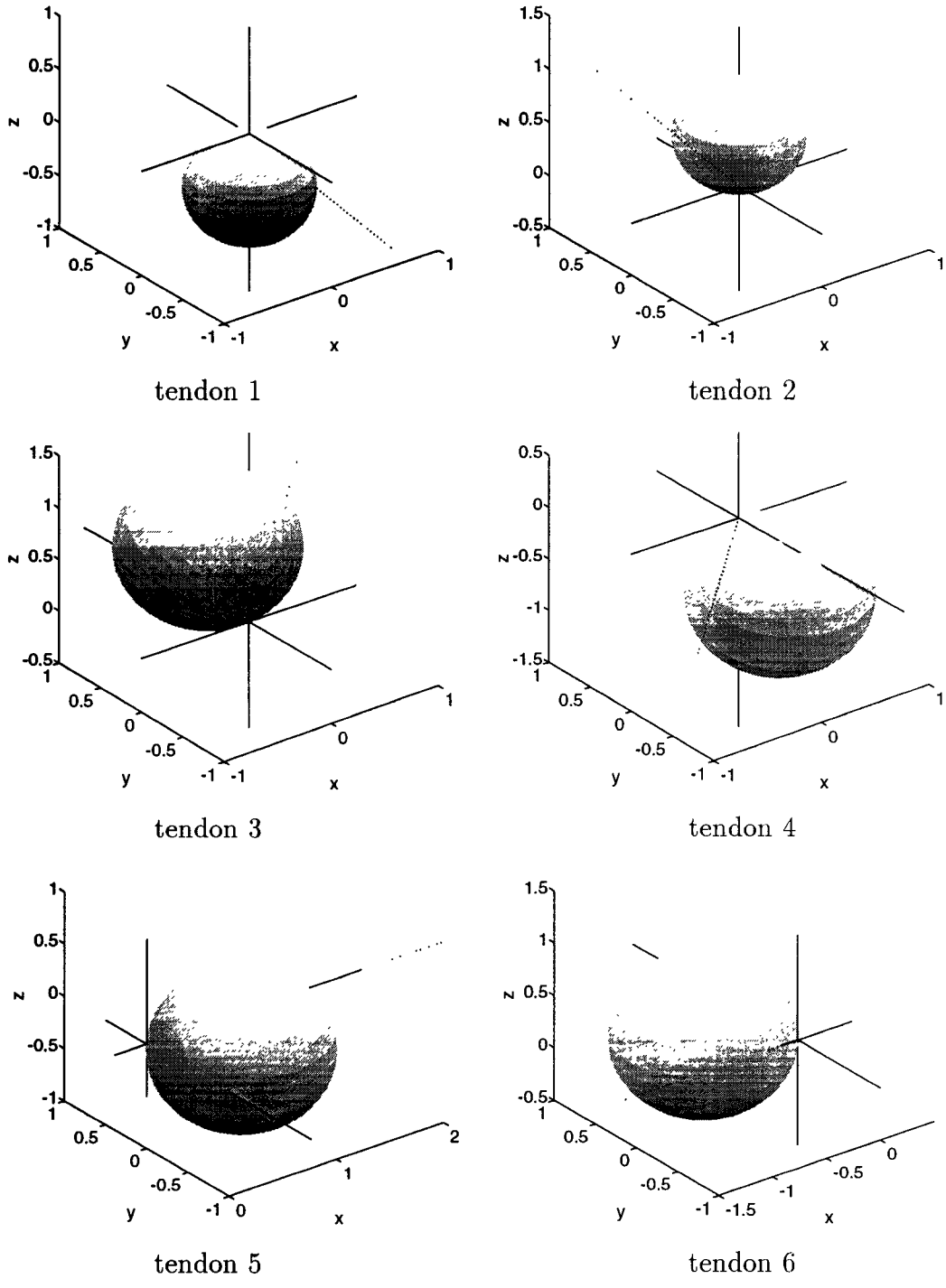

Figure 4.16: Spherical plots of the six tendon forces versus direction of applied force for structure (a) evaluated at position 1. The radial distance represents the tendon force and the phase angle represents the direction of applied force.

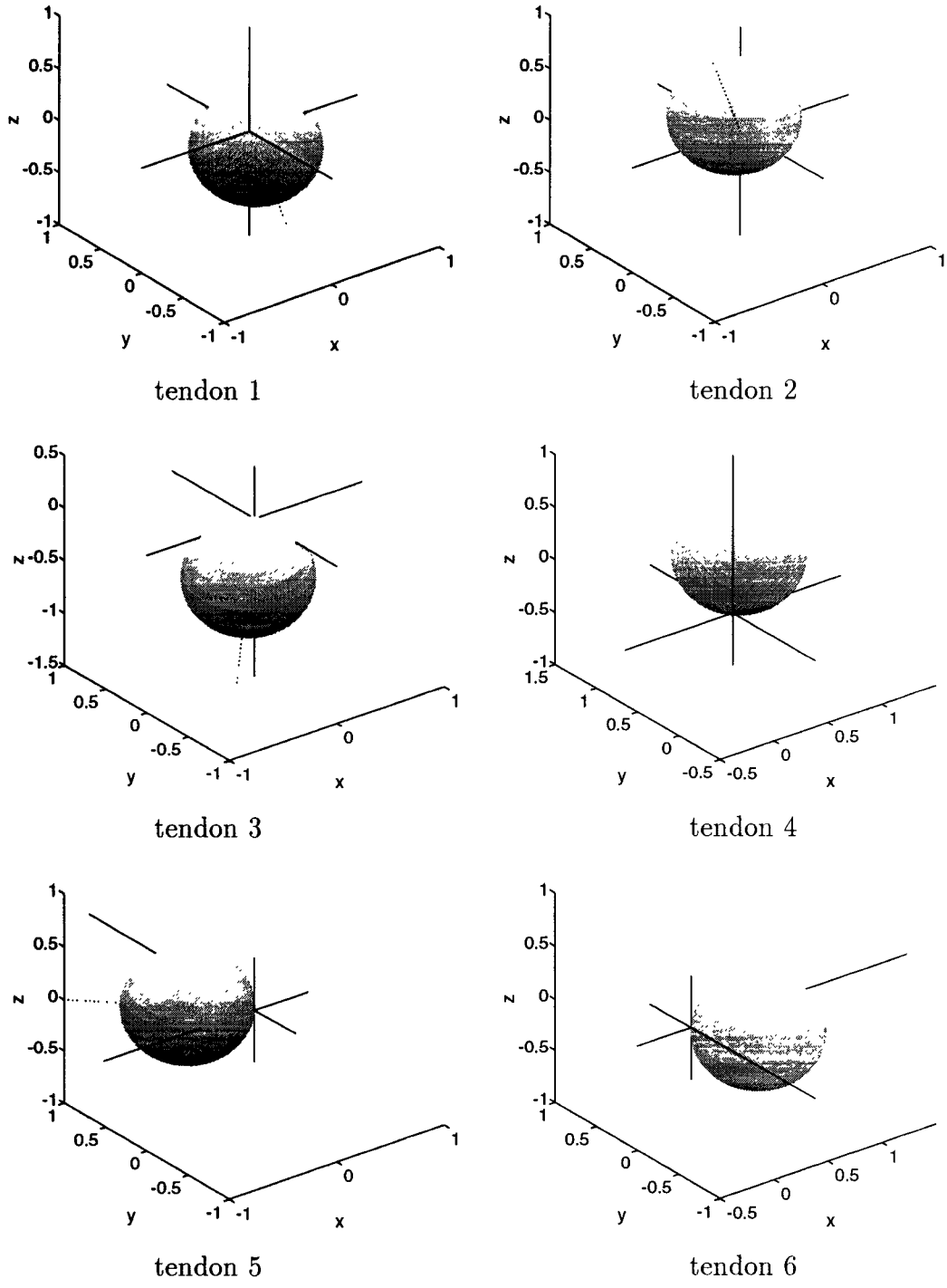

Figure 4.17: Spherical plots of the six tendon force versus direction of applied force for structure (b) evaluated at position 1. The radial distance represents the tendon force and the phase angle represents the direction of applied force.

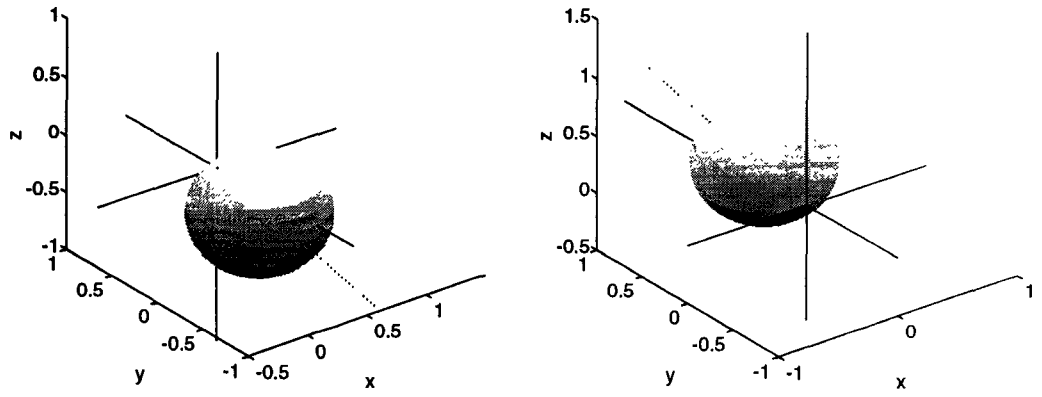

tendon 1

tendon 2

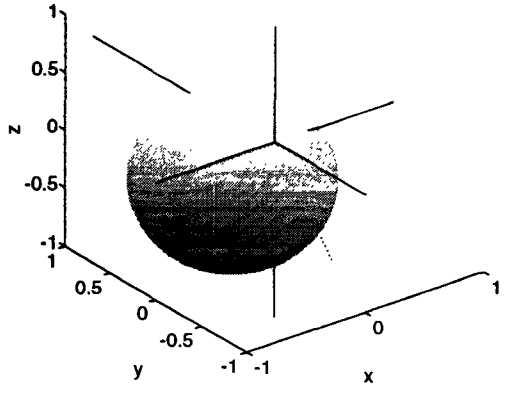

tendon 3

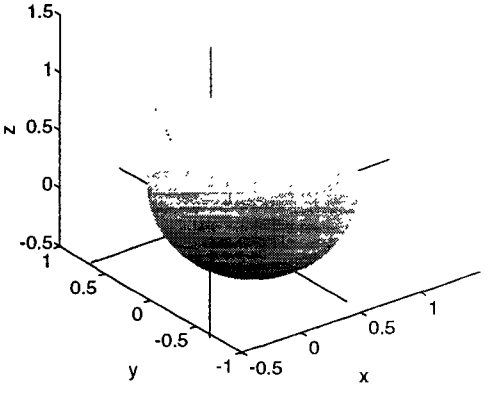

tendon 4

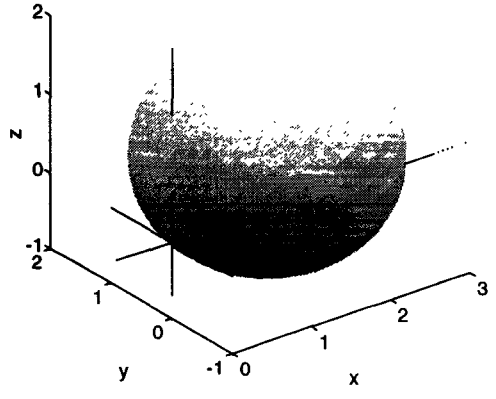

tendon 5

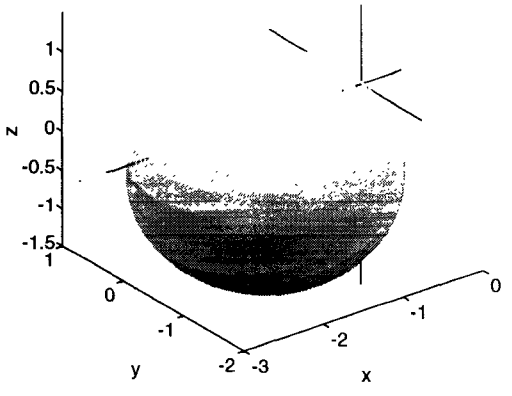

tendon 6

Figure 4.18: Spherical plots of the six tendon forces versus direction of applied force for structure (a) evaluated at position 2. The radial distance represents the tendon force and the phase angle represents the direction of applied force.

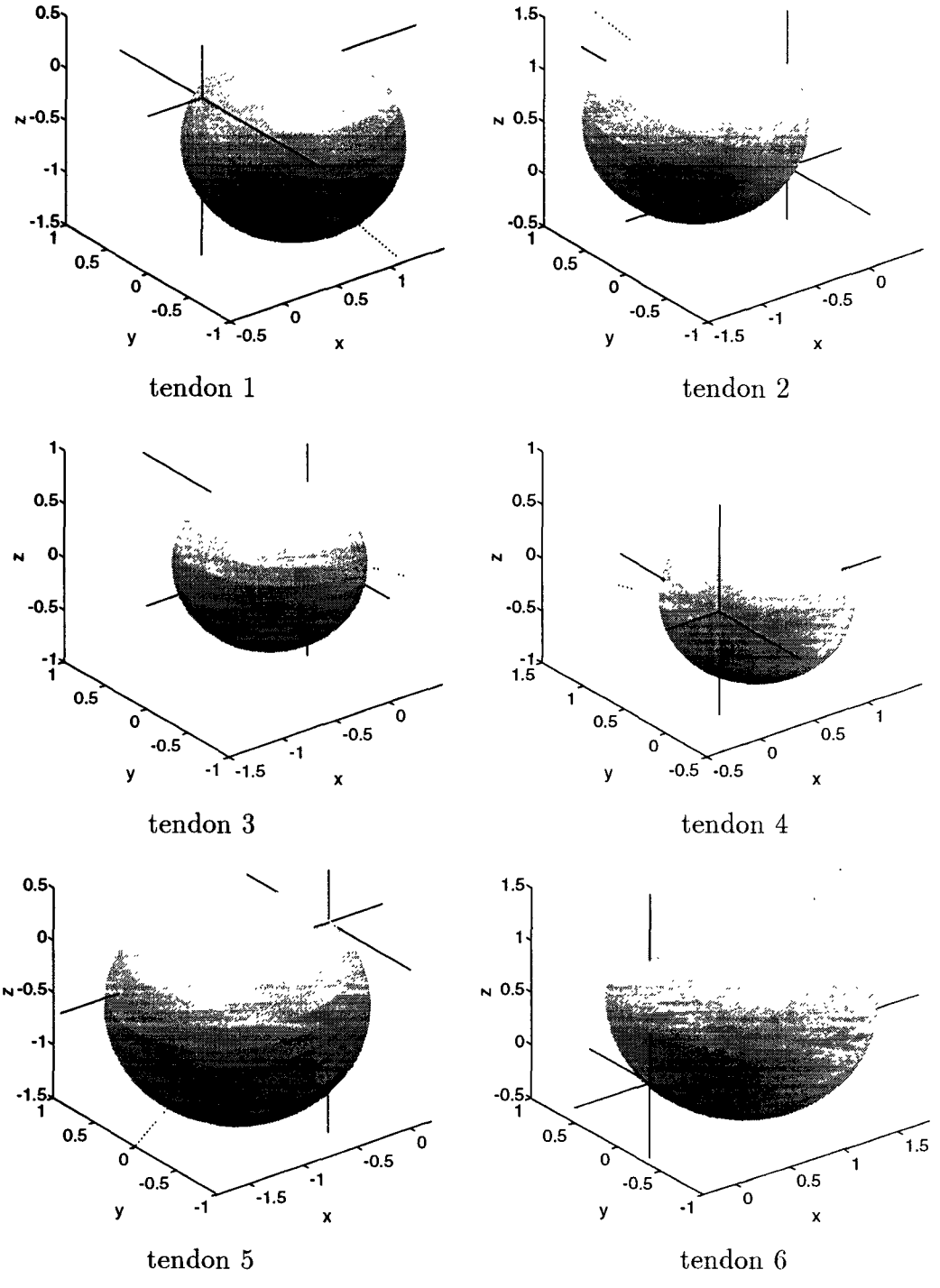

Figure 4.19: Spherical plots of the six tendon force versus direction of applied force for structure (b) evaluated at position 2. The radial distance represents the tendon force and the phase angle represents the direction of applied force.

Structure		(a)	(b)
position	max. tensions	1 1 1.414 1.414 1.414 1.414	1 1 1 1 1 1
1	ratio	1 : 1 : 1.4 : 1.4 : 1.4 : 1.4	1 : 1 : 1 : 1 : 1 : 1
	solo directions ϕ, ψ (deg)	125.3 45 54.7 225 90 45 90 225 90 0 90 180	135 45 45 225 135 225 45 45 90 135 90 315
	Cond($\mathbf{A}^{+T}\mathbf{J}^T$)	4.0489	1
position	max. tensions	1 1 1.414 1.414 2.798 2.798	1.677 1.677 1.450 1.450 1.978 1.978
2	ratio	1 : 1 : 1.4 : 1.4 : 2.8 : 2.8	1.2 : 1.2 : 1 : 1 : 1.4 : 1.4
	solo angles ϕ, ψ (deg)	128.1 297.3 51.9 117.3 145.1 32.8 34.9 212.8 90 0 90 180	118.3 288.4 61.7 108.4 68.8 256.9 111.2 76.9 145.1 147.2 34.9 327.2
	Cond($\mathbf{A}^{+T}\mathbf{J}^T$)	3.6313	2.7112

Table 4.8: List of maximum tensions, their ratios, solo directions and the condition numbers

Table 4.8 lists the maximum tensions, their ratios, solo directions and the condition numbers of $\mathbf{A}^{+T}\mathbf{J}^T$ of the manipulator at the two positions. Though both transmission structure matrices have the same null space, the condition numbers of structure (a) at both positions are worse than that of structure (b). Therefore the largest maximum tension ratios in structure (b) are far less than that of structure (a) at both positions

4.4 Summary

Two examples, one two-dof planar manipulator and one three-dof spatial manipulator, are used to demonstrate the methodology introduced in Chapter 3. It is shown that manipulators which possess isotropic transmission characteristics do have more even force distribution among their tendons. It is also shown that the space of the homogeneous solution plays a very important role in tendon force distribution.

Finally, we note that the isotropic transmission characteristics exist only at isotropic points. The selection of isotropic points has a great influence on the static characteristics over the entire workspace of a manipulator. Thus careful consideration should be given to the selection of this position to achieve a global optimal design of such manipulators.

Chapter 5

Attributes of Isotropic Transmission Structures

5.1 Introduction

The criteria for the design of tendon-driven manipulators with isotropic transmission characteristics and the transmission structures that satisfy the criteria were derived in Chapter 3. The analytical solutions provide the whole solution domain for constructing a manipulator with isotropic transmission structures (ITS). However, the features of ITS weren't discussed. In this chapter, the attributes of manipulators with ITS are discussed. Since there are two types of ITS for an n degree-of-freedom (dof) manipulator: one with $n+1$ tendons and the other with $2n$ tendons; their similarities and differences will also be examined. In what follows, the terms "$n+1$ ITS" and "$2n$ ITS" represent an n-dof ITS with

n+1 and $2n$ tendons, respectively.

A tendon-driven manipulator with ITS has many unique features. In this chapter, the tension control algorithm, maximum tension, kinematic performance, and the sum of the tendon forces will be considered. Since a manipulator with $2n$ ITS has many redundant tendons, one might be interested in knowing how will such a manipulator will perform when one or more tendons malfunction. Finally, the controllability under such conditions will be studied.

5.2 Minimum Tension Control

It has been shown in Chapter 2 that the fundamental relationship between tendon forces and joint torques are related by

$$\underline{\tau} = \mathbf{A}^T \underline{\xi} \tag{5.1}$$

The inverse transformation of eq. (5.1) can be expressed as

$$\underline{\xi} = \mathbf{A}^{+T} \underline{\tau} + \mathbf{H} \underline{\lambda} \tag{5.2}$$

Given a vector of joint torques, $\underline{\tau}$, the tendon forces in eq. (5.2) is underdetermined. Hence, a tension control algorithm should be imposed on the system to regulate the value of $\underline{\lambda}$ and to maintain positive tensions. One obvious method to control tendon forces is the algorithm which finds the minimum p-norm tension forces for p = 1, 2, 3, $\cdots$, or ∞. In this section, the effects of different minimum p-norm tension control algorithms in regulating tendon forces of a manipulator are discussed.

For a transmission structure with $n+1$ tendons, $\underline{\lambda}$ and $\mathbf{H}$ in eq. (5.2) are a scalar and a vector, respectively. To maintain non-negative tensions, the minimum value of λ is given by

$$\lambda_{min} = \max_j \{ -\frac{(\mathbf{A}^{+T}_{n+1})_j \ \underline{\tau}}{h_j} \} \tag{5.3}$$

where $(\ )_j$ denotes the j-th row of the matrix in the parentheses, h_j denotes the jth component of $\mathbf{H}$, and $\max_j\{\ \}$ denotes the maximum value among all the possible choices of j, for j=1, 2, 3, $\cdots$, $n+1$. Since all elements in $\mathbf{H}$ are positive for an admissible transmission structure and since any λ that is less than λ_{min} will result in at least one negative tendon force, we conclude that eq. (5.2) with λ = λ_{min} yields the minimum p-norm tendon forces, where p could be any positive real number. In other words, any minimum p-norm tension control algorithm results in the same λ and, therefore, the same tendon forces.

For a transmission structure with $2n$ tendons, $\underline{\lambda}$ is no longer a scalar and the elements of matrix $\mathbf{H}$ are not necessarily all positive. Generally speaking, applying different minimum p-norm tension control algorithms to the manipulator will result in different $\underline{\lambda}$ and different tendon forces. However, there are some exceptions, and a manipulator with $2n$ ITS is one of them.

For a $2n$ ITS, the null matrix $\mathbf{H}$ in eq. (5.2) can be arranged into the form given by eq. (3.14). The null matrix decouples each λ_i, for i=1, 2, 3, $\cdots$, n, from each other in the homogeneous solution space. Each λ_i regulates only one pair of opposing tendons called a "dual transmission line." It is obvious that the minimum λ_i which maintains positive tendon forces in a "dual transmission

line" is equal to

$$(\lambda_i)_{min} = \max\{-(\mathbf{A}_{2n}^{+T})_{2i-1}\ \underline{\tau}, -(\mathbf{A}_{2n}^{+T})_{2i}\ \underline{\tau}\}, \quad i = 1, 2, 3, \cdots, n \tag{5.4}$$

Substituting eq. (3.27) into $\mathbf{A}^{+T} = \mathbf{A}(\mathbf{A}^T\mathbf{A})^{-1}$, we obtain

$$\mathbf{A}_m^{+T} = c_m \tilde{\mathbf{P}}_m^T \mathbf{U}^T (\mathbf{L}\tilde{\mathbf{J}})(c_m^2 (\mathbf{L}\tilde{\mathbf{J}})^T \mathbf{U} \tilde{\mathbf{P}}_m \tilde{\mathbf{P}}_m^T \mathbf{U}^T \mathbf{L}\tilde{\mathbf{J}})^{-1} \tag{5.5}$$

where $\tilde{\mathbf{J}}$ is the Jacobian matrix when the end-effector is located at a designated isotropic point. Using eq. (3.16), we can simplify eq. (5.5)

$$\mathbf{A}_m^{+T} = \frac{\mu}{\alpha_m} \tilde{\mathbf{P}}_m^T \mathbf{U}^T (\mathbf{L}\tilde{\mathbf{J}})((\mathbf{L}\tilde{\mathbf{J}})^T \mathbf{L}\tilde{\mathbf{J}})^{-1} \tag{5.6}$$

Since $\mathbf{L}\tilde{\mathbf{J}}$ is a full rank matrix, we obtain

$$\mathbf{A}_m^{+T} = \frac{\mu}{\alpha_m} \tilde{\mathbf{P}}_m^T \mathbf{U}^T (\mathbf{L}\tilde{\mathbf{J}})(\mathbf{L}\tilde{\mathbf{J}})^{-1} (\mathbf{L}\tilde{\mathbf{J}})^{-T} \tag{5.7}$$

Simplifying eq. (5.7), yields

$$\mathbf{A}_m^{+T} = \frac{\mu}{\alpha_m} \tilde{\mathbf{P}}_m^T \mathbf{U}^T (\mathbf{L}\tilde{\mathbf{J}})^{-T} \tag{5.8}$$

Since $\tilde{\mathbf{P}}_{2n}^T$ contains n pairs of opposing vectors, matrix $\mathbf{A}_{2n}^{+T}$ in eq. (5.8) also contains n pairs of opposing vectors, that is

$$(\mathbf{A}_{2n}^{+T})_{2i-1} = -(\mathbf{A}_{2n}^{+T})_{2i} \tag{5.9}$$

Equation (5.4) thus can be further simplified into

$$(\lambda_i)_{min} = \mid (\mathbf{A}_{2n}^{+T})_{2i}\ \underline{\tau}\ \mid \quad i = 1, 2, 3, \cdots, n \tag{5.10}$$

Therefore, all minimum p-norm tension control algorithms will yield the same $(\underline{\lambda})_{min}$ with the values given by eq. (5.10). Moreover, it is clear that all minimum

p-norm tension control algorithms applied to a manipulator with a transmission structure whose null matrix $\mathbf{H}$ can be expressed in a decoupled form (i.e. each row has only one nonzero element) will yield the same tendon forces.

Therefore, we conclude that applying different minimum p-norm tension control algorithms to a tendon-driven manipulator with either $n+1$ or $2n$ ITS will not result in different tendon forces. We called such control algorithms "the minimum tension control algorithm" for manipulators with ITSs.

5.3 Maximum Tensions

For a given manipulator posture, tendon forces required to generate a force $\underline{f}$ at the end-effector can be calculated by eq. (2.7). By confining the magnitude of the output force to one unit, each tendon force will vary as the output force changes its direction. Under this condition, the minimum tension control algorithm presented in section 5.2 will be applied to evaluate the maximum tension in each tendon.

For a manipulator with $n+1$ ITS to output a unit force $\underline{f}$, the minimum λ is given by eq. (5.3),

$$\lambda_{min} = \max_j \{-(\mathbf{A}_{n+1}^{+T}\mathbf{J}^T)_j \ \underline{f}\} \tag{5.11}$$

Substituting eq. (5.11) into eq. (2.7) and applying the Cauchy-Schwarz inequality, the maximum tension in each tendon can be obtained as

$$\max(\xi_i) = \max_j \{\| \ [(\mathbf{A}_{n+1}^{+T})_i - (\mathbf{A}_{n+1}^{+T})_j]\mathbf{J}^T \ \|\}, \quad i = 1, 2, 3, \cdots, n+1 \tag{5.12}$$

Substituting eq. (5.8), for $m = n+1$, into eq. (5.12), yields

$$\max(\xi_i) = \mid \frac{\mu}{\alpha_{n+1}} \mid \max_j \{ \parallel [(\tilde{\mathbf{P}}^T_{n+1})_i - (\tilde{\mathbf{P}}^T_{n+1})_j] \mathbf{U}^T (\mathbf{L}\tilde{\mathbf{J}})^{-T} \mathbf{J}^T \parallel \}, \quad i = 1, 2, 3, \cdots, n+1 \tag{5.13}$$

If we let $\mathbf{L}$ be an identity matrix and the end-effector be located at the isotropic point, i.e., $\mathbf{J} = \tilde{\mathbf{J}}$, then eq. (5.13) becomes

$$\max(\xi_i) = \mid \frac{\mu}{\alpha_{n+1}} \mid \max_j \{ \parallel [(\tilde{\mathbf{P}}^T_{n+1})_i - (\tilde{\mathbf{P}}^T_{n+1})_j] \mathbf{U}^T \parallel \}, \quad i = 1, 2, 3, \cdots, n+1 \tag{5.14}$$

Since $\mathbf{U}$ does not affect the norm in eq. (5.14), eq. (5.14) can be further simplified into

$$\max(\xi_i) = \mid \frac{\mu}{\alpha_{n+1}} \mid \max_j \{ \parallel (\tilde{\mathbf{P}}^T_{n+1})_i - (\tilde{\mathbf{P}}^T_{n+1})_j \parallel \}, \quad i = 1, 2, 3, \cdots, n+1 \tag{5.15}$$

Hence, the maximum tendon force in each tendon when the end-effector is located at an isotropic point has a value of

$$\max(\xi_i) = \sqrt{2} \mid \mu \mid, \quad i = 1, 2, 3, \cdots, n+1 \tag{5.16}$$

For a manipulator with a $2n$ ITS to output a unit force $\underline{f}$ at the end-effector, we use eq. (5.10) and (2.6) to obtain the minimum $\underline{\lambda}$ as

$$(\lambda_i)_{min} = \mid (\mathbf{A}^{+T}_{2n})_{2i} \mathbf{J}^T \underline{f} \mid, \quad i = 1, 2, 3, \cdots, n \tag{5.17}$$

Substituting eq. (5.17) into eq. (2.7), the force in each tendon can be derived as

$$\xi_{2i-1} = \max\{0, [(\mathbf{A}^{+T}_{2n})_{2i-1} - (\mathbf{A}^{+T}_{2n})_{2i}] \mathbf{J}^T \underline{f}\} \tag{5.18}$$

$$\xi_{2i} = \max\{0, [(\mathbf{A}^{+T}_{2n})_{2i} - (\mathbf{A}^{+T}_{2n})_{2i-1}] \mathbf{J}^T \underline{f}\} \tag{5.19}$$

Applying the Cauchy-Schwarz inequality to eqs. (5.18) and (5.19), we obtain the maximum tendon forces as

$$\max(\xi_{2i-1}) = \max(\xi_{2i}) = \parallel [(\mathbf{A}^{+T}_{2n})_{2i-1} - (\mathbf{A}^{+T}_{2n})_{2i}] \mathbf{J}^T \parallel \tag{5.20}$$

Substituting eq. (5.9) into (5.20), yields

$$\max(\xi_j) = 2 \parallel (\mathbf{A}_{2n}^{+T})_j \mathbf{J}^T \parallel; \quad j = 1, 2, 3, \cdots, 2n \tag{5.21}$$

Again when $\mathbf{J} = \tilde{\mathbf{J}}$ and $\mathbf{L} = \mathbf{I}_n$, and substituting eq. (5.8) into eq. (5.21), we obtain

$$\max(\xi_j) = \mid \frac{2\mu}{\alpha_{2n}} \mid\mid\mid (\tilde{\mathbf{P}}_{2n}^T)_j \parallel, \quad j = 1, 2, 3, \cdots, 2n \tag{5.22}$$

Hence, substituting eq. (3.13) into (5.22) yields the maximum tendon force for each tendon at an isotropic point as

$$\max(\xi_j) = \sqrt{2} \mid \mu \mid, \quad j = 1, 2, 3, \cdots, 2n \tag{5.23}$$

Since μ is a global amplification factor, we can select μ to be equal for both n+1 ITS and $2n$ ITS. Hence, at the same designate isotropic points, we have

$$\max(\xi_i)_{n+1} = \max(\xi_j)_{2n} \tag{5.24}$$

If we further confine the product of all singular values of an ITS to be equal to one, from eq. (3.10), μ is then equal to

$$\mid \mu \mid = \sqrt[n]{\sigma_1 \sigma_2 \cdots \sigma_n} \tag{5.25}$$

where σ_i ($i = 1, \cdots, n$) are the singular values of $\mathbf{L}\tilde{\mathbf{J}}$.

Hence, the maximum force in each tendon at an isotropic point has a value of

$$\max(\xi_k) = \sqrt{2}\sqrt[n]{\sigma_1 \sigma_2 \cdots \sigma_n}, \quad k = 1, 2, 3, \cdots, m \tag{5.26}$$

5.4 Condition Number

Since the Jacobian matrix of a manipulator is position dependent, the condition number of $\mathbf{A}^{+T}\mathbf{J}^T$ is also position dependent. Based on the same designated isotropic point, in what follows, we prove that the condition number of $\mathbf{A}^{+T}\mathbf{J}^T$ for an n+1 ITS is equal to that for an $2n$ ITS in the whole workspace.

From eq. (5.8), the condition number of $\mathbf{A}^{+T}\mathbf{J}^T$ can be expressed as

$$cond(\mathbf{A}^{+T}\mathbf{J}^T) = cond(\frac{\mu}{\alpha_m}\tilde{\mathbf{P}}_m^T\mathbf{U}^T(\mathbf{L}\tilde{\mathbf{J}})^{-T}\mathbf{J}^T) \tag{5.27}$$

where $cond(\ )$ denotes the condition number of the matrix in the parenthesis. Since the selection of a constant μ/α_m and a rotation matrix $\mathbf{U}$ does not effect the condition number of $\mathbf{A}^{+T}\mathbf{J}^T$, we have

$$cond(\mathbf{A}^{+T}\mathbf{J}^T) = cond(\tilde{\mathbf{P}}_m^T(\mathbf{L}\tilde{\mathbf{J}})^{-T}\mathbf{J}^T) \tag{5.28}$$

From eqs. (3.11) and (3.13), it can be shown that both $\tilde{\mathbf{P}}_{n+1}^T$ and $\tilde{\mathbf{P}}_{2n}^T$ have unity condition numbers. Thus, we conclude

$$cond(\mathbf{A}^{+T}\mathbf{J}^T) = cond((\mathbf{L}\tilde{\mathbf{J}})^{-T}\mathbf{J}^T) \tag{5.29}$$

From eq. (5.29), we can see that both n+1 and $2n$ ITS have equal condition numbers in the whole workspace.

5.5 Sum of the Tendon Forces

From the previous discussion, it seems that a manipulator with either an n+1 ITS or an $2n$ ITS possesses many similar features. In this section, both types of

ITS will be compared based on the sum of all tendon forces in order to understand the antagonistic relationship among tendons.

Substituting eq. (5.8) into (5.2), the tendon forces of an ITS are

$$\underline{\xi} = \frac{\mu}{\alpha_m}\tilde{\mathbf{P}}_m^T\mathbf{U}^T(\mathbf{L}\tilde{\mathbf{J}})^{-T}\underline{\tau} + \mathbf{H}\,\underline{\lambda} \tag{5.30}$$

From eq. (5.30), the sum of all tendon forces can be written as

$$\sum_{i=1}^{m}\xi_i = \frac{\mu}{\alpha_m}[\sum_{i=1}^{m}(\tilde{\mathbf{P}}_m^T)_i]\mathbf{U}^T(\mathbf{L}\tilde{\mathbf{J}})^{-T}\underline{\tau} + [\sum_{i=1}^{m}(\mathbf{H})_i]\,\underline{\lambda} \tag{5.31}$$

where $\sum_{i=1}^{m}(\tilde{\mathbf{P}}_m^T)_i$ is a row vector with the sum over each column of $\tilde{\mathbf{P}}_m^T$ and $\sum_{i=1}^{m}(\mathbf{H})_i$ is a row vector with the sum over each column of $\mathbf{H}$. Since both $\sum_{i=1}^{n+1}(\tilde{\mathbf{P}}_{n+1}^T)_i$ and $\sum_{i=1}^{2n}(\tilde{\mathbf{P}}_{2n}^T)_i$ are equal to a zero vector, the sum of tendon forces due to the particular solution in eq. (5.31) is always equal to zero. Hence, the sum of the tendon forces are completely determined by the homogeneous solution. The homogeneous solution has no effect on joint torques. Hence, the tension sum indicates the antagonistic relationship among tendons for an ITS. Since $\mathbf{H}_{n+1}$ and $\mathbf{H}_{2n}$ of the ITS contain only unit elements, the sum of tendon forces depends on $\underline{\lambda}$. Note that all elements of $\underline{\lambda}$ for both ITS are always positive.

For n+1 ITS, substituting eqs. (3.12) and (5.3) into eq. (5.31), yields

$$\sum_{i=1}^{n+1}\xi_i = (n+1)\lambda_{min} = (n+1)\max_j\{-(\mathbf{A}_{n+1}^{+T})_j\ \underline{\tau}\} \tag{5.32}$$

Substituting eq. (5.8) and (2.6) into (5.32), gives

$$\sum_{i=1}^{n+1}\xi_i = (n+1)\max_j\{-(\frac{\mu}{\alpha_{n+1}})(\tilde{\mathbf{P}}_{n+1}^T)_j\mathbf{U}^T(\mathbf{L}\tilde{\mathbf{J}})^{-T}\mathbf{J}^T\underline{f}\} \tag{5.33}$$

At an isotropic point, if $\mathbf{L}$ is equal to an identity matrix, eq. (5.33) becomes

$$\sum_{i=1}^{n+1}\xi_i = (n+1)\max_j\{-(\frac{\mu}{\alpha_{n+1}})(\tilde{\mathbf{P}}_{n+1}^T)_j\mathbf{U}^T\underline{f}\} \tag{5.34}$$

If we confine the magnitude of the output force $\underline{f}$ to one unit, then the application of the Cauchy-Schwarz inequality gives the maximum of $\sum_{i=1}^{n+1} \xi_i$ as

$$\max(\sum_{i=1}^{n+1} \xi_i) = (n+1) \mid \frac{\mu}{\alpha_{n+1}} \mid \max_j\{\| (\tilde{\mathbf{P}}_{n+1}^T)_j \|\} = \sqrt{n^2+n} \mid \mu \mid \qquad (5.35)$$

From a geometric interpretation, each row of $\tilde{\mathbf{P}}_{n+1}^T$ represents a position vector of an apex of a regular simplex. The quantity "$-(\tilde{\mathbf{P}}_{n+1}^T)_j \mathbf{U}^T \underline{f}$" is the dot product of the vector "$-\mathbf{U}^T \underline{f}$" and the position vector of an apex of a regular simplex. Hence, the smallest value of $\max_j\{-(\tilde{\mathbf{P}}_{n+1}^T)_j \mathbf{U}^T \underline{f}\}$ happens when the vector "$-\mathbf{U}^T \underline{f}$" points to the center of a face of the regular simplex. Since this direction is opposite to the position vector of an apex, the smallest value of $\max_j\{-(\tilde{\mathbf{P}}_{n+1}^T)_j \mathbf{U}^T \underline{f}\}$ is the negative dot product of any two position vectors of the apexes. Hence, we have

$$\min\{\max_j\{-(\tilde{\mathbf{P}}_{n+1}^T)_j \mathbf{U}^T \underline{f}\}\} = \frac{1}{n} \qquad (5.36)$$

Substituting eq. (5.36) into (5.34), yields

$$\min(\sum_{i=1}^{n+1} \xi_i) = \frac{n+1}{n} \mid \frac{\mu}{\alpha_{n+1}} \mid = \sqrt{\frac{n+1}{n}} \mid \mu \mid \qquad (5.37)$$

For $2n$ ITS, substituting eqs. (3.14) and (5.10) into eq. (5.31), we obtain the sum of the tendon forces as

$$\sum_{i=1}^{2n} \xi_i = 2 \sum_{i=1}^{n} \lambda_i = 2 \sum_{i=1}^{n} \mid (\mathbf{A}_{2n}^{+T})_{2i} \ \underline{\tau} \mid \qquad (5.38)$$

Since all rows of $(\tilde{\mathbf{P}}_{2n}^T)_{2i}$ for $i = 1, 2, 3, \cdots, n$, form an identity matrix, substituting eq. (5.8) into eq. (5.38), yields

$$\sum_{i=1}^{2n} \xi_i = 2 \mid \frac{\mu}{\alpha_{2n}} \mid \sum_{i=1}^{n} \mid (\mathbf{U}^T (\mathbf{L}\tilde{\mathbf{J}})^{-T})_i \ \underline{\tau} \mid \qquad (5.39)$$

Using eq. (5.39) in a manner similar to that use for n+1 ITS, the sum of the tendon forces generating a unit force when the end-effector is located at an isotropic point is given by

$$\sum_{i=1}^{2n} \xi_i = 2 \mid \frac{\mu}{\alpha_{2n}} \mid \sum_{i=1}^{n} \mid (\mathbf{U}^T)_i \ \underline{f} \mid \tag{5.40}$$

The maximum sum of the forces $\sum_{i=1}^{2n} \xi_i$ generating a unit force happens when $\mathbf{U}^T \underline{f}$ points in the $[\pm 1, \pm 1, \cdots, \pm 1]$ direction and is given by

$$\max(\sum_{i=1}^{2n} \xi_i) = 2 \mid \frac{\mu}{\alpha_{2n}} \mid \max\{\sum_{i=1}^{n} \mid (\mathbf{U}^T)_i \ \underline{f} \mid\} = \sqrt{2n} \mid \mu \mid \tag{5.41}$$

The minimum sum $\sum_{i=1}^{2n} \xi_i$ happens when $\mathbf{U}^T \underline{f}$ points in the $[0, \cdots, 0, \pm 1, 0, \cdots, 0]$ direction and is equal to

$$\min(\sum_{i=1}^{2n} \xi_i) = 2 \mid \frac{\mu}{\alpha_{2n}} \mid \min\{\sum_{i=1}^{n} \mid (\mathbf{U}^T)_i \ \underline{f} \mid\} = \sqrt{2} \mid \mu \mid \tag{5.42}$$

If we choose the same $\mid \mu \mid$ for both n+1 and $2n$ ITS matrices, we obtain

$$\sqrt{\frac{n+1}{n}} \mid \mu \mid \leq \sqrt{2} \mid \mu \mid \leq \sqrt{2n} \mid \mu \mid \leq \sqrt{n^2+n} \mid \mu \mid \tag{5.43}$$

where the equal sign holds only for n=1. Therefore, the maximum tension sum of an n+1 ITS is larger than that of an $2n$ ITS, while the minimum tension sum of an n+1 ITS is smaller than that of an $2n$ ITS. For an n+1 ITS, the maximum tension sum is n times the minimum tension sum. For an $2n$ ITS, the maximum tension sum is $\sqrt{n}$ times the minimum tension sum. This means an n+1 ITS generates higher antagonistic tendon forces than an $2n$ ITS does.

The two-dof planar manipulator shown in Fig. 4.1 is chosen to evaluate the sum of the tendon forces. One 2×3 ITS matrix and one 2×4 ITS matrix are selected for comparison. The 2×3 ITS matrix is the transmission structure (c) in

Table 4.1 whereas the 2×4 ITS matrix is transmission structure (b) in Table 4.3. Both ITS are designed so that their isotropic points are located the same x = ℓ and y = 0 position.

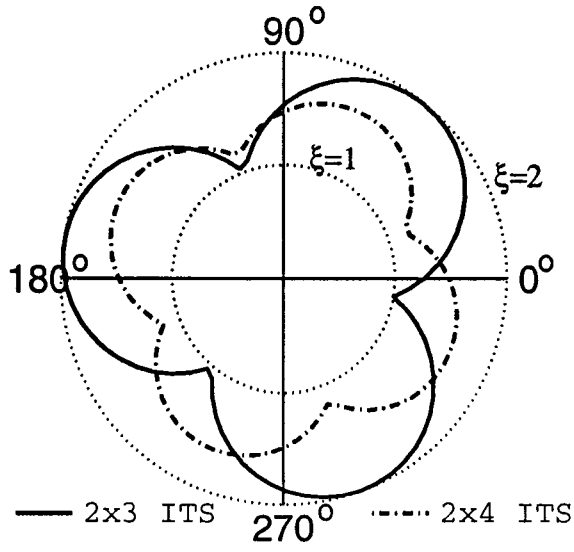

Figure 5.1: Polar plots of the tension sums for the manipulator shown in Fig. 4.1 with two different ITS: one is a 2× 3 ITS, and the other is a 2× 4 ITS

Figure 5.1 shows polar plots of the sum of tendon forces working against a unit external force acting at the end-effector from all possible directions while the end-effector is located at the isotropic point. Note that by selecting a different **U** in eq. (3.15) to derive a different ITS, the resulting polar plots can be obtained by rotating the original polar plots by an appropriate angle. From Fig. 5.1, we can see the tension sum of the 2×4 ITS has smaller variation than that of 2×3 ITS does. The maximum tension sum of the 2×3 ITS is also larger than that of the 2×4 ITS while the minimum tension sum of the 2×3 ITS is less than that of the 2×4 ITS. Therefore, a 2×3 ITS has higher antagonistic forces than a 2×4 ITS.

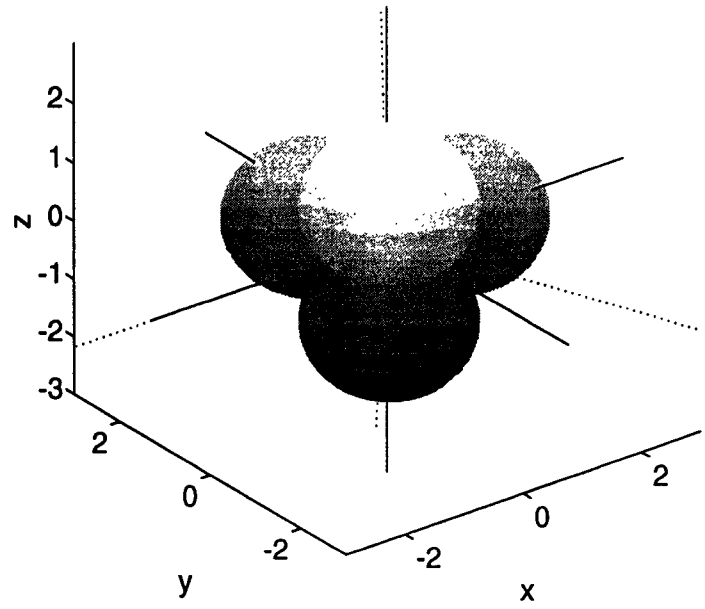

Figure 5.2: Spherical plots of the tension sum for the manipulator shown in Fig. 4.8 with a 3× 4 ITS

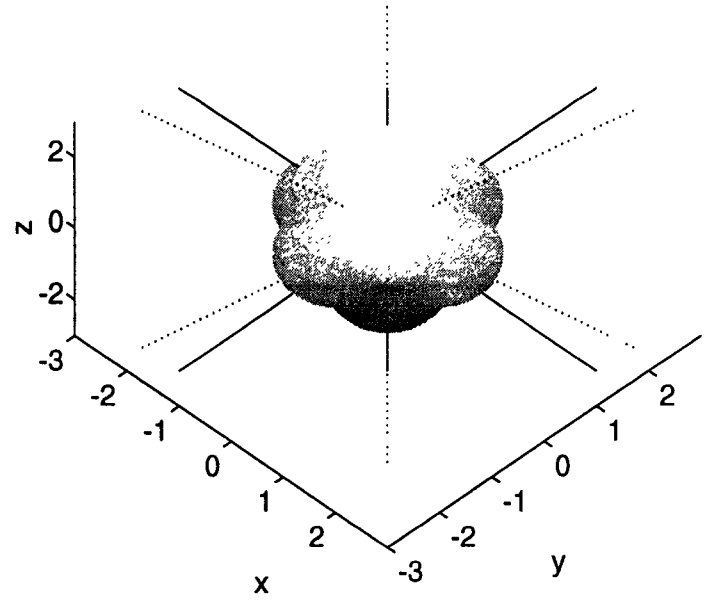

Figure 5.3: Spherical plots of the tension sum for the manipulator shown in Fig. 4.8 with a 3× 6 ITS

Figures 5.2 and 5.3 show spherical plots of tension sum for the manipulator shown in Fig. 4.8 with two different ITS when a unity external force is applied at the end-effector and when the end-effector is located at the designated isotropic point ($x = 0, y = z = \ell/\sqrt{2}$). The 3× 4 ITS shown in Fig. 5.2 is the structure (b) listed in Table 4.5, and the 3× 6 ITS shown in Fig. 5.3 is the structure (b) listed in Table 4.7. Again, the tension sum for an ITS with six tendons assumes lower antagonistic forces than that with four tendons.

5.6 Controllability of $2n$ ITS

Since a $2n$ ITS employs more tendons than required to fully control an n-dof manipulator, one might be interested to learn its controllability when one or more tendons malfunction. To answer this question, we should examine whether the resulting transmission structure complies with the conditions of admissible transmission structure presented in Chapter 2.

Due to the existence of "dual transmission lines," a general $2n$ ITS matrix can be expressed as

$$\mathbf{A}_{2n}^{T} = \begin{bmatrix} a_{11} & -a_{11} & a_{12} & -a_{12} & \cdots & a_{1n} & -a_{1n} \\ a_{21} & -a_{21} & a_{22} & -a_{22} & \cdots & a_{2n} & -a_{2n} \\ \vdots & \vdots & \vdots & \vdots & \vdots & \vdots & \vdots \\ a_{n1} & -a_{n1} & a_{n2} & -a_{n2} & \cdots & a_{nn} & -a_{nn} \end{bmatrix} \tag{5.44}$$

where the $2i$-th columns, i= $1, 2, 3, \cdots, n$, represents the dual of the ($2i$-1)-th column. The null matrix $\mathbf{H}$ is given by eq. (3.14).

When the $(2i\text{-}1)$th (or $2i$th) tendon malfunctions, the resulting transmission structure matrix is obtained by deleting the $(2i\text{-}1)$th (or $2i$th) column from the matrix $\mathbf{A}_{2n}^T$. Hence, the corresponding null matrix $\mathbf{H}$ can be obtained by deleting the $(2i\text{-}1)$th (or $2i$th) row and the ith column. Thus, the $(2i\text{-}1)$th row of the resulting null matrix $\mathbf{H}$ contains all zero elements which means positive tension in the corresponding $(2i\text{-}1)$th tendon can not always be maintained. Therefore, the resulting transmission structure matrix is not an admissible transmission structure.

Following the same procedure when another tendon malfunctions, the resulting null matrix $\mathbf{H}$ will contain another row with all zero elements. Hence, we conclude that when one or more tendons malfunction, a manipulator with a $2n$ ITS becomes uncontrollable.

5.7 Conclusions

In this chapter, many features of ITS have been described. The existence of a unique minimum tension control methodology for ITS eases and unifies the design of the control system. With the discussion of the maximum tensions, the global amplification factor μ can be regulated so that a manipulator with any ITS will possess the same maximum tendon force in each tendon against a unit external force acting at the end-effector. It is shown that the condition number of the matrix product $\mathbf{A}^{+T}\mathbf{J}^T$ of a manipulator with either type of ITS is the same in the whole workspace. The sum of the tendon forces differentiates between the two types of ITS. The study of controllability when one or more

tendons are broken reveals that 2n ITS is no better than n+1 ITS.

Chapter 6

Design of a Three-DOF Manipulator Having Equal Maximum Tensions within its Entire Workspace

6.1 Introduction

For a manipulator designed without any structural optimization, tension in each tendon against an external force applied at the end-effector will vary as a function of the direction of applied force and the position of the end-effector. As a result, the maximum tension for each tendon in the whole workspace would be different from one another. If equal strength tendons are used, the largest

maximum tension among all tendons should be used for the sizing of tendons. This, however, will be inefficient. If different strength tendons are adopted, the transmission structure will be degraded due to the diverse attributes of the tendons. Therefore, a manipulator with the feature of equal maximum tensions in its whole workspace is crucial in the design of a manipulator with equal strength of its actuators and tendons. A manipulator with this feature is also expected to simplify the process of design.

Lee and Tsai (1991a) developed a methodology to implement all possible tendon routings for an n-dof manipulator controlled by more than n actuators. A methodology to optimize the tendon routings and pulley sizes for an n-dof manipulator with $n+1$ or $2n$ actuators based on the concept of local isotropic transmission characteristics was presented in Chapter 3. An isotropic transmission structure ensures a unity condition number of the static force transformation matrix and equal maximum tensions in all tendons against a unity force applied at the end-effector, when the end-effector is located at an isotropic point. However, as the end-effector moves away from the isotropic point, maximum tension in each tendon may become different.

Generally speaking, the feature of equal maximum tensions cannot be achieved simply by designing its transmission structure, except for some particular manipulator configurations. For example, a manipulator with all perpendicular joint axes. In this chapter, we present the design of a particular three-dof manipulator which possesses the feature of equal maximum tensions in its entire workspace. The description of the manipulator follows.

6.2 Description of the Three-dof Manipulator

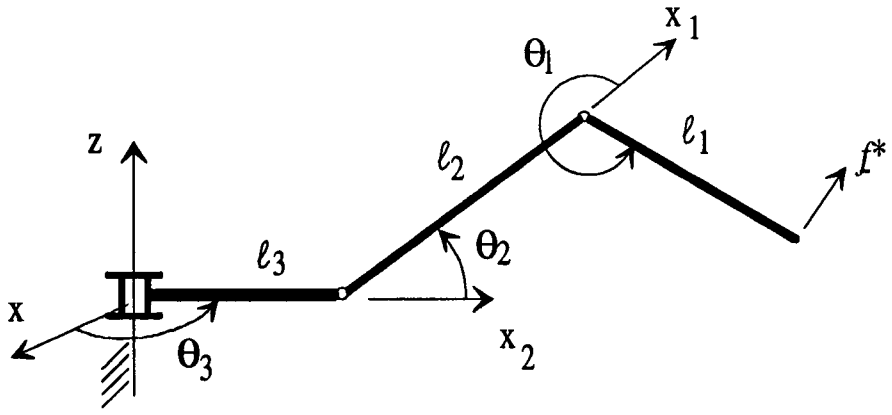

Figure 6.1: The three-dof link structure of the Salisbury finger

To improve static performance of existing devices with the aforementioned features and to illustrate the methodology, the linkage structure and the four tendons (actuators) of a three-dof manipulator (taken from the Stanford/JPL hand) was adopted. Figure 6.1 shows its linkage structure; the first and the second joint axes are parallel to each other, and the third joint axis is perpendicular the second. Note that the links and joints as shown in Fig. 6.1 are numbered from the outermost to the proximal, where ℓ_1, ℓ_2, ℓ_3, and θ_1, θ_2, θ_3 are the corresponding link lengths and joint angles. Although, the end-effector of this manipulator travels in a complex three dimensional space, its linkage structure and tendon routings are simple enough to be applied by the methodology developed here.

By letting θ_3 be equal to 90°, the Jacobian matrix of the manipulator, which represents the transformation from the joint space to the end-effector space, can

be written as

$$\mathbf{J} = \ell_2 \begin{bmatrix} 0 & 0 & -(C_2 + l_{32} + C_{12}l_{12}) \\ -S_{12}l_{12} & -S_2 - S_{12}l_{12} & 0 \\ C_{12}l_{12} & C_2 + C_{12}l_{12} & 0 \end{bmatrix}. \tag{6.1}$$

where $C_2 = Cos(\theta_2), S_2 = Sin(\theta_2), C_{12} = Cos(\theta_1 + \theta_2), S_{12} = Sin(\theta_1 + \theta_2)$, $l_{12} = \ell_1/\ell_2$ and $l_{32} = \ell_3/\ell_2$. Hence, l_{12} and l_{32} are two non-dimensional link length ratios.

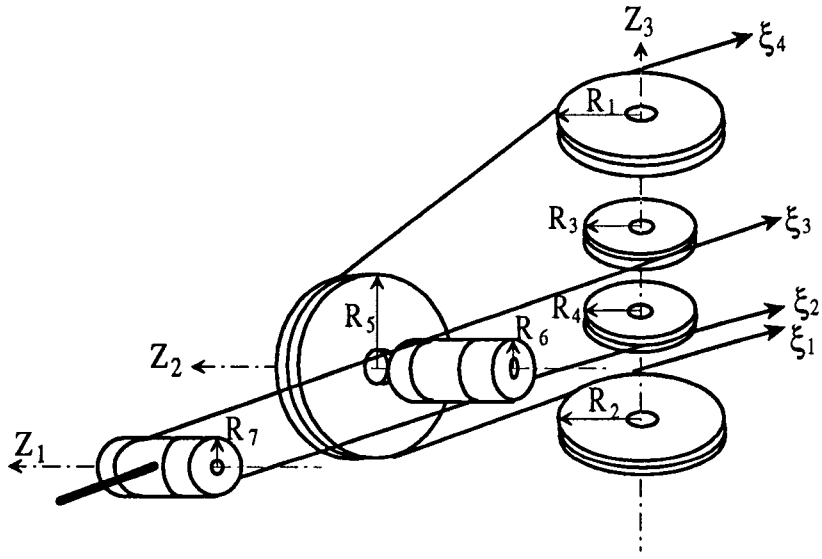

Figure 6.2: The tendon routings and pulleys of the Salisbury finger

Figure 6.2 shows the tendon routings and pulley arrangement of the Stanford/JPL finger. The power is transmitted from the actuators to the joints through four tendons.

6.3 Structure Matrix with Equal Maximum Tensions

Consider an external force $\underline{f}^* = [f_x^*, f_y^*, f_z^*]^T$ applied at the end-effector. Applying the minimum tension control algorithm to regulate and to maintain positive tendon forces, λ in eq. (2.15) is given by:

$$\lambda = \max_j \{\frac{(\mathbf{A}^{+T}\mathbf{J}^T)_j \underline{f}^*}{h_j}\} \quad j = 1,\ 2,\ 3,\ \text{and}\ 4 \tag{6.2}$$

where $(\ )_j$ denotes the j-th row of the matrix in the parentheses, $\max\{\ \}_j$ denotes the maximum value among all the possible choices of j and h_j is the jth element of $\underline{h}$ in eq. (2.15).

Substituting eq. (6.2) into eq. (2.15), we obtain scalar forms of eq. (2.15) as

$$\xi_i = \max_j \{[-(\mathbf{A}^{+T}\mathbf{J}^T)_i + (\mathbf{A}^{+T}\mathbf{J}^T)_j \frac{h_i}{h_j}]\underline{f}^*\}, \qquad i = 1,\ 2,\ 3,\ \text{and}\ 4 \tag{6.3}$$

Confining the externally applied force on a unit sphere and applying the Cauchy-Schwarz inequality to eq. (6.3) result in

$$\max(\xi_i) = \max_j \{\| \ (\mathbf{A}^{+T}\mathbf{J}^T)_i - (\mathbf{A}^{+T}\mathbf{J}^T)_j \frac{h_i}{h_j} \ \|\}, \qquad i = 1,\ 2,\ 3,\ \text{and}\ 4 \tag{6.4}$$

When all four maximum tendon forces are equal, it is clear that the elements of $\underline{h}$ should satisfy

$$\frac{h_i}{h_j} = 1; \qquad i, j = 1,\ 2,\ 3,\ \text{and}\ 4 \tag{6.5}$$

i.e.,

$$\underline{h} = [1, 1, 1, 1]^T \tag{6.6}$$

Note that eq. (6.6) is one of the criteria for an isotropic transmission structure. Using eq. (6.6), the condition of equal maximum tensions can be stated as

$$max(g_{12}, g_{13}, g_{14}) = max(g_{21}, g_{23}, g_{24}) = max(g_{31}, g_{32}, g_{34}) = max(g_{41}, g_{42}, g_{43}) \quad (6.7)$$

where

$$g_{ij} = g_{ji} = \| \left[(\mathbf{A}^{+T})_i - (\mathbf{A}^{+T})_j \right] \mathbf{J}^T \|; \quad i, j = 1,\ 2,\ 3,\ \text{and}\ 4 \qquad (6.8)$$

There are a total of six norms involved in eq. (6.7), namely: g_{12}, g_{13}, g_{14}, g_{23}, g_{24}, and g_{34}. The Jacobian matrix $\mathbf{J}$ depends on the posture of a manipulator, as do the six norms. It is clear that, for eq. (6.7) to be valid, the six norms must satisfy one of the following two conditions:

1. Three of the six norms are equal to each other and the other three are always less than or equal to the first three norms in the whole workspace.
2. Each maximum tendon force is determined from an equivalent set of norms, $max(g_{12}, g_{13}, g_{14})$, provided the following conditions are satisfied:

$$g_{12} = g_{34}, \qquad (6.9)$$

$$g_{13} = g_{24}, \quad \text{and} \qquad (6.10)$$

$$g_{14} = g_{23} \qquad (6.11)$$

Condition 1 results in rank-deficient transmission structure matrices, which are not admissible. In what follows, we will only consider condition 2.

Equation (6.9) can be rewritten as

$$\| \left[(\mathbf{A}^{+T})_1 - (\mathbf{A}^{+T})_2 \right] \mathbf{J}^T \| = \| \left[(\mathbf{A}^{+T})_3 - (\mathbf{A}^{+T})_4 \right] \mathbf{J}^T \| \qquad (6.12)$$

To derive matrix $\mathbf{A}$, we first express matrix $\mathbf{A}^{+T}$ as:

$$\mathbf{A}^{+T} = \begin{bmatrix} a_{11} & a_{12} & a_{13} \\ a_{21} & a_{22} & a_{23} \\ a_{31} & a_{32} & a_{33} \\ a_{41} & a_{42} & a_{43} \end{bmatrix} \tag{6.13}$$

where a_{ij} ($i,\ j = 1,\ 2,\ 3,$ and 4) are the unknown elements of $\mathbf{A}^{+T}$.

Substituting eqs. (6.1) and (6.13) into eq. (6.12), we obtain

$$\begin{aligned} &[(a_{12} - a_{22})^2 - (a_{32} - a_{42})^2](1 + 2l_{12}C_1) + \\ &[(a_{13} - a_{23})^2 - (a_{33} - a_{43})^2](C_2 + l_{32} + C_{12}l_{12})^2 + \\ &[(a_{12} - a_{22})(a_{11} - a_{21}) - (a_{32} - a_{42})(a_{31} - a_{41})]2l_{12}C_1 + \\ &[(a_{12} - a_{22} + a_{11} - a_{21})^2 - (a_{32} - a_{42} + a_{31} - a_{41})^2]l_{12}^2 = 0 \end{aligned} \tag{6.14}$$

Since θ_1 and θ_2 can take any two arbitrary angles, we conclude that

$$(a_{13} - a_{23})^2 - (a_{33} - a_{43})^2 = 0 \tag{6.15}$$

$$\begin{aligned} &(a_{12} - a_{22})^2 - (a_{32} - a_{42})^2 + \\ &\quad (a_{12} - a_{22})(a_{11} - a_{21}) - (a_{31} - a_{41})(a_{32} - a_{42}) = 0 \end{aligned} \tag{6.16}$$

$$\begin{aligned} &(a_{32} - a_{42})^2 - (a_{12} - a_{22})^2 = \\ &\quad l_{12}^2[(a_{12} - a_{22} - a_{11} - a_{21})^2 - (a_{32} - a_{42} + a_{31} - a_{41})^2] \end{aligned} \tag{6.17}$$

Similarly, from eqs. (6.10) and (6.11), we obtain

$$(a_{13} - a_{33})^2 - (a_{23} - a_{43})^2 = 0 \tag{6.18}$$

$$\begin{aligned} &(a_{12} - a_{32})^2 - (a_{22} - a_{42})^2 + \\ &\quad (a_{11} - a_{31})(a_{12} - a_{32}) - (a_{21} - a_{41})(a_{22} - a_{42}) = 0 \end{aligned} \tag{6.19}$$

$$(a_{22}-a_{42})^2-(a_{12}-a_{32})^2=$$

$$l_{12}^2[(a_{12}-a_{32}-a_{11}-a_{31})^2-(a_{22}-a_{42}+a_{21}-a_{41})^2] \tag{6.20}$$

and

$$(a_{13}-a_{43})^2-(a_{23}-a_{33})^2=0 \tag{6.21}$$

$$(a_{12}-a_{42})^2-(a_{22}-a_{32})^2+$$

$$(a_{12}-a_{42})(a_{11}-a_{41})-(a_{21}-a_{31})(a_{22}-a_{32})=0 \tag{6.22}$$

$$(a_{22}-a_{32})^2-(a_{12}-a_{42})^2=$$

$$l_{12}^2[(a_{12}-a_{42}-a_{11}-a_{41})^2-(a_{22}-a_{32}+a_{21}-a_{31})^2] \tag{6.23}$$

Since eq. (6.6) is a null vector of $\mathbf{A}^T$, and thus the null vector of $\mathbf{A}^+$, $\mathbf{A}^{+T}$ must satisfy the following constraints:

$$a_{11}+a_{21}+a_{31}+a_{41}=0 \tag{6.24}$$

$$a_{12}+a_{22}+a_{32}+a_{42}=0 \tag{6.25}$$

$$a_{13}+a_{23}+a_{33}+a_{43}=0 \tag{6.26}$$

Equations (6.15) through (6.26) are a set of twelve equations in twelve unknowns. However, only nine of them are independent. By solving eqs. (6.15) to (6.26) and eliminating those solutions which yield rank-deficient matrices, we obtain

$$\mathbf{A}^{+T}=\begin{bmatrix} -a_{12}\pm\frac{a_{22}}{l_{12}} & a_{12} & a_{13} \\ \pm\frac{a_{12}}{l_{12}}-a_{22} & a_{22} & -a_{13} \\ a_{12}\mp\frac{a_{22}}{l_{12}} & -a_{12} & a_{13} \\ \mp\frac{a_{12}}{l_{12}}+a_{22} & -a_{22} & -a_{13} \end{bmatrix} \tag{6.27}$$

Since

$$(\mathbf{A}^{+T})^{+} = \mathbf{A}^{T} \tag{6.28}$$

we have

$$\mathbf{A}^{T} = (\mathbf{A}^{+}\mathbf{A}^{+T})^{-1}\mathbf{A}^{+} \tag{6.29}$$

By introducing the new variables,

$$a = \frac{1}{4a_{11}}, \quad b = \frac{a_{12}}{2(a_{12}^2 - a_{22}^2)}, \quad \text{and} \quad c = \frac{a_{22}}{2(a_{12}^2 - a_{22}^2)} \tag{6.30}$$

we obtain $\mathbf{A}^T$ as

$$\mathbf{A}^{T} = \begin{bmatrix} \mp cl_{12} & \pm bl_{12} & \pm cl_{12} & \mp bl_{12} \\ b \mp cl_{12} & -c \pm bl_{12} & -b \pm cl_{12} & c \mp bl_{12} \\ a & -a & a & -a \end{bmatrix} \tag{6.31}$$

Therefore, the three-dof manipulator with its structure matrix in the form of eq. (6.31) possesses the feature of equal maximum tensions in its whole workspace. Note that the link ratio l_{32} has no effect on the structure matrix.

6.4 Addition of Isotropic Transmission Characteristics

When the end-effector of a manipulator locates at an isotropic point, the maximum tensions on the four tendons are equal to one another. This feature is compatible with that of equal maximum tensions. The link ratio l_{32} and the four free variables in eq. (6.31) leave enough room for introducing more design constraints. Therefore, we can impose the concept of isotropic transmission to the design of this manipulator.

To achieve isotropic transmission characteristics, as discussed in Chapter 3, two criteria should be satisfied: the first is eq. (6.6), and the second is

$$\mathbf{A}^T\mathbf{A} = \frac{1}{\mu^2}\mathbf{J}^T\mathbf{J} \tag{6.32}$$

where μ is an arbitrary constant.

Since eq. (6.31) satisfies (6.6) automatically, we need only to consider eq. (6.32). Substituting eq. (6.31) into eq. (6.32), we obtain, upon simplification, the following two independent equations:

$$\frac{-2bc}{b^2+c^2} = \pm C_1 \tag{6.33}$$

and

$$\frac{2a^2}{b^2+c^2} = (l_{32} + C_2 + l_{12}C_{12})^2 \tag{6.34}$$

From eqs. (6.33) and (6.34), it is clear that the link ratios l_{12} and l_{32} and the location of isotropic point can be chosen arbitrary, as long as the Jacobian matrix is not singular. After selecting the link ratios and the location of the isotropic point, eqs. (6.33) and (6.34) become two constraints for the matrix in eq. (6.31). Therefore, there is one free variable that serves as an amplification factor for the whole transmission structure.

The following section provides a numerical example to illustrate the characteristics of this type of manipulators. The results are compared with that of the Salisbury finger.

6.5 Numerical Examples

The link proportion of the Salisbury finger from the distal link to the proximal link is 1 : 1 : 0.685. The radii of the pulleys shown in Fig. 6.2 are R_1=1.0795cm, R_2=.8255cm, R_3=R_4=R_6=.5969cm, R_5=1.1862cm, and R_7=.6350cm. Hence, the transmission structure matrix of the manipulator can be written as

$$\begin{bmatrix} 0 & -.6350 & .6350 & 0 \\ -1.1862 & -.5969 & .5969 & 1.1862 \\ -.8255 & .5969 & .5969 & -1.0795 \end{bmatrix} \tag{6.35}$$

To demonstrate the effect of equal maximum tensions and the isotropic transmission characteristics, a new transmission structure is developed. The link arrangement and link proportion are the same as that of the Salisbury finger. The variable c in eq. (6.31) is set to zero to maintain the same tendon routings as that of the Salisbury finger for comparison. Thus, the isotropic points can be chosen only at the locations where the joint angle θ_1 is equal to $\pm 90°$. The new transmission structure is designed so that the manipulator possesses isotropic transmission characteristics when $\theta_1 = 90°$ and $\theta_2 = 0°$, and the point (x=0, y=$\ell_3 + \ell_2$, z=ℓ_1) is one of the isotropic points on the locus. The transmission structure matrix can be derived from eqs. (6.31) and (6.34) by letting $b = -1$. After discarding the solutions that involve different routings from that of the Salisbury finger and after reordering columns of the transmission structure, such that the new transmission structure matrix has the same form as the matrix in

eq. (6.35), we obtain

$$\mathbf{A}^T = \begin{bmatrix} 0 & -1 & 1 & 0 \\ -1 & -1 & 1 & 1 \\ -1.192 & 1.192 & 1.192 & -1.192 \end{bmatrix} \tag{6.36}$$

The maximum tendon force on each tendon of the two transmission structures is computed by using eq. (6.4) at three different end-effector positions: the first is at x=0, y=$\ell_3 + \ell_2$, z=ℓ_1, the second is at x=0, y=$\ell_3 + \sqrt{2}\ell_2$, z=0, and the third is at x=0, y=ℓ_3, z=$\sqrt{2}\ell_2$. The first position is an isotropic point for the new transmission structure.

Structures		(a)	(b)
κ		1.899	0.5942
position 1	max. tensions	[1.514, 2.363, 2.415, 1.453]	[1.683, 1.683, 1.683, 1.683]
	ratio	1.042 : 1.626 : 1.662 : 1	1 : 1 : 1 : 1
position 2	max. tensions	[1.75, 2.749, 2.792, 1.699]	[1.899, 1.899, 1.899, 1.899]
	ratio	1.03 : 1.618 : 1.643 : 1	1 : 1 : 1 : 1
position 3	max. tensions	[1.13, 2.104, 2.104, 1.13]	[1.681, 1.681, 1.681, 1.681]
	ratio	1 : 1.862 : 1.862 : 1	1 : 1 : 1 : 1

Table 6.1: List of κ's, maximum tensions, and their ratios at three end-effector positions

In what follows, we let $\ell_2 = 1$ unit for simplicity. To achieve a fair comparison, each transmission structure matrix is multiplied by a constant κ. The value

of κ is chosen so that the product of the three singular values of each $\mathbf{A}^T$ is equal to one. Table 6.1 lists the values of κ, the maximum tensions and their ratios at the three positions. In Table 6.1, structure (a) represents the Salisbury finger and (b) represents the structure with the transmission structure matrix derived in eq. (6.36). Structure (a) has different maximum tensions at the three representative positions, and the ratios of its maximum tensions are never equal to 1:1:1:1. Structure (b) has equal maximum tensions at all three positions, and the ratios of its maximum tensions are always equal to 1:1:1:1.

Figures 6.3 and 6.4 show the spherical plots of the four tendon forces for structures (a) and (b), respectively, evaluated at position 1. In a spherical plot, the radial distance represents the tendon force and the phase angle represents the direction of the applied force. Except for a change in orientation, the four spherical plots shown in Fig. 6.4 are identical in shape with each other while those shown in Fig. 6.3 are different from one another.

6.6 Summary

Through static force analysis, a design methodology for determining tendon routings and pulley sizes of a particular three-dof tendon-driven manipulator is developed. The manipulator features the characteristics of equal maximum tensions and isotropic transmission. The characteristics of equal maximum tensions ensure that all tendons subject to equal maximum tensions in its whole workspace when an external force is applied at the end-effector in all possible orientations. The isotropic transmission with appropriately selected isotropic

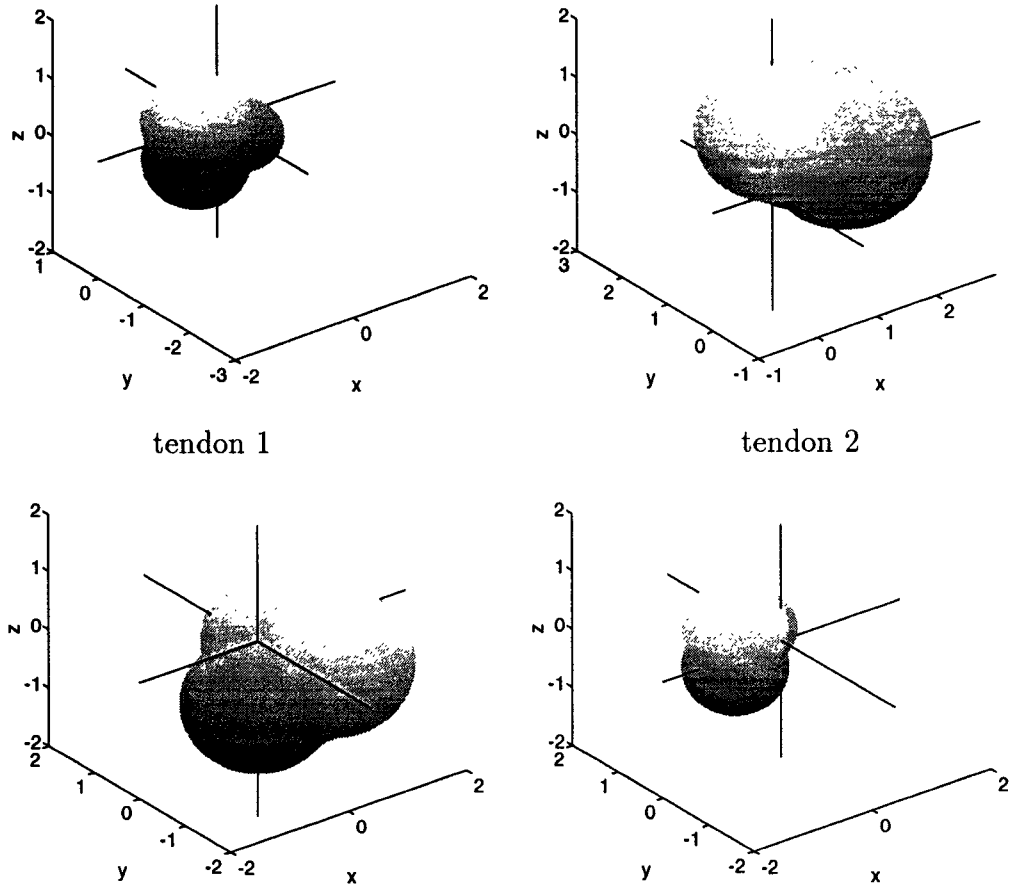

Figure 6.3: Spherical plots of the six tendon forces versus direction of applied force for structure (a) evaluated at position 1. The radial distance represents the tendon force and the phase angle represents the direction of applied force.

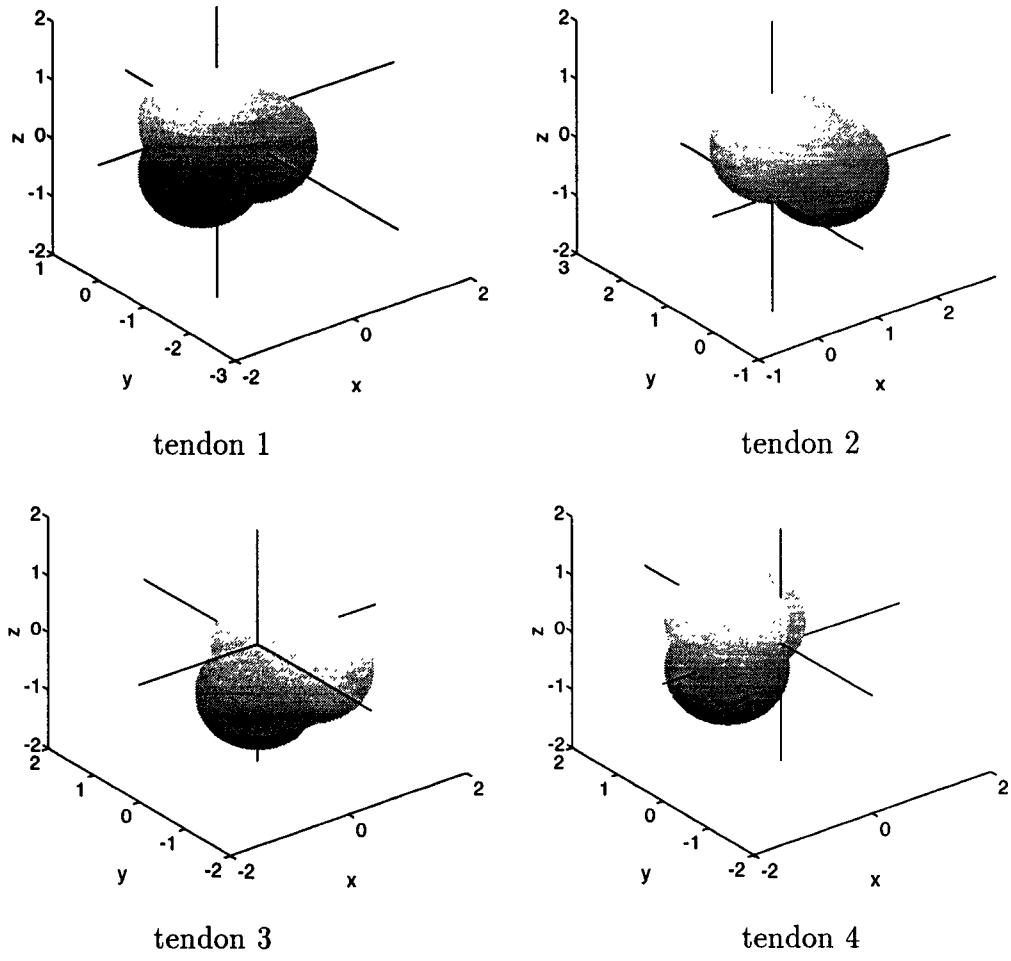

Figure 6.4: Spherical plots of the six tendon forces versus direction of applied force for structure (b) evaluated at position 1. The radial distance represents the tendon force and the phase angle represents the direction of applied force.

points helps to improve the static performance of the manipulator.

Chapter 7

Summary and Future Study

7.1 Summary

This work deals with the synthesis of the mechanical power transmission structure in tendon-driven manipulators. Four topics were addressed: (1) kinematically admissible transmission structures, (2) design of transmission structures with isotropic transmission characteristics, (3) attributes of isotropic transmission structures, and (4) the design of a three-dof manipulator with equal maximum tensions everywhere in its workspace.

Due to the constraint of uni-directional force, the synthesis of tendon transmission mechanism is different from that of bi-directional force transmission mechanisms. In the first topic, the fundamental rules for kinematically admissible transmission structures was addressed; and then an efficient algorithm to check for kinematically admissible transmission structures was derived. The

rules and the algorithm are then simplified for transmission structures with the minimum number of tendons, $n+1$ tendons, required to independently control each joint of a manipulator.

Based on the analysis of the static force transmission from the end-effector space to the actuator space, the design objective is then aimed at the creation of transmission structures with isotropic transmission characteristics. It is shown that only transmission structures with $n+1$ and $2n$ tendons can be designed to possess these characteristics. The design equations and their analytic solutions for creating such transmission structures are derived. It is shown that the designated isotropic point can be chosen at any place where the Jacobian matrix is nonsingular, thereby, increasing the solution space of optimal design of tendon-driven manipulator.

Comparisons for manipulators with the $n+1$ type, $2n$ type isotropic transmission structures and other non-isotropic type transmission structures are illustrated through many different examples. It is shown that manipulators with isotropic transmission structures have more uniform force distribution among their tendons. Furthermore, it is also shown that a better global performance can be achieved through proper selection of the designated isotropic point.

To broaden the understanding of the isotropic transmission characteristics, many attributes of a manipulator with an isotropic transmission structure was discussed. The analysis of minimum p-norm tension leads to a unique control tension algorithm. The analysis of maximum tension proves that the maximum tension in each tendon can be made equal to one another. The condition number

of the transformation matrix $\mathbf{A}^{+T}\mathbf{J}^{T}$ is shown to be the same for both the n+1 type and the $2n$ type isotropic transmission structures. The difference in the sum of tensions for the n+1 and $2n$ type isotropic transmission structures reveals that the $2n$ type transmission structures has smaller antagonistic forces among their tendons. A study of the controllability of the $2n$ type isotropic transmission structures shows that all $2n$ tendons are necessary for independently controlling each joint.

Since the maximum tension in each tendon is equal at an isotropic point, it is interesting to extend the feature to the whole workspace. A special three-dof spherical manipulator with isotropic transmission structure was designed to possess the characteristics of equal maximum tensions everywhere within its workspace.

Although only small size manipulators are mentioned in this work, the results are equally applicable to other applications. Examples include construction robots and space robots where the actuators have to be installed on a base and the power transmission mechanisms should be compact and lightweight. Such large scale manipulators usually require isotropic transmission characteristics within a reasonable working range.

7.2 Future Study

So far, we have established kinematic design constraints and static design methodologies for tendon-driven manipulators. Based on kinematic and static analysis,

this work provides a fundamental analytical and theoretical basis for the design of such mechanisms. However, in real-world applications, the design goals are far more complicated than what the analysis can achieve. There is no doubt that many issues remain to be investigated.

Experimental validation

To verify the concept of the isotropic transmission characteristics and to further understand the characteristics of a tendon-driven manipulator, it is necessary to build an experimental prototype. By using different pulleys and tendon routings, the effects of isotropic transmission structures can be demonstrated and compared. This protype can also serve as a test bed for different force controllers and tension sensors. The physical properities of a tendon-driven manipulator can then be studied. Such investigation is essential to better design a manipulator.

Global performance

As mentioned in the conclusion of Chapter 4, the selection of isotropic points has a great influence on the static characteristics over the entire workspace of a manipulator. The selection of isotropic points depends on the link lengths and joint configuration of a manipulator. To achieve global optimal performance, the link lengths, joint configuration, tendon routings and pulley sizes should be carefully considered as a whole. The development of a new theory or methodology based on these parameters is crucial to the global optimal design of a tendon-driven manipulator. And this is a subject worth pursuing.

Redundant manipulators

Although in this work, the Jacobian matrix is assumed to be a square matrix

to avoid confusion, the design concept can be extended to those manipulators with nonsquare Jacobian matrices. The number of degrees of freedom for such a manipulator is more than that required to perform a primary task. The existence of redundancy offers the possibility to perform a secondary function such as obstacle avoidance and optimal path planning. As the design criteria for such manipulators are more complex than non-redundant manipulators, we feel that this is a completely new topic for the design of tendon-driven manipulators.

Dynamic effect

A tendon-driven mechanism is widely adopted in the design of dexterous hands for its lightness and compactness, where the primary tasks of a dextrous hand are to grasp and to manipulate objects. Such tasks usually involve slow motions and static analysis of this system can lead to satisfactory results. As we should free ourself from such limited applications and widen our applications, the importance of large and fast motions of a manipulator will never be over-exaggerated. The main concerns in the design of a manipulator for these applications are the dynamic effect and kinematic performance within its entire workspace. Such a design problem is a necessary challenge for the completeness of the design methodologies for tendon-driven manipulators.

Tendon compliance, system friction and control strategies

As mentioned before, human tendon-sheath system has nearly the lowest friction. However, today's tendon-technology falls far behind the works of the nature in this perspective. As a tendon stretches under tension, the tendon unavoidably slides against pulleys. This phenomenon generates friction and causes wear and fatigue. The selection of tendons affects the reliability and strength of

tendon-driven manipulators. Together with tendon compliance, the nonlinear characteristic of friction also cause problems in the design of the control system (Townsend and Salisbury, 1987). Since a tendon-driven manipulator performs under the control of antagonistic forces among its tendons, the control strategies has great influence on the performance of the system. An innovative methodogy for sensor-based adaptive nonlinear control needs to be developed.

The above discussions only reveal portions of the challenges to the design of tendon-driven manipulators. As the understanding of all these matters and other relative technologies increase, the design and the capability of tendon-driven manipulators can be improved. Before that, much work needs to be done.

Bibliography

Ali, M., Kyriakopoulos, K. J., and Stephanou, H. E., 1993, "The Kinematics of the Anthrobot-2 Dextrous Hand," *Proc. of IEEE Int'l. Conf. on Robotics and Automation*, pp. 705–710.

Angeles, J., 1992, "The Design of Isotropic Manipulator Architectures in the Presence of Redundancies," The Int'l Journal of Robotics Research, Vol. 11, No. 3, pp. 196–201.

Asada, H., and Cro Granito, J. A., 1985, "Kinematic and Static Characterization of Wrist Joints and Their Optimal Design," *Proc. of IEEE Int'l. Conf. on Robotics and Automation*, pp. 244–250.

Ben-Israel, A., and Greville, T. N. E., 1974, *Generalized Inverses: Theory and Applications*, Wiley, New York, NY.

Chen, D.-Z., and Tsai, L.-W., 1993, "Kinematic and Dynamic Synthesis of Geared Robotic Mechanisms," ASME Journal of Mechanical Design, Vol. 115, No. 2, pp. 241–246.

Coxeter, H. S. M., 1973, *Regular Polytopes*, Dover Publications, New York, NY., 3 edition.

Fu, K. S., Gonzalez, R. C., and Lee, C. S. G., 1987, *Robotics: Control, Sensing, Vision, and Intelligence*, McGraw-Hill Inc., New York, N.Y.

Golub, G. H., and Van Loan, C. F., 1983, *Matrix Computations*, The John Hopkins University Press, Baltimore, Maryland.

Gosselin, C., and Angeles, J., 1988, "A New Performance Index for the Kinematic Optimization of Robotic Manipulators," *ASME Trends and Developments in Mechanisms, Machines and Robotics, DE-Vol. 15-3*, pp. 441–447.

Jacobsen, S. C., Iversen, E. K., Knutti, D. F., Johnson, R. T., and Biggers, K. B., 1986, "Design of The UTAH/MIT Dextrous Hand," *Proc. of IEEE Int'l. Conf. on Robotics and Automation*, pp. 1520–1532.

Jacobsen, S. C., Ko, H., Iversen, E. K., and Davis, C. C., 1989, "Antagonistic Control of a Tendon Driven Manipulator," *Proc. of IEEE Int'l. Conf. on Robotics and Automation*, pp. 1334–1339.

Jacobsen, S. C., Wood, J. E., Knutti, D. F., and Biggers, K. B., 1984, "The Utah/MIT Dextrous Hand: Work in Progress," The International Journal of Robotics Research, Vol. 3, No. 4, pp. 21–50.

Klein, C. A., and Blaho, B. E., 1987, "Dexterity Measures for the Design and Control of Kinematically Redundant Manipulators," Int'l. J. of Robotics Research, Vol. 6, No. 2, pp. 72–83.

Lee, J.-J., 1991, "Tendon-Driven Manipulators: Analysis, Synthesis, and Control," PhD thesis, Dept. of Mech. Eng., The University of Maryland, College Park, MD.

Lee, J.-J., and Tsai, L.-W., 1991a, "On the Structural Synthesis of Tendon-Driven Manipulators Having Pseudo-Triangular Matrix," The Int'l. J. of Robotics Research, Vol. 10, No. 3, pp. 255–262.

Lee, J.-J., and Tsai, L.-W., 1991b, "Topological Analysis of Tendon-Driven Manipulators," *Proceedings of the 8th World Congress on the Theory of Ma-*

chines and Mechanisms, pp. 479–482, Prague, Czechoslovakia.

Melchiorri, C., and Vassura, G., 1992, "Mechanical and Control Features of the University of Bologna Hand Version 2," *Proc. of IEEE/RSJ Int'l. Conf. on Intelligent Robots and Systems*, pp. 187–193, Raleigh, NC.

Morecki, A., Busko, Z., Gasztold, H., and Jaworek, K., 1980, "Synthesis and Control of the Anthropomorphic Two-Handed Manipulator," *Proc. 10th Int'l. Symposium on Industrial Robots*, pp. 461–474, Milan, Italy.

Okada, T., 1977, "On a Versatile Finger System," *Proc. 7th Int'l. Symposium on Industrial Robots*, pp. 345–352, Tokyo, Japan.

Press, W. H., Flannery, B. P., Teukolsky, S. A., and Vetterling, W. T., 1988, *Numerical Recipes in C: The Art of Scientific Computing*, Cambridge University Press, Cambridge.

Rouff, C. F., and Salisbury, J. K., 1990, *Multi-Fingered Robotic Hand*, U.S. Patent 4,921,293.

Rovetta, A., 1977, "On Specific Problems of Design of Multipurpose of Mechanical Hands in Industrial Robots," *Proc. 7th Int'l. Symposium on Industrial Robots*, pp. 337–341, Tokyo, Japan.

Salisbury, J. K., 1982, "Kinematic and Force Analysis of Articulated Hands," PhD thesis, Department of Mechanical Engineering, Stanford University, Stanford, CA.

Salisbury, J. K., and Craig, J. J., 1982, "Articulated Hands: Force Control and Kinematic Issues," The Int'l. J. of Robotics Research, Vol. 1, No. 1, pp. 4–17.

Salisbury, J. K., and Roth, B., 1983, "Kinematic and Force Analysis of Articulated Mechanical Hands," ASME J. of Mechanisms, Transmissions and Automation in Design, Vol. 105, No. 1, pp. 35–41.

Strang, G., 1988, *Linear Algebra and Its Applications*, Harcourt Brace Jovanovich, Inc., Orlando, FL, 3rd edition.

Sugano, S., and Kato, I., 1987, "WABOT-2: Autonomous Robot with Dexterous Finger-Arm," *Proc. of IEEE Int'l. Conf. on Robotics and Automation*, pp. 90–97, Raleigh, North Carolina.

Townsend, W. T., and Salisbury, J. K., 1987, "The Effect of Coulomb Friction and Stiction on Force Control," *Proc. of IEEE Int'l. Conf. on Robotics and Automation*, pp. 240–245, Raleigh.

Yoshikawa, T., 1985, "Manipulability of Robotic Mechanisms," Int'l. J. of Robotics Research, Vol. 4, No. 2, pp. 3–9.